

Session 6. Magnetic nozzles and plasma plumes



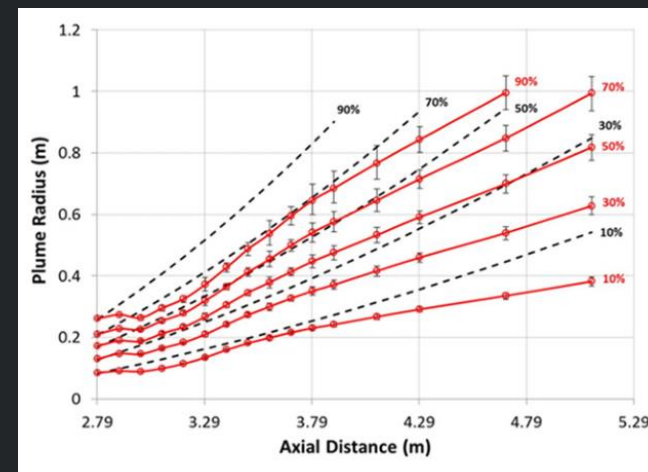
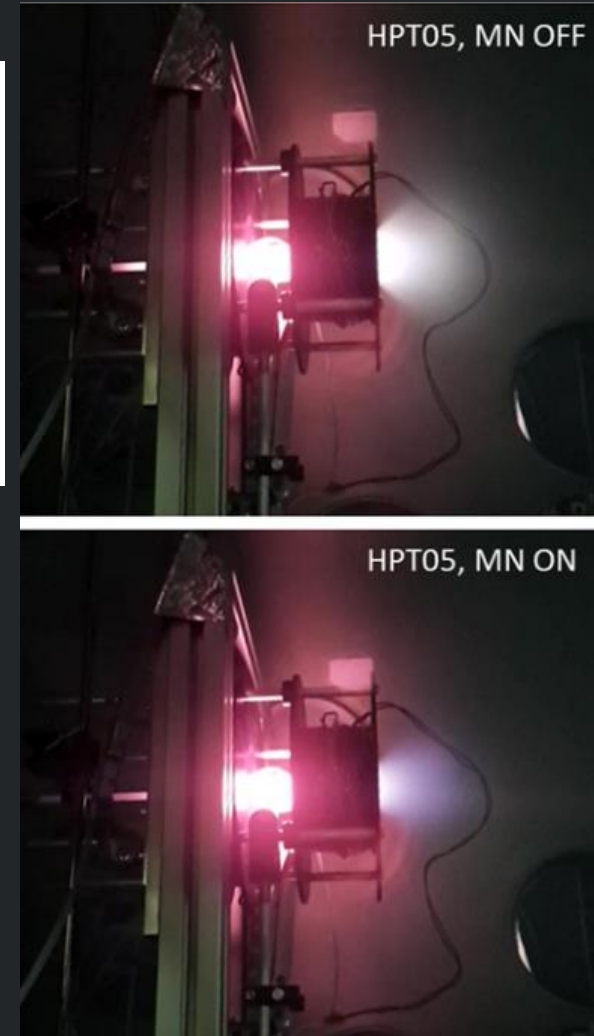
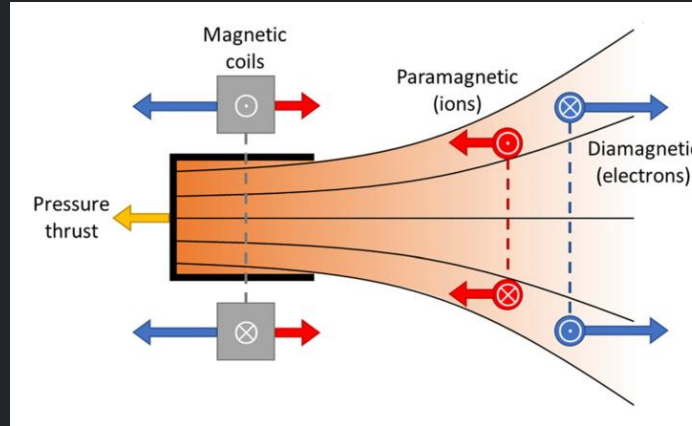
**ExB Plasmas
Workshop
2022**

Madrid, online event

Universidad Carlos III de Madrid, February 16-18, 2022

Magnetic nozzles and plasma plumes

- Basic mechanisms in the MN have been observed experimentally and explained from fluid models:
 - Magnetic thrust generation based on the repulsion of azimuthal plasma currents by the coils; electron pressure driven
 - Plume divergence angle in the MN is lower than in the comparable unmagnetized plasma expansion (i.e. radial plasma confinement)
 - Thermal electron energy to ion kinetic energy conversion via the self-consistent electrostatic field
 - Quasineutral flow, supersonic acceleration of ions
 - Unmagnetized ion detachment thanks to the increasing ion inertia ($\propto M_i^2$)
- Unmagnetized plumes: Main concerns:
 - Understanding electron kinetics, cooling, etc
 - Interaction with S/C surfaces

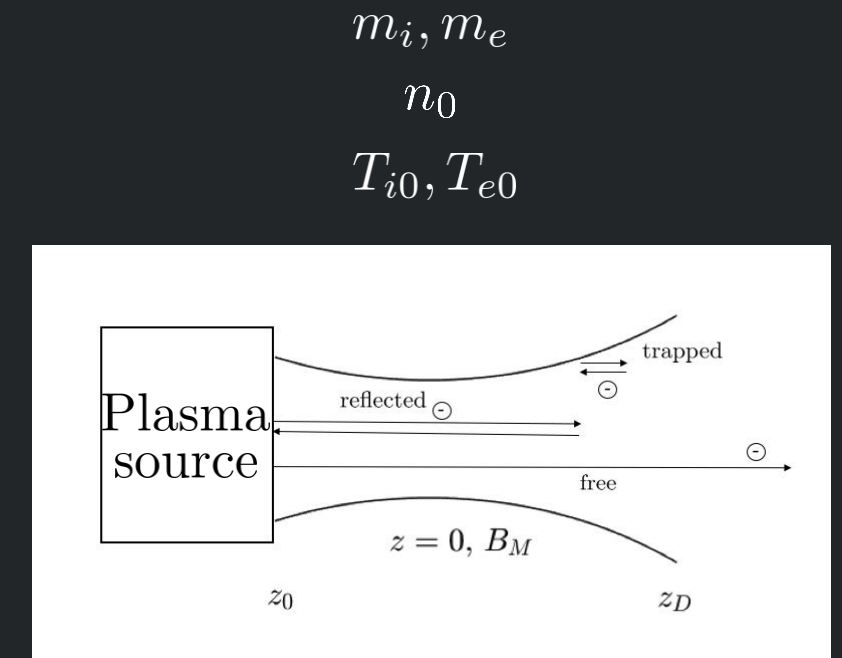


Active lines of work

- Kinetic evolution of the EVDF in the plasma expansion
 - Trapped electrons, cooling, anisotropy, heat fluxes Jiewei Zhou
 - Experimental results on electron cooling Alfio Vinci
 - Experimental measurement of trapped electrons June Young Kim
- Ion kinetic effects and instabilities in the MN Andrei Smolyakov
- Facility effects Ben Jorns
- Oscillations and instabilities in the MN Ben Jorns
- Advances in performance of associated EP thrusters Kazunori Takahashi
- Stretch of the magnetic nozzle Kazunori Takahashi
- Electron detachment Justin Little
- 3D plume modeling in the geomagnetic field Filippo Cichocki
- Numerical boundary conditions for fluid/hybrid/kinetic codes Mario Merino
- Advanced magnetic configurations Mario Merino

Kinetics of electrons (Zhou)

- Kinetic paraxial models of fully magnetized plasmas.
- Collisionless steady-state models based on conservation of E, μ :
 - Model of stationary Vlasov equation (integrated with the conservation of two motion properties). *Global* electron response
 - Martínez-Sánchez et al, Physics of Plasmas 22 053501 2015
 - Ahedo et al, PSST 29 045017 2020
 - Merino et al, PSST 30 115006 2021
 - Analogous models exist for unmagnetized plumes
 - Merino et al, PSST 27 035013 2018
 - Three subpopulations of electrons are found: reflected, trapped and free electrons.
 - Trapped electrons cannot be characterized, they originate from transient processes and collisions.
- In parallel, time-dependent and low-collisional models have been developed to characterize the trapped electrons:
 - Sánchez-Arriaga et al (PSST 27 035002 2018).
 - Zhou et al (PSST 30 045009 2021).

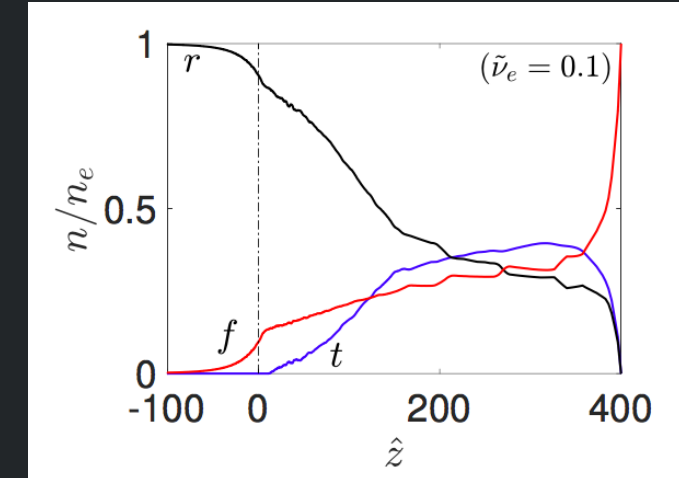


Kinetics of electrons (Zhou)

- VLASMAN: guiding center Boltzmann-Poisson model of the magnetized plasma expansion.
 - Boltzmann equation: solves for the average gyrophase VDF.
 - Collisions: Bhatnagar–Gross–Krook operator for electrons.

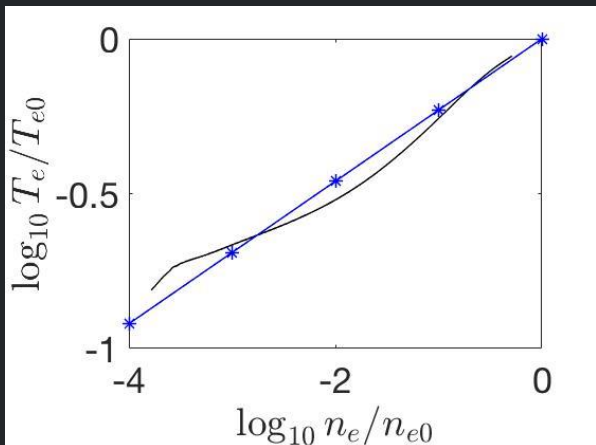
$$\begin{aligned} \frac{\partial \bar{f}_\alpha}{\partial t} + v_{\parallel} \frac{\partial \bar{f}_\alpha}{\partial z} + a_\alpha \frac{\partial \bar{f}_\alpha}{\partial v_{\parallel}} &= \frac{\delta \bar{f}_\alpha}{\delta t} \\ B \frac{\partial}{\partial z} \left(\frac{1}{B} \frac{\partial \phi}{\partial z} \right) &= -\frac{e}{\epsilon_0} \sum_{\alpha=e,i} Z_\alpha n_\alpha \end{aligned} \quad \left. \begin{array}{l} \frac{\delta \bar{f}_i}{\delta t} = 0 \\ \frac{\delta \bar{f}_e}{\delta t} = \nu_e (\bar{f}_{Me} - \bar{f}_e) \end{array} \right\}$$

- Simulation results for a weakly collisional case:
 - Set-up: $m_i/m_e = 100$, $T_{i0}/T_{e0} = 1$, $v_e = 0.1/\tau_{te}$.
 - Result: trapped region partially populated (12.7% of the region), and trapped electrons are not fully dominant downstream.



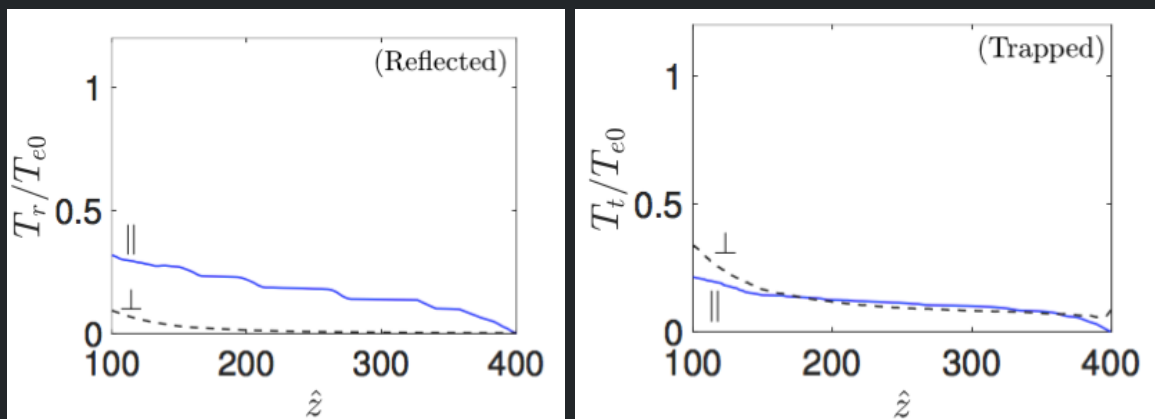
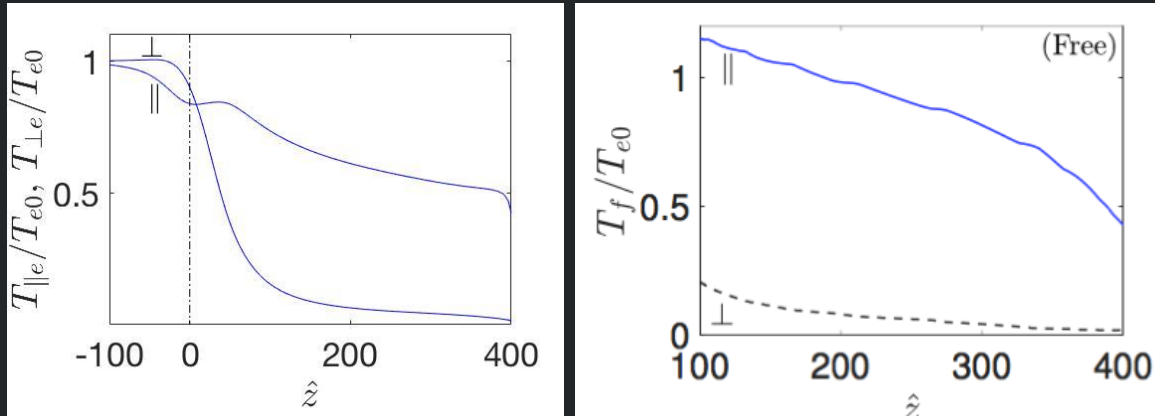
Kinetics of electrons (Zhou)

- Cooling of electrons and development of anisotropy downstream.
- Behavior separating in subpopulations:
 - Free electrons are hot and anisotropic.
 - Reflected electrons are cool and anisotropic.
 - Trapped electrons are cool and isotropic.
- Amount of trapped electrons regulate the cooling rate and level of anisotropy.
- Polytropic fitting as many experiments do, obtaining $k = 1.239$.



$$T_e \propto n_e^{k-1}$$

$$1 + \frac{n_e dT_e}{T_e dn_e} \approx k$$



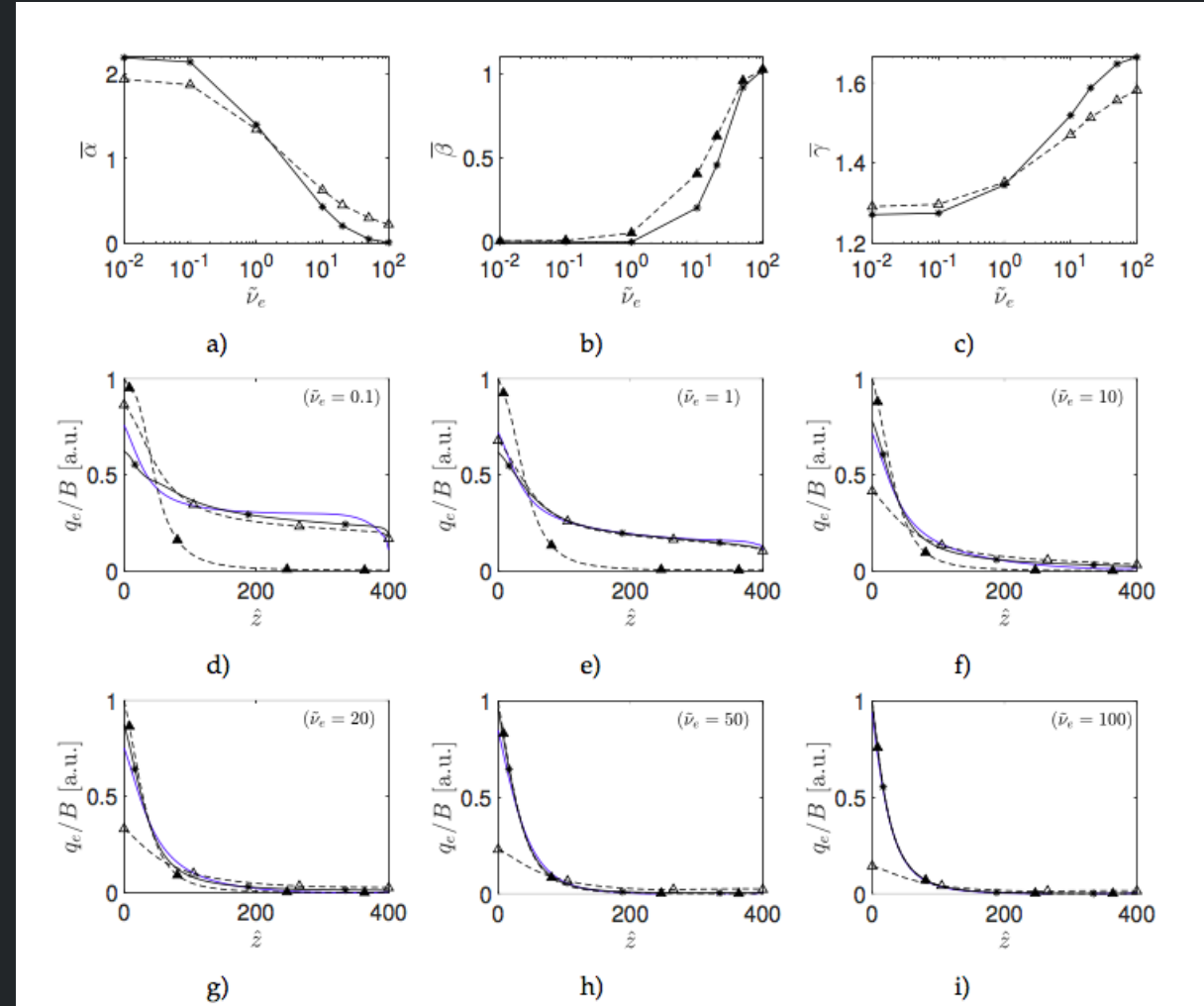
- In agreement with experimental works:
 - Little et al, Physical Review Letters 117 225003 2016.
 - Kim et al, New Journal of Physics 20 063033 2018.
 - Correyero et al, PSST 28 095004 2019.

Kinetics of electrons (Zhou)

- Fitting of the electron heat flux against a hybrid model, convective term/diffusive term.

$$q_e = \bar{\alpha} n_e T_e u_e - \bar{\beta} \frac{5 n_e T_e}{2 m_e \nu_e} \frac{dT_e}{dz}$$

- High-collisional limit, heat flux is diffusive.
- Low-collisional limit, heat flux is convective.
- Similar laws for low-collisional limits are found in other fields:
 - Malone et al, Physical Review Letters 34(12) 721-724 1975.
 - Stangeby et al, Nuclear Fusion 50 125003 2010.

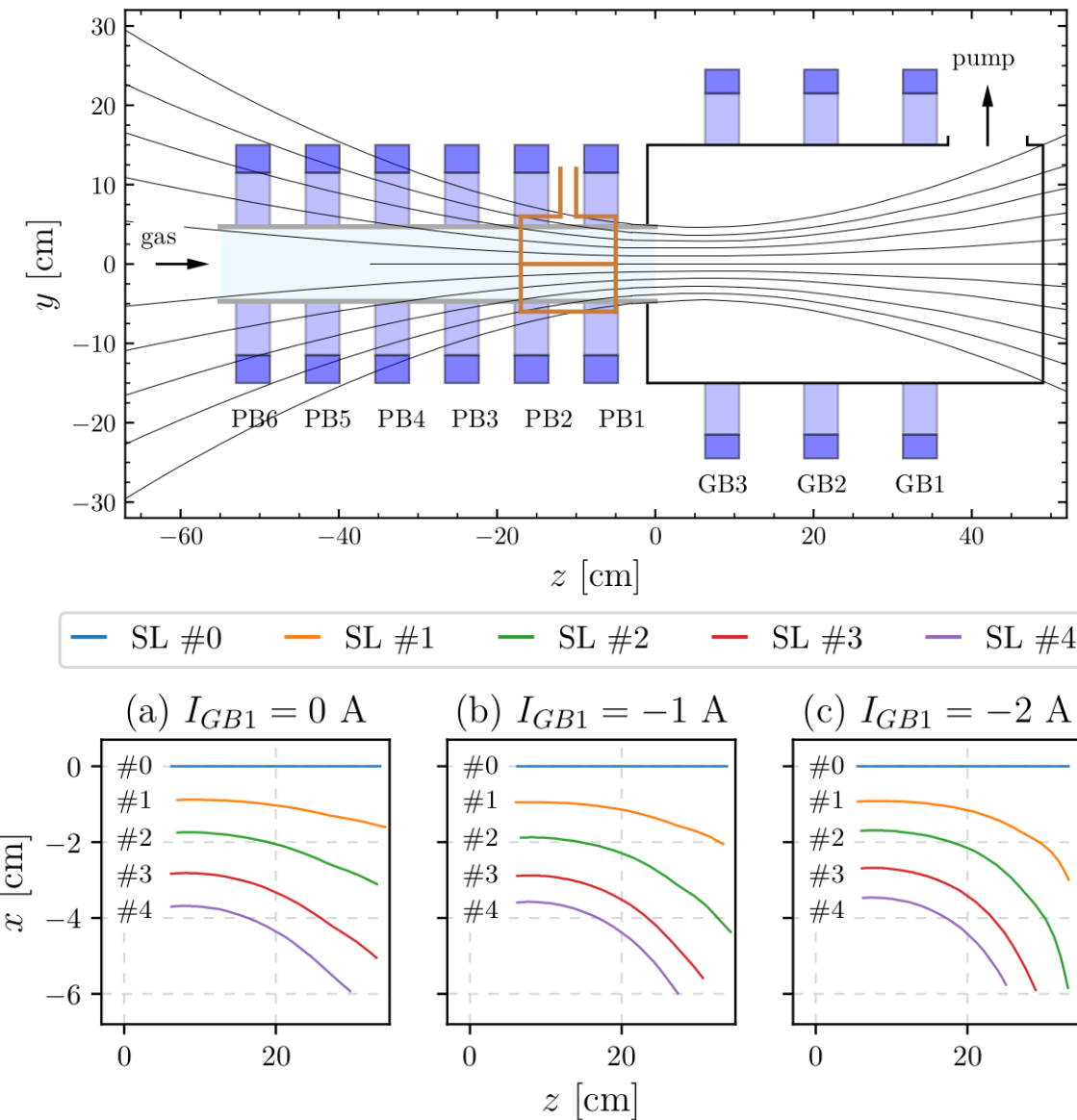


Context

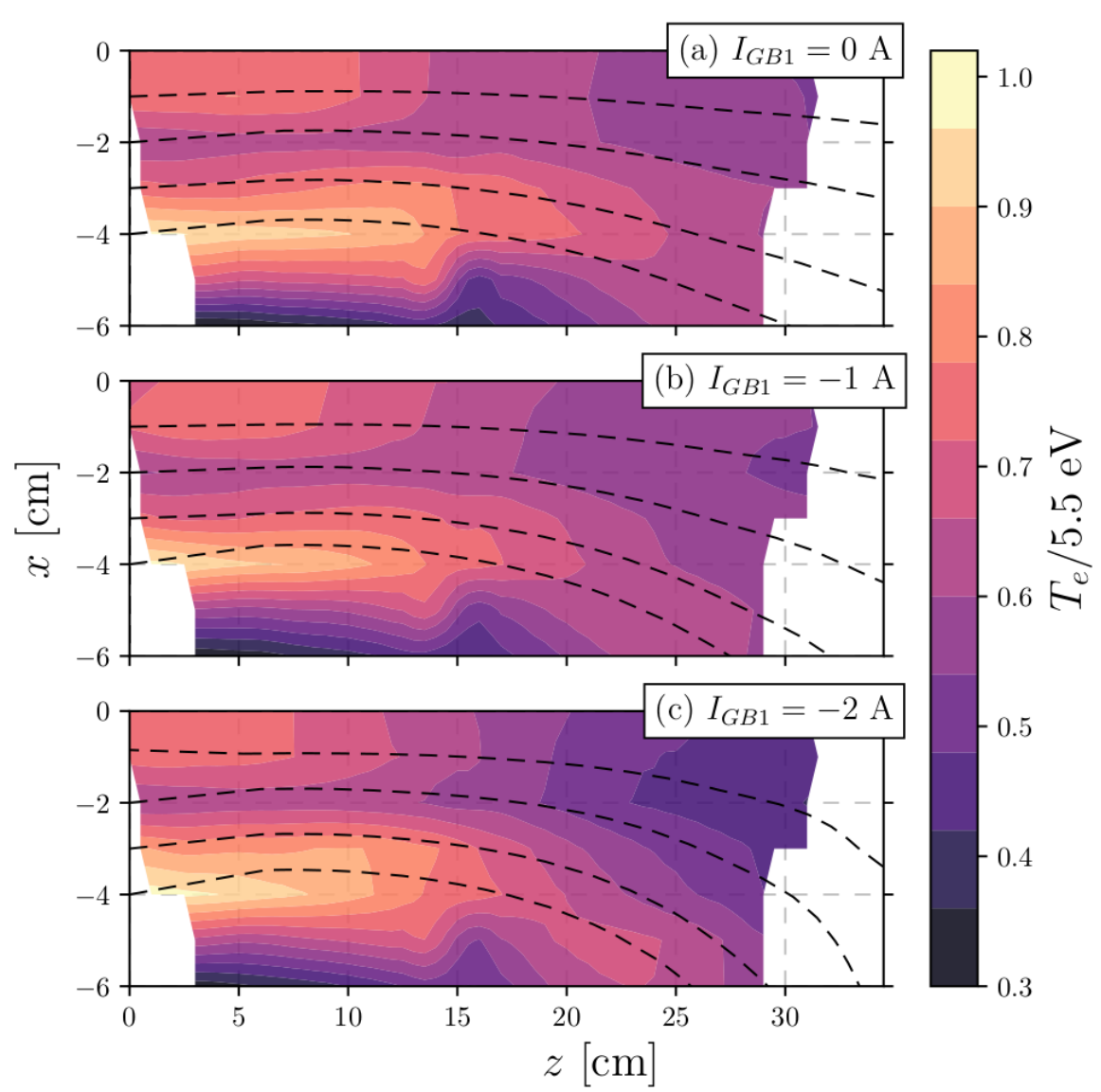
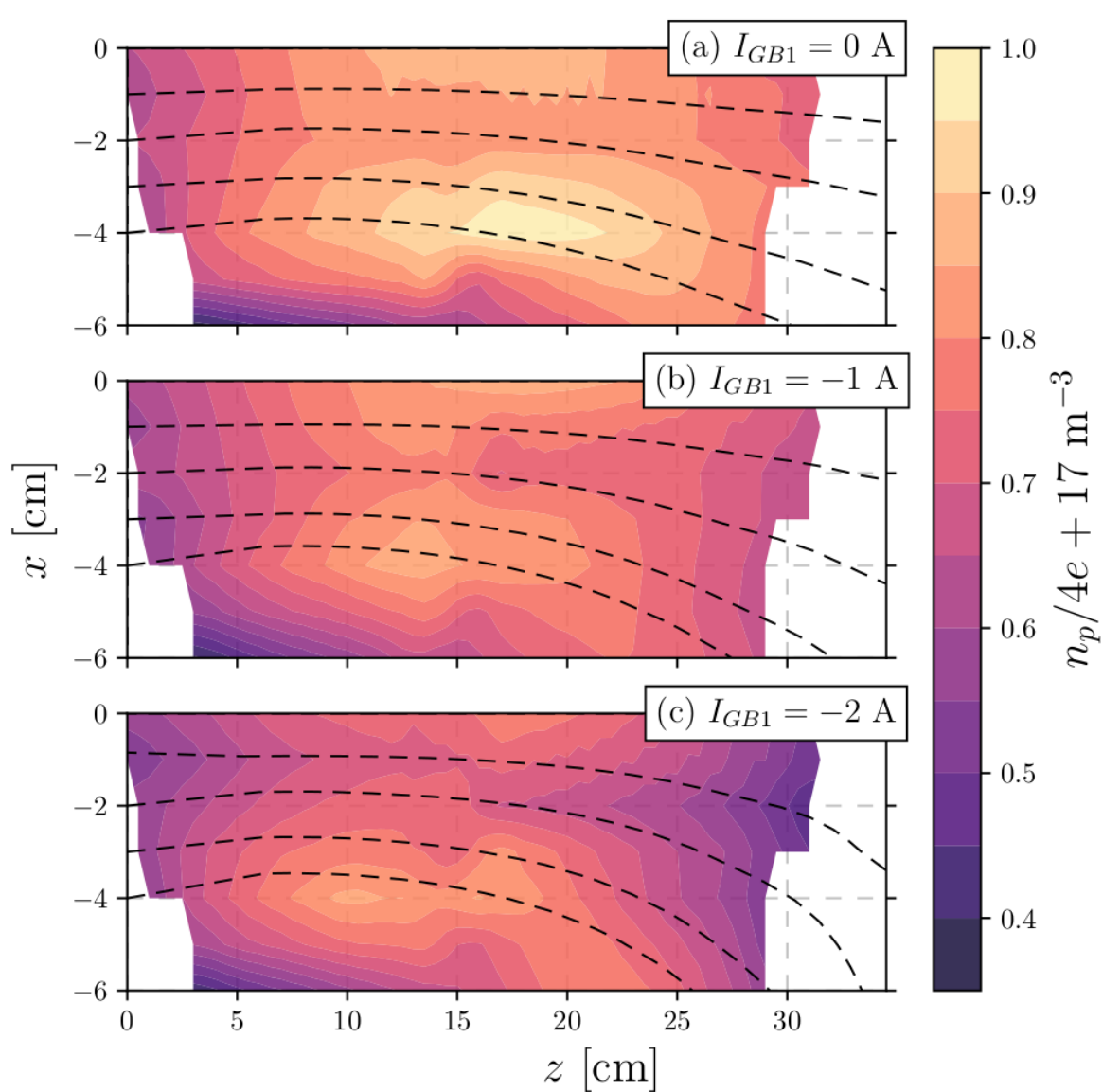
- The electron thermodynamics is a pivotal aspect in the plasma plume dynamics in terms of energy transfer
- The information is “stored” in the effective polytropic index γ_e
- Previous experimental studies:
 - Little and Choueiri, “*Electron Cooling in a Magnetically Expanding Plasma*”, Phys. Rev. Lett. **117**, 225003
Results: $\gamma_e \cong 1.15 \pm 0.03$ with no dependence on $|\mathbf{B}|$ ($Nu \ll 1$ dominant conductive flux)
 - Zhang *et al.*, “*Thermodynamic Study on Plasma Expansion along a Divergent Magnetic Field*”, Phys. Rev. Lett. **116**, 025001, 15 January 2016
Results: $\gamma_e \cong 1.17 \pm 0.02$, adiabatic expansion with non-Maxwellian electrons
 - Takahashi *et al.*, “*Thermodynamic Analogy for Electrons Interacting with a Magnetic Nozzle*”, Phys. Rev. Lett. **125**, 165001, 16 October 2020
Results: $1.1 < \gamma_e < 5/3$ continuously changing with $|\mathbf{B}|$
 - Kim *et al.*, “*Dependence of the polytropic index of plasma on magnetic field*”, New J. Phys. **23** 052001
Results: $\gamma_e \cong 2$ as the radial $|\mathbf{E}|$ constraints the cross-field transport
- These analyses relate to γ_e along the magnetic nozzle axis only
- **Question:** what happens in 2-D?

Experimental setup

- Helicon plasma source: $\phi = 9.4$ cm, $L = 55$ cm
- Expansion chamber: $\phi = 30$ cm, $L = 50$ cm
- $P_{IN} = 800$ W @ 13.56 MHz
- $\dot{m} = 0.2$ mg/s Xe
- $I_{GB3} = 9$ A and
 - $I_{GB1} = 0$ A for MN config.(a)
 - $I_{GB1} = -1$ A for MN config.(b)
 - $I_{GB1} = -2$ A for MN config.(a)
- $B_{max} \cong 9$ mT in all cases
- Plasma properties (n_e, T_e, V_p) are measured using a RF-compensated Langmuir probe



Results (1/3) - 2D electron properties

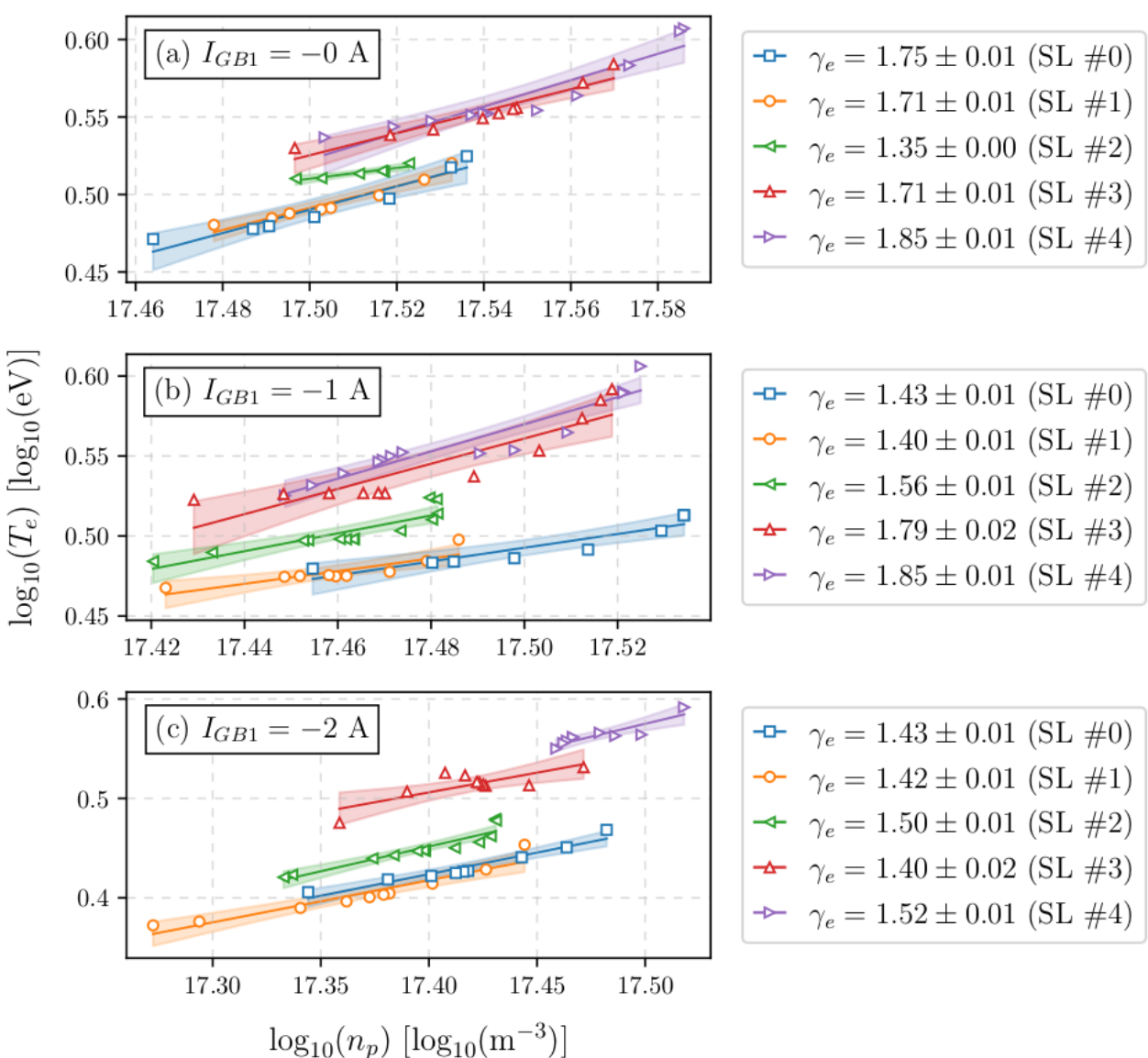


Results (2/3) - Electron cooling rate

- γ_e has dissimilar values along distinct SLs
 - MN config.(a) $\rightarrow 1.35 < \gamma_e < 1.85$
 - MN config.(b) $\rightarrow 1.40 < \gamma_e < 1.85$
 - MN config.(c) $\rightarrow \gamma_e \approx 1.4 - 1.5$
- Possible explanations:
 - Where $\gamma_e < 5/3$, ionization within the plume serves as additional degree of freedom. From [1], $\gamma_e = \gamma_e(T_i/T_e, n_p/n_n)$ yields:

$$\gamma_e \approx 1.3 - 1.5 \quad \text{for } T_i/T_e = n_p/n_n \sim 10^{-2}$$

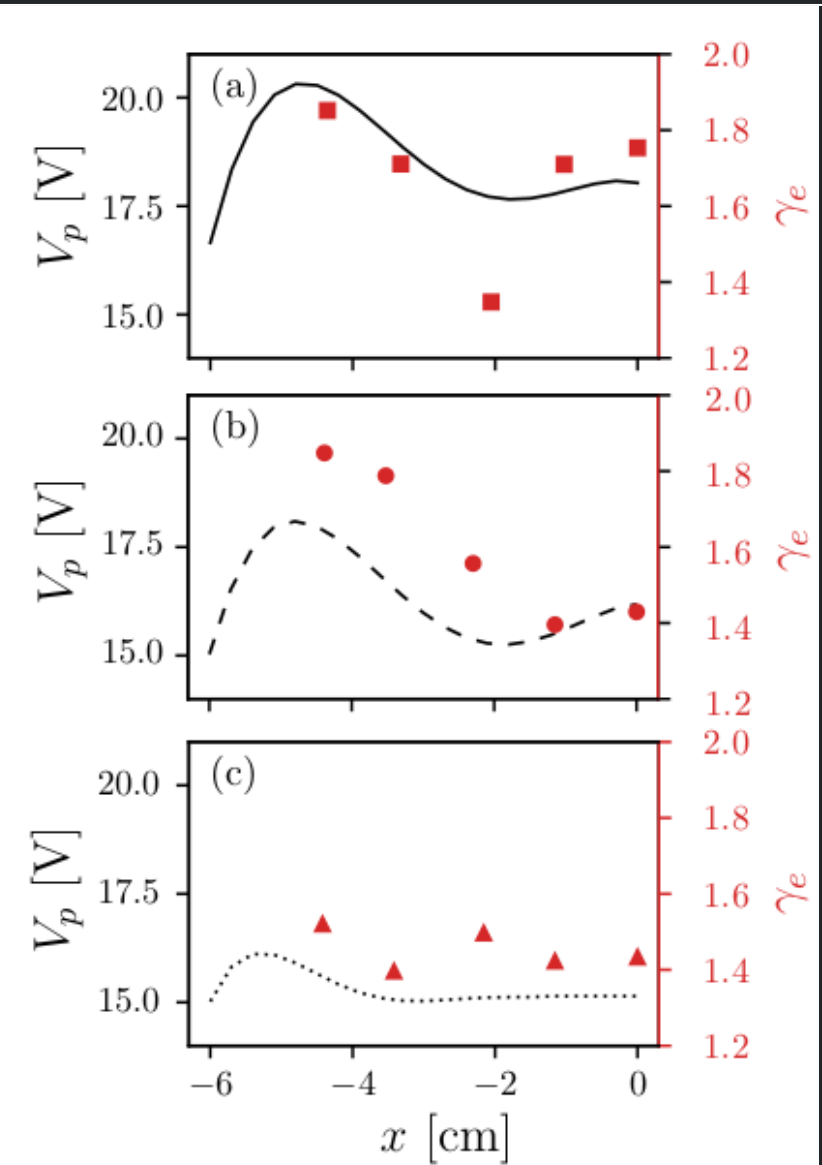
(it weakly depends on T_i/T_e and n_p/n_n for typical low-pressure lab plasmas)



[1] Burm *et al.*, "The isentropic exponent in plasmas", Physics of Plasmas **6** (1999)

Results (3/3) - Electron cooling rate

- γ_e has dissimilar values along distinct SLs
 - MN config.(a) $\rightarrow 1.35 < \gamma_e < 1.85$
 - MN config.(b) $\rightarrow 1.40 < \gamma_e < 1.85$
 - MN config.(c) $\rightarrow \gamma_e \approx 1.4 - 1.5$
- Possible explanations:
 - $\gamma_e > 5/3$ on-axis only in config.(a) may result from a stronger electron magnetization ($|\mathbf{B}|$ is larger downstream)
 - $\gamma_e > 5/3$ off-axis where V_p increases may result from a larger parallel conductivity (longitudinal transport promoted over transverse transport) as $D_{\perp} \sim (k_B T_e)^{-1/2}$



Conclusion

- In short:
 - In a 2-D description, simple gas dynamics cannot grasp the MN plume expansion
 - The real picture seems relatively complex featuring different cooling rates along different streamlines
 - In some conditions, the electrons degrees of freedom reduce to 2 (inhibited cross-field transport)
 - In some conditions, accounting for ionization within the plume effectively predicts the polytropic index
- Next steps:
 - Additional measurements to be performed on different kind of sources (ECRT, ...)
 - Additional measurements on different device scales
 - Use Thomson scattering to infer n_e and T_e

Recent Experimental Researches on Electron Cooling

- The effect of trapped electrons on the electron cooling rate is highlighted from 2018.

Importance of trapped electrons (1 to 5/3)

| Paper | Pressure | Source type | Magnetic field | Vacuum chamber |
|----------------------|-----------------------|---|---|--|
| [2014] J. P. Sheehan | 0.1 mTorr | Helicon (6.78 MHz) VASIMR VX-200 30 kW | • Electromagnets (2000 G at nozzle throat) | • Vacuum chamber was grounded (4.2 m in diameter and 10 m long) |
| [2015] T Lafleur | 3.8 to 7.5 μ Torr | ECR (2.45 GHz) | • Electromagnet (<1000 G inside the source) | • Vacuum chamber (1 m diameter, 4 m long) |
| [2016] J. M. Little | 0.02 mTorr | ICP (13.56 MHz) | • Electromagnet (peak magnetic field, 105-420 G) | • Vacuum chamber (2.4 m diameter, 7.6 m long) |
| [2016] Y. Zhang | 0.3 mTorr | Helicon (13.56 MHz) | • Electromagnet (peak magnetic field, 150 G) | • Expansion chamber (0.32 m diameter, 0.3 m long) |
| [2018] K. Takahashi | 0.5 mTorr | DC (remove axial electric field) | • Electromagnet (peak magnetic field, ~220 G) | • Expansion chamber (0.15 m diameter, 0.5 m long (estimated)) |
| [2018] J.Y. Kim | 0.45 mTorr | ECR (2.45 GHz) | • Electromagnet (450 G at nozzle throat) | • Expansion chamber (0.6 m diameter, 0.66 m long) |
| [2019] J.Y. Kim | 0.4 mTorr | ICP (13.56 MHz) Pulsed signal to extract and confine the source plasma | • Electromagnet (70 G at nozzle throat) | • Expansion chamber (0.6 m diameter, 0.66 m long) |
| [2019] S. Correyero | 2.1 to 2.8 μ Torr | ECR (2.45 GHz) | • Electro-magnet or Permanent magnet (fixed at 900 G for both types at the thrust back plate) | • The vacuum chamber, known as B09, (0.8 m diameter, 2 m long) |
| [2020] K. Takahashi | 0.5 mTorr | DC (remove axial electric field) | • Electromagnet (peak magnetic field, 264 G) | • Expansion chamber (0.15 m diameter, 0.5 m long (estimated)) |
| [2021] J.Y. Kim | 0.4 mTorr | DC (remove axial electric field, fixed radial electric field) | • Electromagnet (230 G at nozzle throat) | • Expansion chamber (0.6 m diameter, 0.66 m long) |
| [2021] J.Y. Kim | 0.4 mTorr | DC (remove axial electric field, fixed radial electric field) | • Electromagnet (230 G at nozzle throat) | • Expansion chamber (0.6 m diameter, 0.66 m long) |

Recent Experimental Researches on Electron Cooling

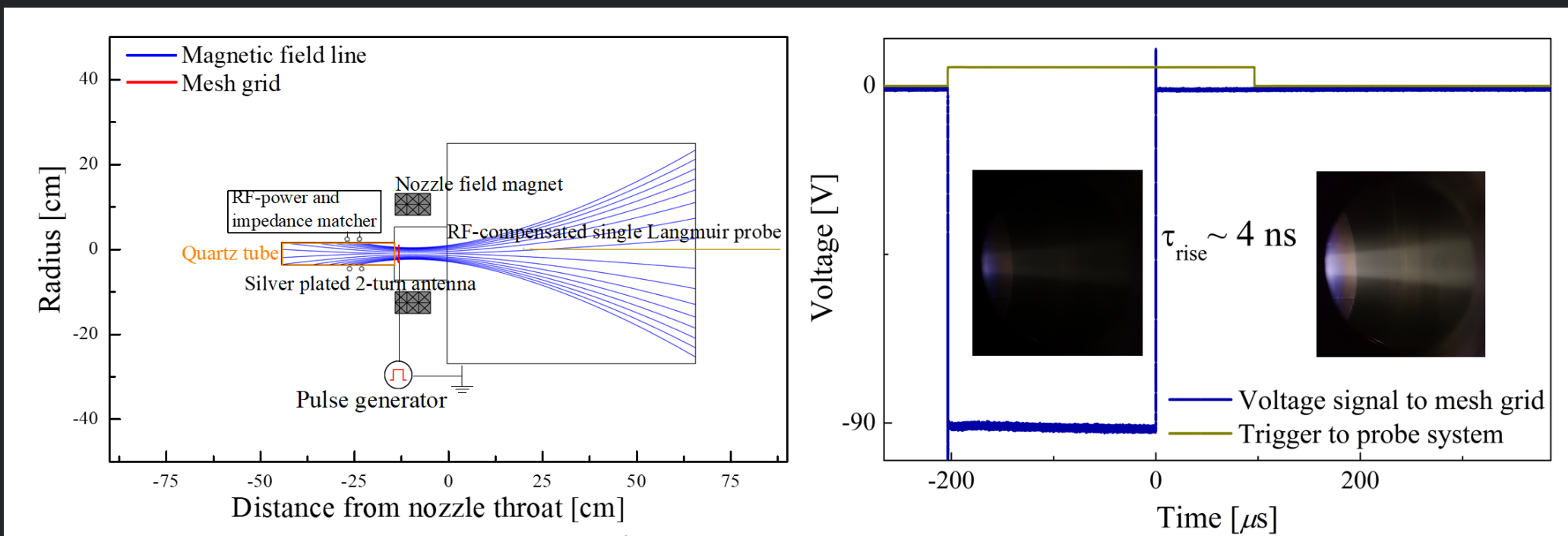
- $1 < \text{Polytropic index } \gamma_e < 2$
- Existence of trapped electrons effectively explains the difference in γ_e

Importance of trapped electrons (1 to 5/3)

| Paper | Electron Diagnostics | Polytropic index | Remark |
|----------------------|---|---|--|
| [2014] J. P. Sheehan | Planar Langmuir probe T_e : Semi-log plot of the electron current n_e : Electron saturation current | $\frac{\partial V_p}{\partial z} = 1.17 \frac{\partial T_{e,parallel}}{\partial z}$ | <ul style="list-style-type: none"> • Spatially varying γ_e due to detachment, turbulence, collision, and radiative loss |
| [2015] T Lafleur | Cylindrical Langmuir probe T_e : EEPF | 1.2 to 1.55 (proportional to magnetic field) | <ul style="list-style-type: none"> • Ratio of the maximum ion energy to the upstream electron temperature <ul style="list-style-type: none"> • No distinctive dependence on flow rate |
| [2016] J. M. Little | Cylindrical Langmuir probe n_e and T_e : Fitting of I-V Curve and EEPF (Maxwellian assumption) | 1.15 | <ul style="list-style-type: none"> • Current status: Potentially significant power loss due to unrecovered electron thermal energy • For efficient ion acceleration, γ_e should be increased to 5/3 |
| [2016] Y. Zhang | Cylindrical Langmuir probe n_e and T_e : Druyvesteyn theory | 1.17 | <ul style="list-style-type: none"> • Non-local kinetics of electrons along magnetic field line • Use of traditional thermodynamics concept is wrong |
| [2018] K. Takahashi | Cylindrical Langmuir probe n_e and T_e : Druyvesteyn theory | 1 or 5/3 | <ul style="list-style-type: none"> • 1, when Axial electric field exists • 5/3, when Axial electric field is removed (radial electric field exists) |
| [2018] J.Y. Kim | Cylindrical Langmuir probe n_e and T_e : Druyvesteyn theory | 1 to 5/3 | <ul style="list-style-type: none"> • Spatially varying γ_e by isothermally behaving electrons |
| [2019] J.Y. Kim | Cylindrical Langmuir probe n_e and T_e : Druyvesteyn theory | Temporal variation of γ_e | <ul style="list-style-type: none"> • 5/3, at initial expansion • <5/3 due to appearance of isothermally behaving trapped electrons |
| [2019] S. Correyero | Cylindrical Langmuir probe n_e and T_e : Druyvesteyn theory | | <ul style="list-style-type: none"> • Spatially varying polytropic index |
| [2020] K. Takahashi | Cylindrical Langmuir probe n_e and T_e : Druyvesteyn theory | 1 to 5/3 (dependent on magnetic field strength) | <ul style="list-style-type: none"> • Closes to 1, when radial electric field is removed • Closes to 5/3, when radial electric field is strengthened (prevent ions from cross-field transport → Confinement of electrons) |
| [2021] J.Y. Kim | Cylindrical Langmuir probe n_e and T_e : Druyvesteyn theory | 2 (independent on magnetic field strength) | <ul style="list-style-type: none"> • If the axial and radial electric is fixed with varying the magnetic field strength → The polytropic index is 2 • Changes in degree of freedom from 3 to 2 by radial electric field |
| [2021] J.Y. Kim | Cylindrical Langmuir probe n_e and T_e : Druyvesteyn theory | Spatially averaged: 1.88 | <ul style="list-style-type: none"> • Introduction of kappa distribution and non-extensive thermodynamics <ul style="list-style-type: none"> • Explains evolution of EEPFs by entropy (Kappa distribution) |

Measurement of Free and Trapped Electrons

- Time-dependent kinetic analysis of trapped electrons in a magnetic nozzle (Kim et al. PSST 2019)
- Mesh grid effectively divides the magnetic nozzle into source and diffusion region
- Box-car average mode gives time-resolved diagnostics of magnetically expanding plasma
- Probe system is synchronized with the voltage signal to mesh grid

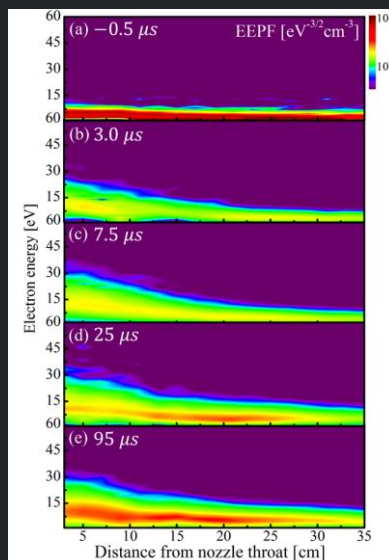


ICP (13.56 MHz) magnetic nozzle in SNU

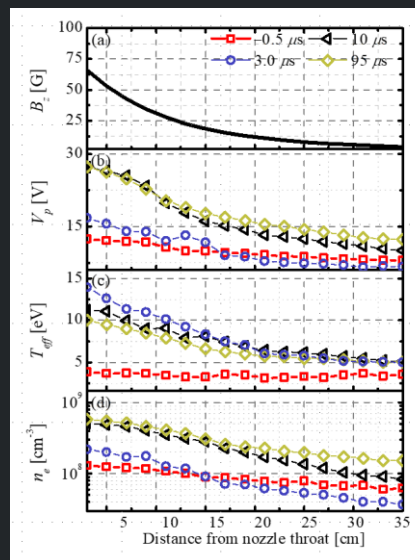
Periodically expanded plasma using mesh-grid

Measurement of Free and Trapped Electrons

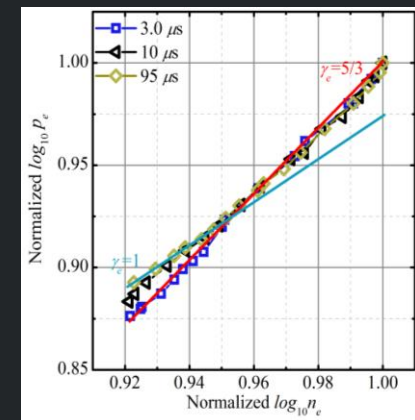
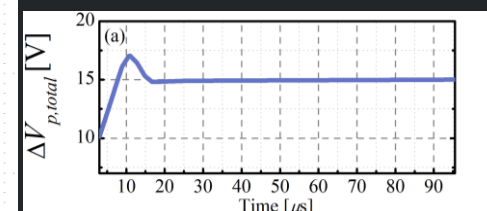
- The accumulation of electrons seen in the EEPFs directly attributes to changes of electron properties over time
 - Build-up of plasma potential structure → Electron trapping begins
 - Temporal changes in the electron temperature (decrease at the nozzle throat over time)
 - Re-constructed plasma potential structure
- Kinetic features of an MN are strongly affected by the non-stationary motion of the trapped electrons; thus, the temporal behavior of the trapped electrons must be considered for prediction and analysis of nozzle performances



Time evolution of EEPF



Time evolution of plasma properties



Polytropic index strongly affected by the trapped electrons

Introduction of Kappa distribution and Entropy

- Introduction of Kappa distribution and entropy can explain (Kim et al. PRE 2021)

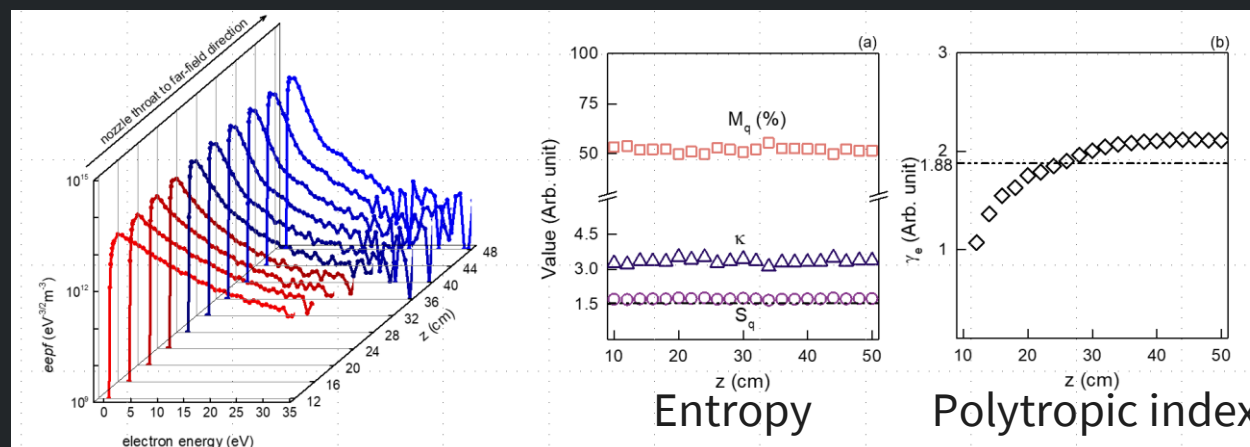
(1) Adiabatic process; Polytropic index closes to adiabatic value (5/3); Overall electron cooling

+

(2) Reversible process; Nearly constant Tsallis entropy s_q along axial direction; Emergence of high-energy tail

=

The formation of the non-Maxwellian distribution in the far-field of magnetic nozzle



By adopting Kappa distribution and entropy, non-Maxwellian distribution in MN can be interpreted in more detail

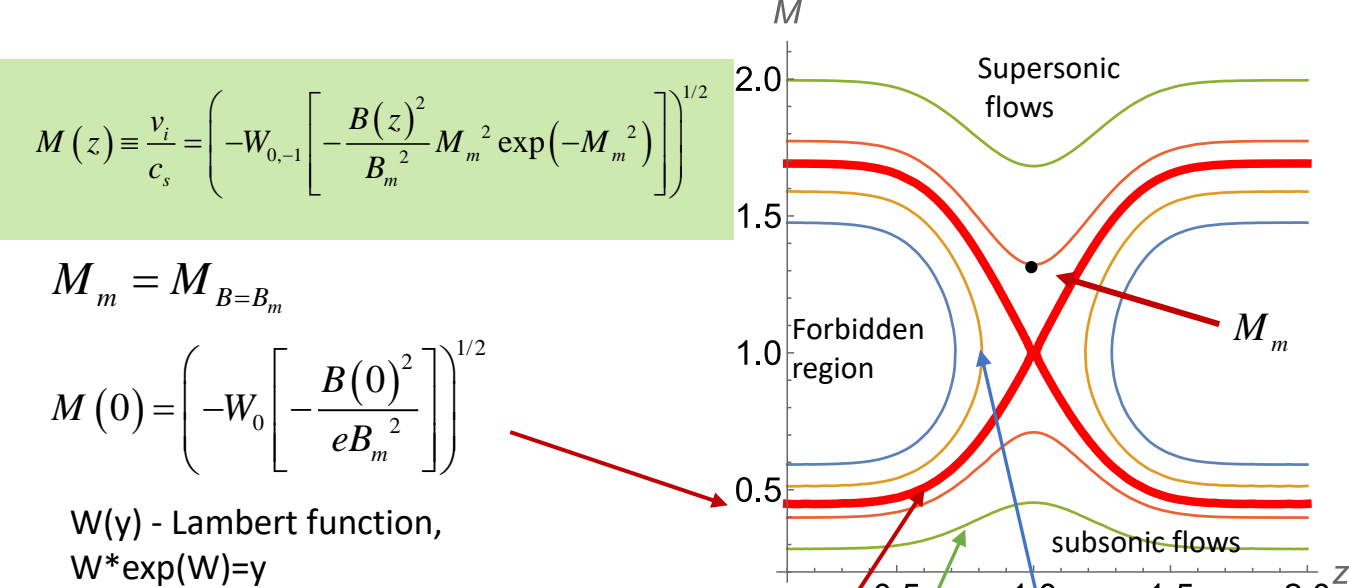
Ion kinetic effects and instabilities in the magnetic nozzle

A.I. Smolyakov¹, M. Jimenez¹, O. Chapurin¹, A. Sabo¹, F. Hunt¹, P. Yushmanov² and S. Putvinskii², ¹Usask, ²TAE Technologies

References: Smolyakov et al., *Physics of Plasmas* **28**(6): 060701; Sabo, et al., ArXiv:2109.02006; Jimenez et al.

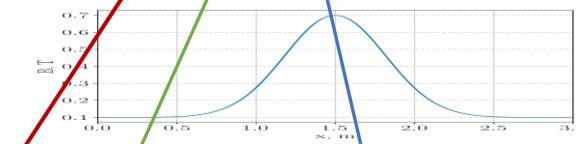
Quasineutral plasma flow in the magnetic nozzle is global (stiff):

The whole velocity profile is uniquely defined by the magnetic field

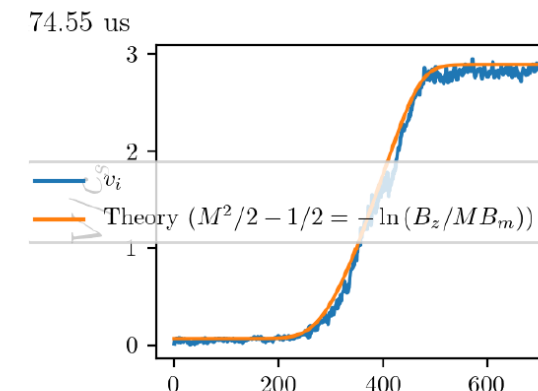
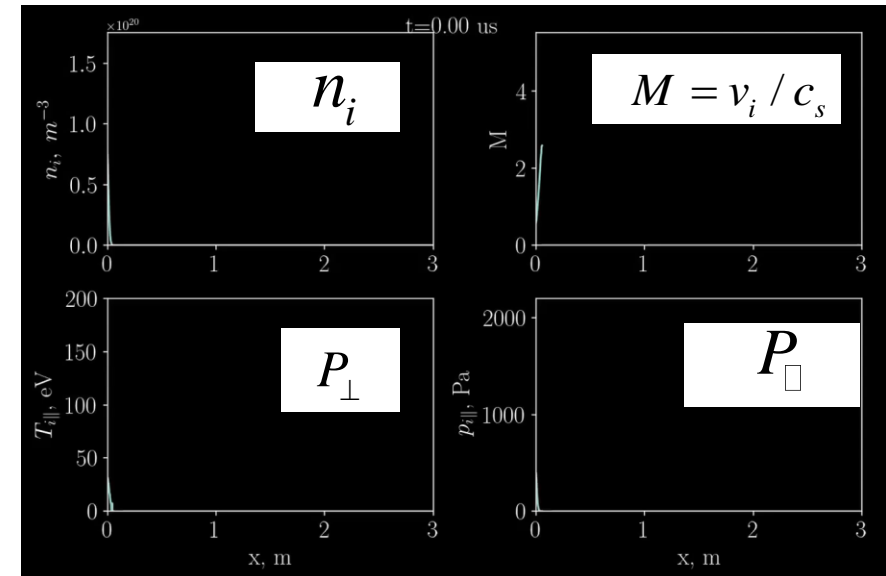


What happens if plasma velocity at the nozzle entrance is “wrong”?

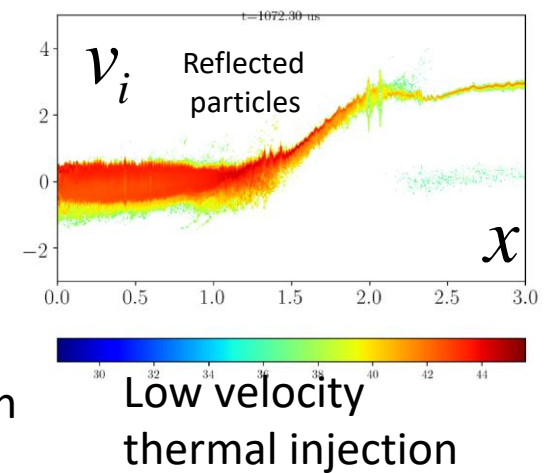
- Unique accelerating solution is structurally stable
- Supersonic laminar flow is stable
- Multivalued solutions, “forbidden region”, wave breaking-> instabilities
- Subsonic solutions are unstable, instabilities



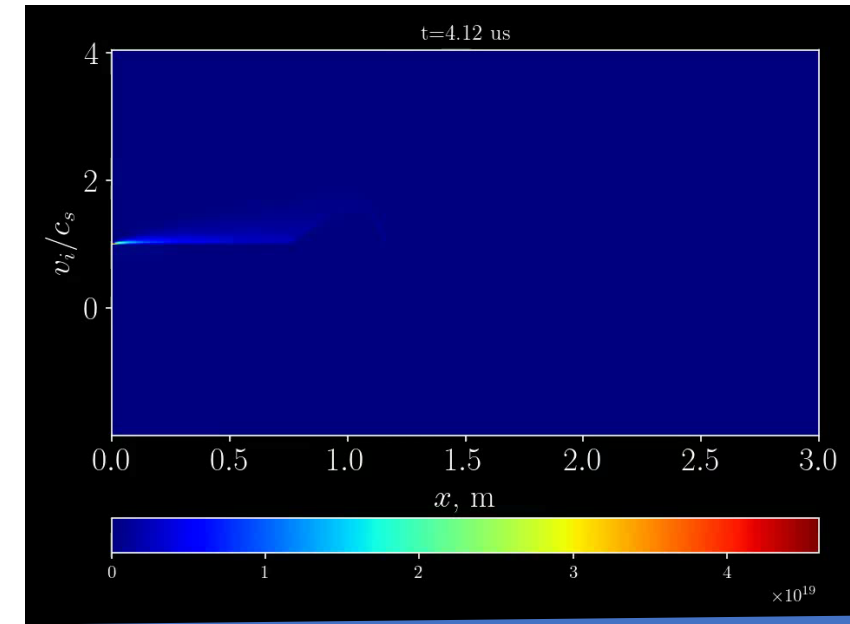
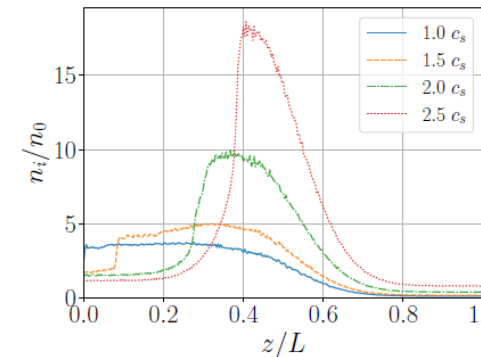
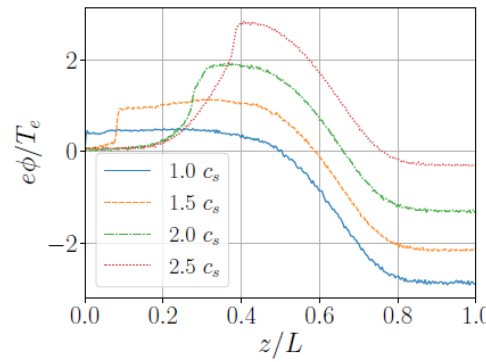
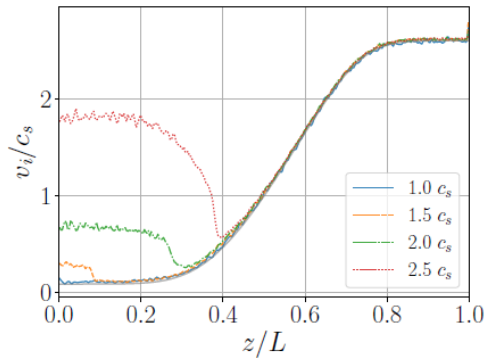
Kinetic effects with hybrid model, drift-kinetic ions, Boltzmann electrons



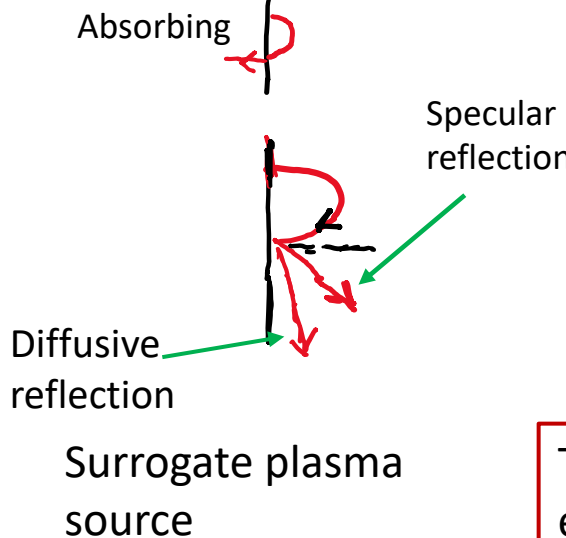
Agreement of fluid solution with kinetic simulations



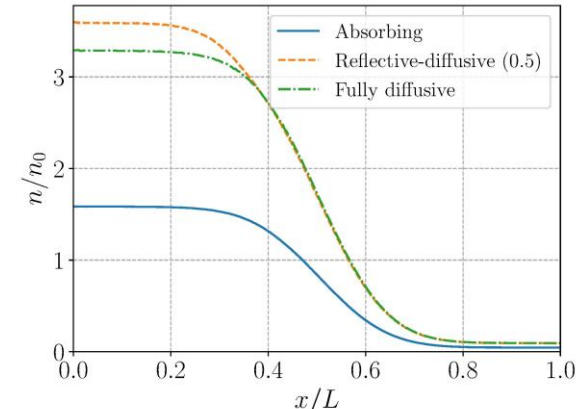
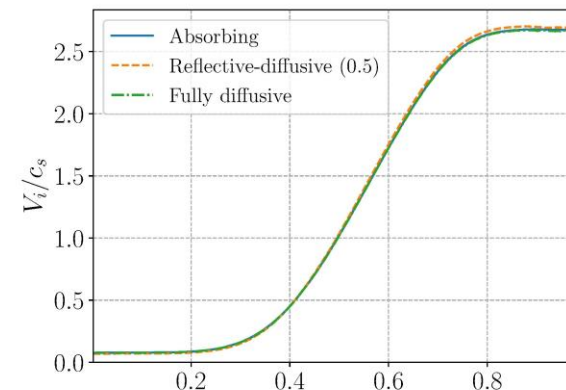
“Stalled flows” and instabilities in the “forbidden region of multivalued solutions”



Instabilities and reflections occur to “force” the flow into the robust accelerating solution



Matching of the MN to plasma source



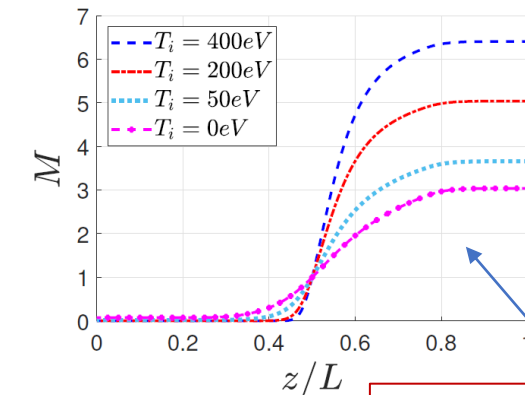
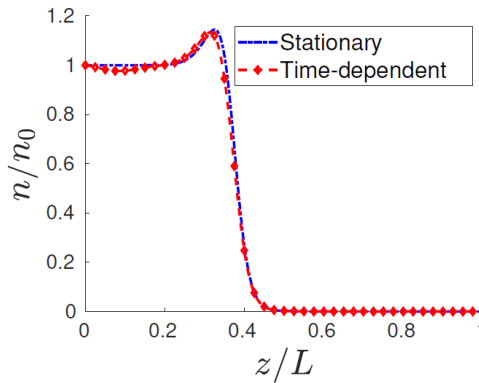
The unique accelerating solution x/L limits the plasma outflow; for a given energy/plasma source defines plasma density in the source region (at the left of the mirror)

Anisotropic ion pressure effects (two-pressure CGL model)

$$\left(M^2 - 1 - \frac{3p_{\parallel}}{nT_e} \right) \frac{\partial M}{\partial z} = - \left(1 + \frac{p_{\perp}}{nT_e} \right) M \frac{\partial \ln B}{\partial z}.$$

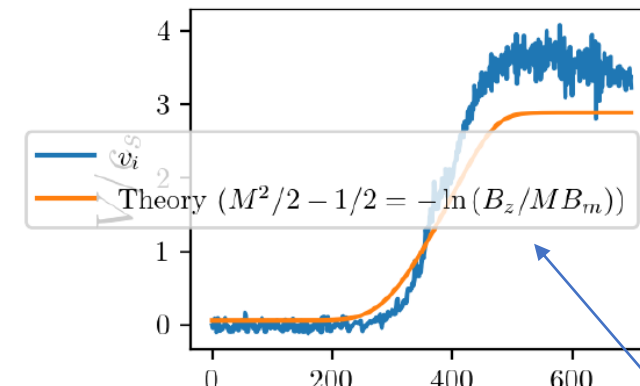
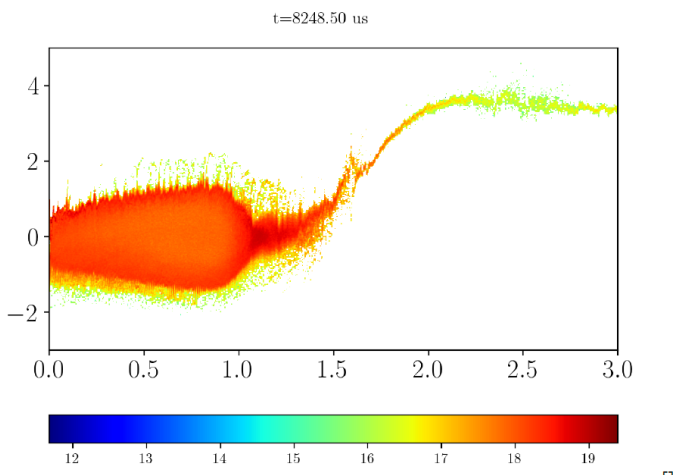
Sonic point modification due to finite ion parallel pressure

Mirror force due to finite ion pressure



Fluid solutions

Reflections in the phase space



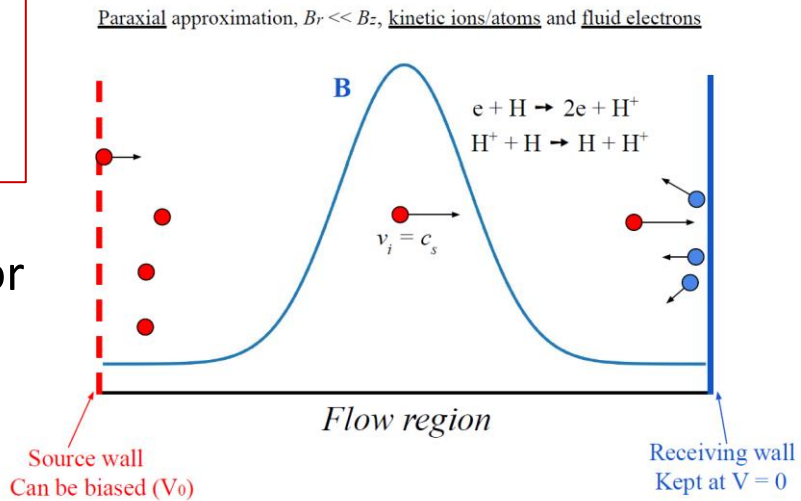
Hybrid (kinetic) solutions

Anisotropy (mirror force) enhances plasma acceleration

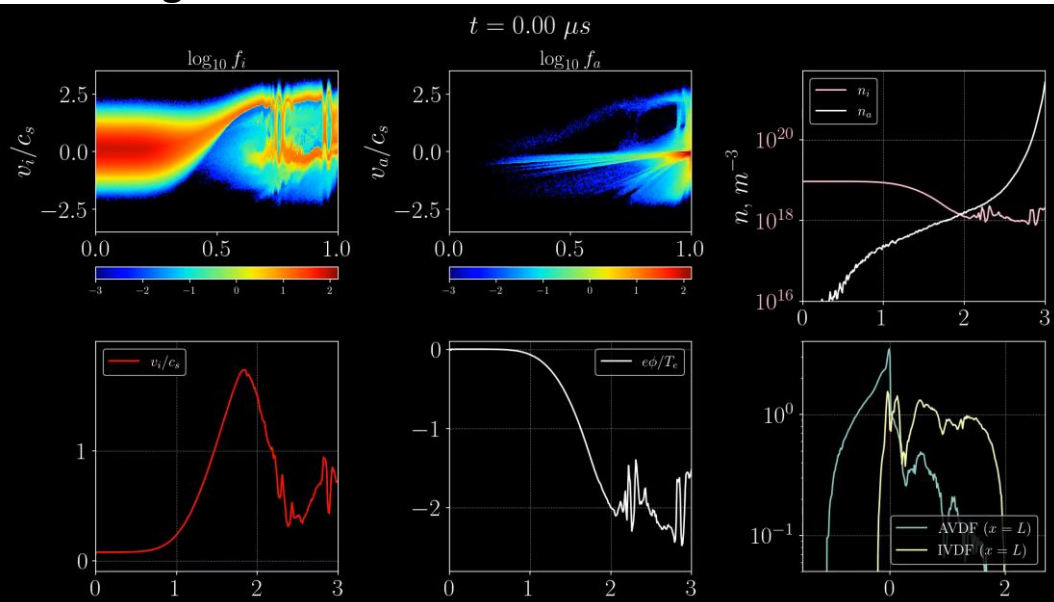
Facility effects and instabilities of the accelerated flow due to charge-exchange interactions with cold neutrals

- Conversion of accelerated ions to cold ions due to CX creates conditions for two-stream type instabilities
- Dramatic flow instabilities may occur for large fraction of cold neutrals
- CX occurs on recycled and/or background neutrals

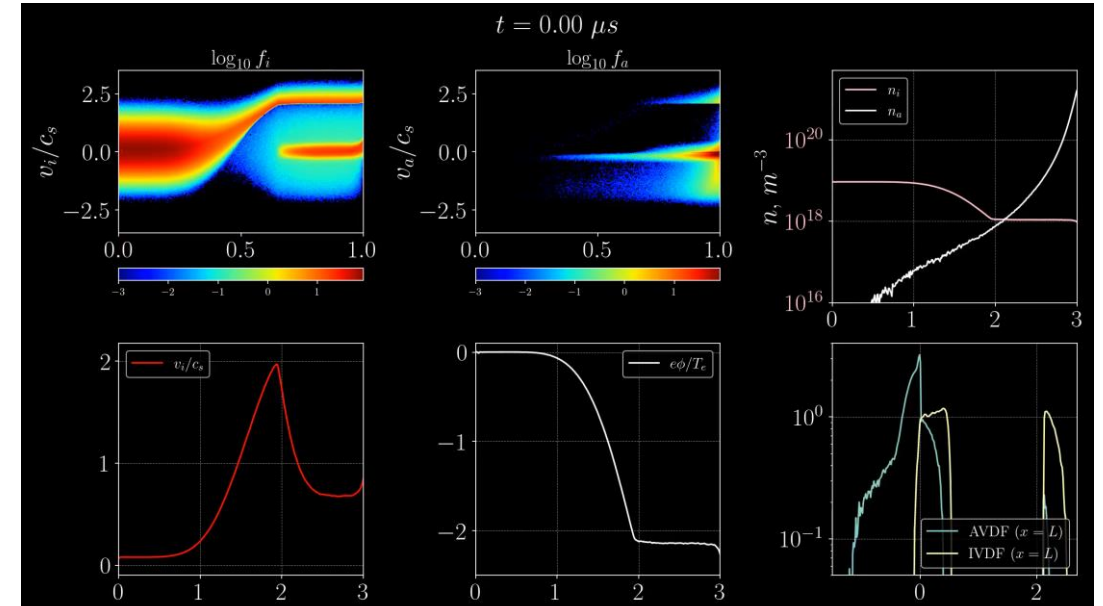
Recycling wall in fusion experiments



Large-fraction of cold neutrals--UNSTABLE



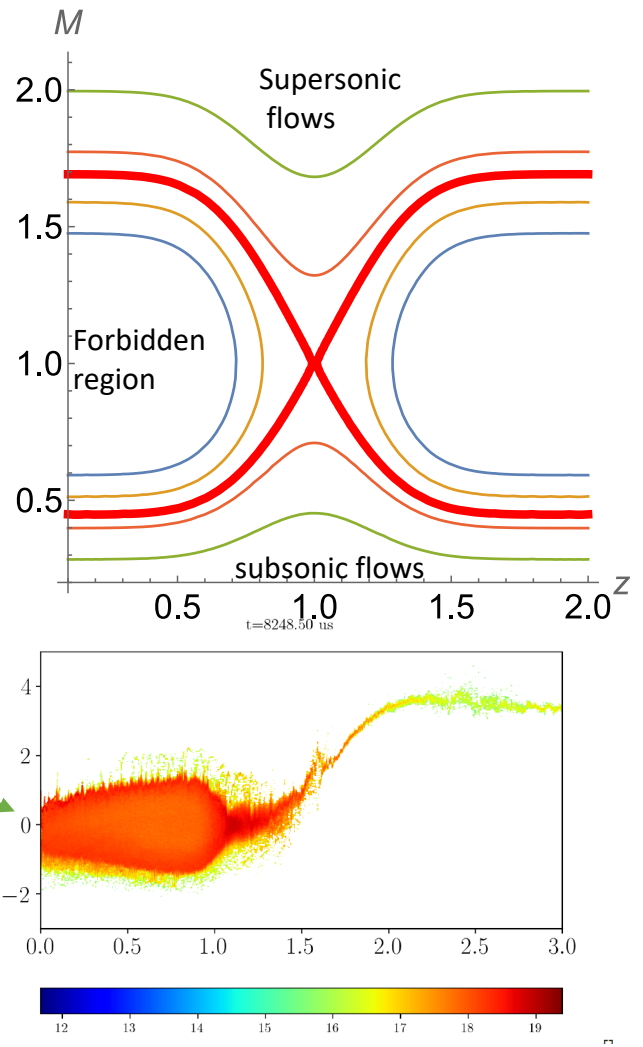
Low fraction of cold neutrals -- STABLE



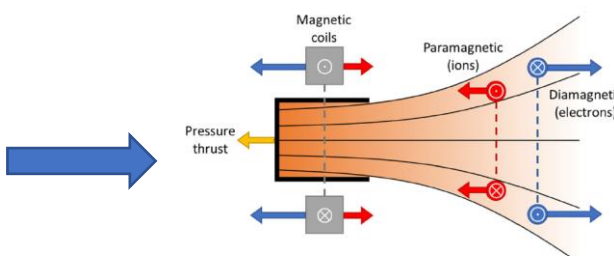
An example in the context of the recycling wall divertor

Summary

- Unique accelerating solution is structurally stable
- Supersonic laminar flows are stable
- Wave breaking and instabilities in multivalued region
- Subsonic solutions are unstable, instabilities?
- Reflection and instabilities force plasma flow into a unique accelerating solution, provide matching to the source region
- Facility effects due to interactions with neutrals
- Caveats:
 - Boltzmann electrons, electron pressure anisotropy and trapping bring additional physics
 - Quasi 1D paraxial model, no diamagnetic effects

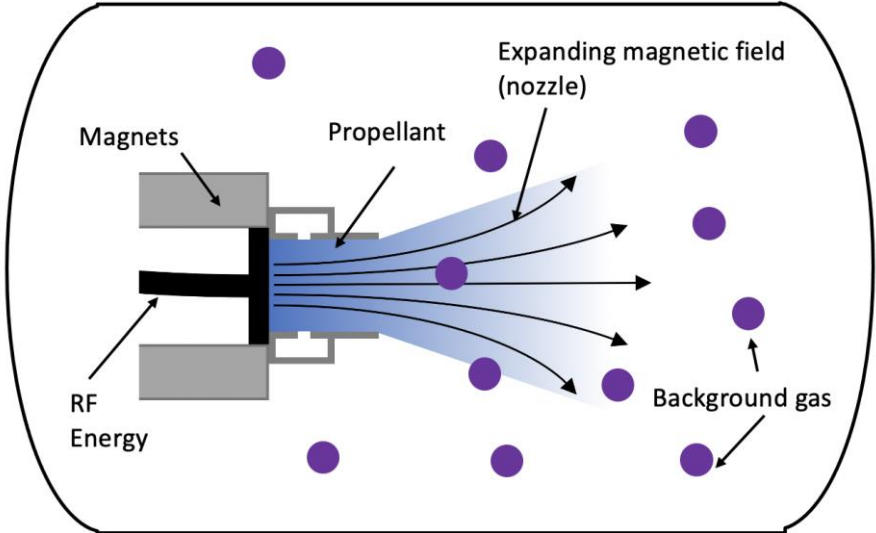


The converging part of the magnetic field region is important, aperture/magnetic field combinations





Pressure-related effects in MNs (B. Jorns)



- Experimental facilities have finite pumping speed. This results in background working gas in the facility that impacts thruster operation.
- Unlike in Hall thrusters where residual gas artificially increases performance, *performance decreases with facility pressure in nozzles*

Known effects in nozzles related to increasing facility pressure

- Thrust efficiency decreases: 9%-3.9% for 5.4 uTorr-9.75 uTorr*
- Plume divergence increases with facility pressure* §
- The location of the “throat” where ion velocity becomes sonic moves**
- The acceleration of ions is depressed†

* T. Vialis, J. Jarrige , and D. Packan, 35th Int. Electric Propulsion Conf. (Atlanta, GA). 2017

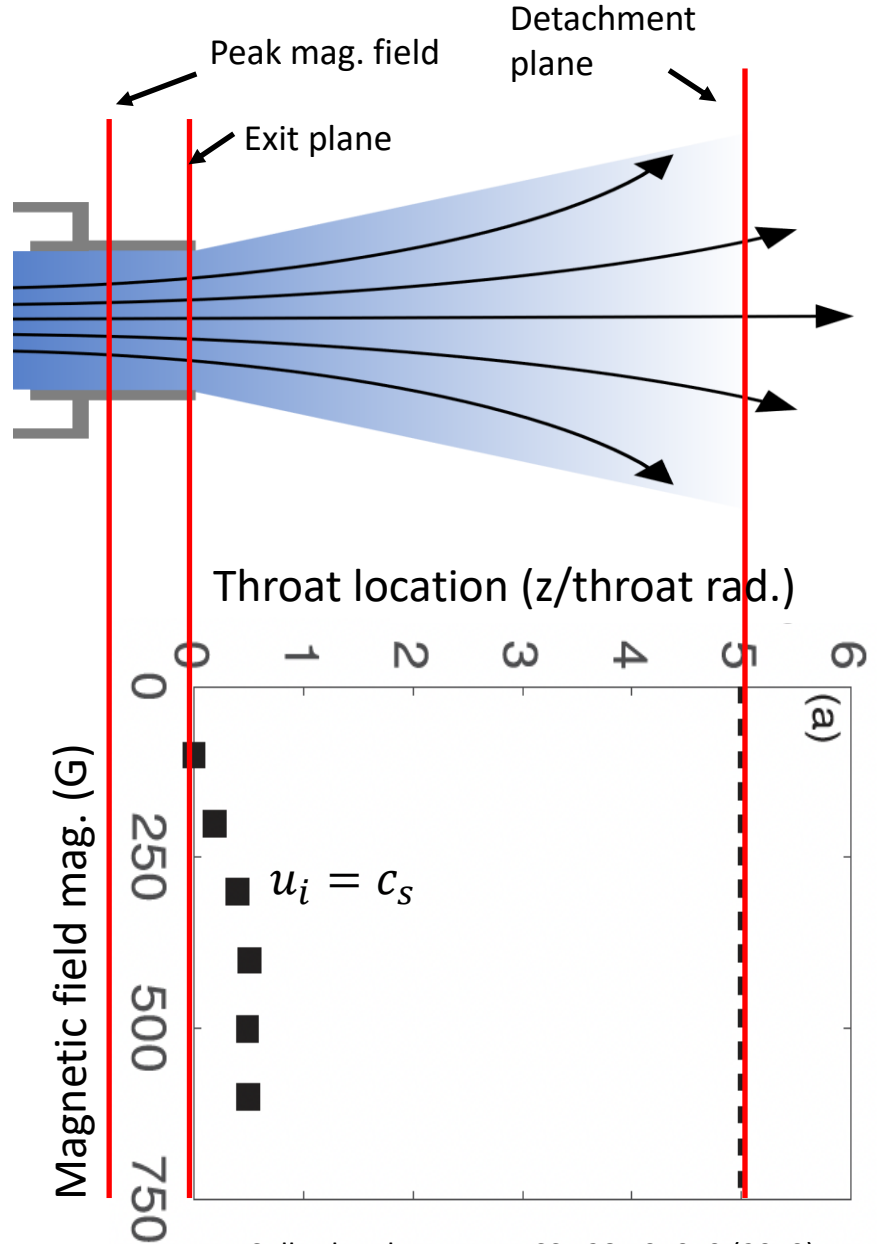
§ N. Caruso and M. Walker, J. Propul. Power. 34 58–65, 2018

**T. Collard and B. Jorns, PSST 28 105019 (2019)

† B. Wachs and B. Jorns, PSST 29 045002 (2020)



Pressure-related effects in MNs: movement of throat



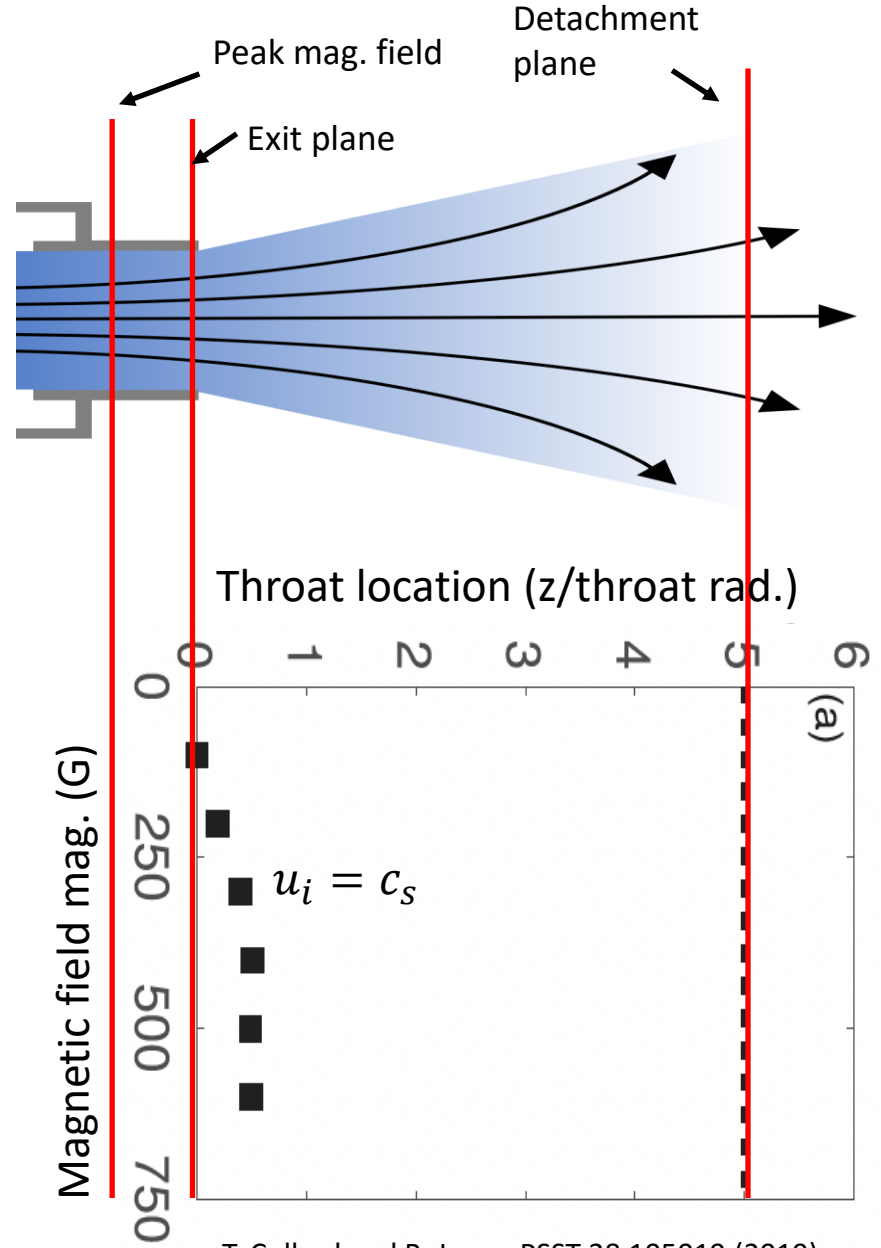
| | |
|-------------------|------------------------------------|
| Source | Inductive (13.56 MHz) |
| Gas | Xenon (3 mg/s) |
| Power | 170 W (Forward) |
| Source dimensions | 1.25 cm (radius) x 1.9 cm (length) |

Approach: experimental measurements of spatial distribution of ion velocity (LIF) and electron temp (Langmuir probe)

Major finding: Location of the throat, defined as point where ions become sonic, is not co-located with position of maximum magnetic field or thruster exit plane.



Pressure-related effects in MNs: movement of throat



| | |
|-------------------|------------------------------------|
| Source | Inductive (13.56 MHz) |
| Gas | Xenon (3 mg/s) |
| Power | 170 W (Forward) |
| Source dimensions | 1.25 cm (radius) x 1.9 cm (length) |

Approach: experimental measurements of spatial distribution of ion velocity (LIF) and electron temp (Langmuir probe)

Major finding: Location of the throat, defined as point where ions become sonic, is not co-located with position of maximum magnetic field or thruster exit plane.

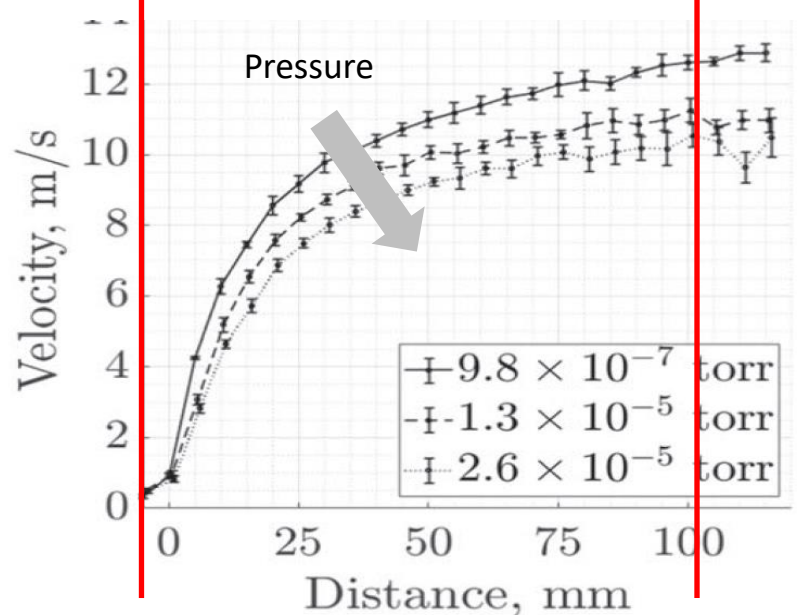
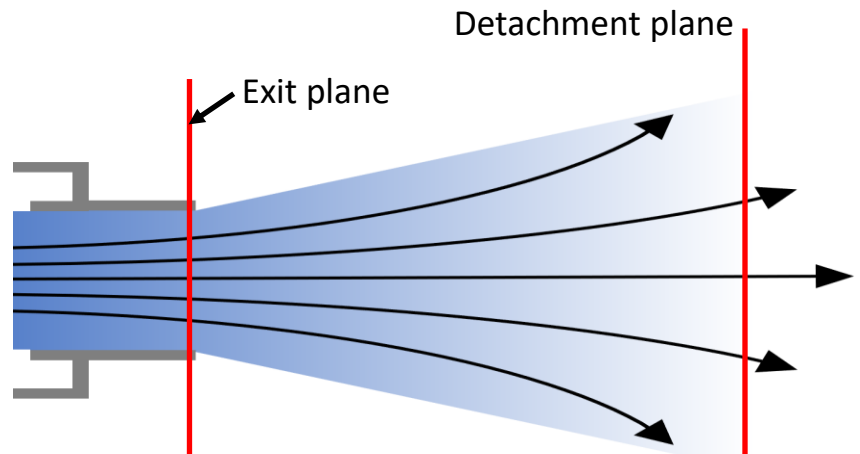
Hypothesis: CEX collisions with neutrals near throat lead to drag on ions, pushing the sonic point downstream.

Supporting evidence: Experimental measurements show anti-correlation between CEX mean free path and location of throat

Implications: For sources with poor ionization fractions or high background pressures, can lower performance (reducing effective expansion ratio). Simulations of real systems should consider neutral population



Pressure-related effects in MNs: ion acceleration



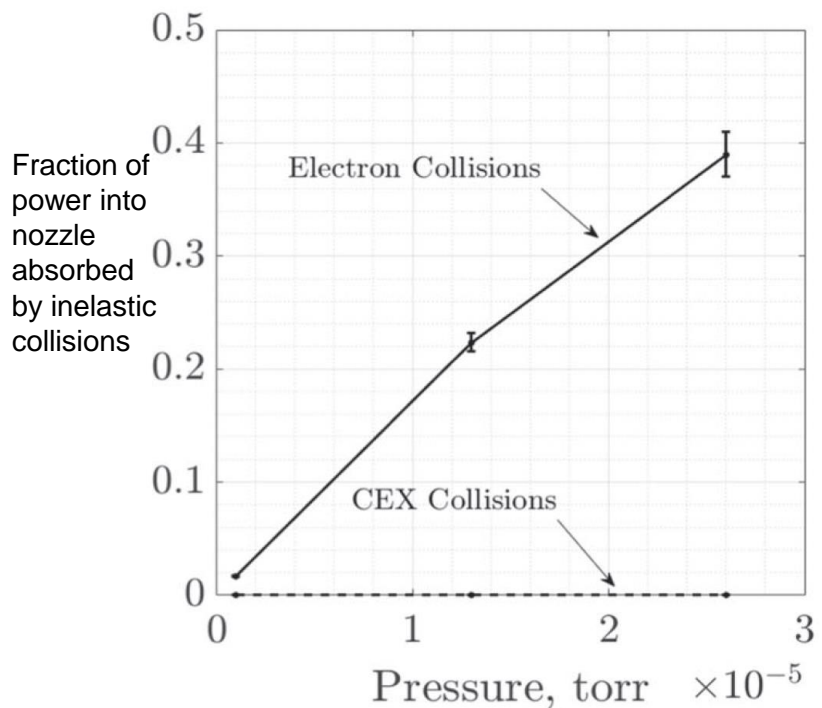
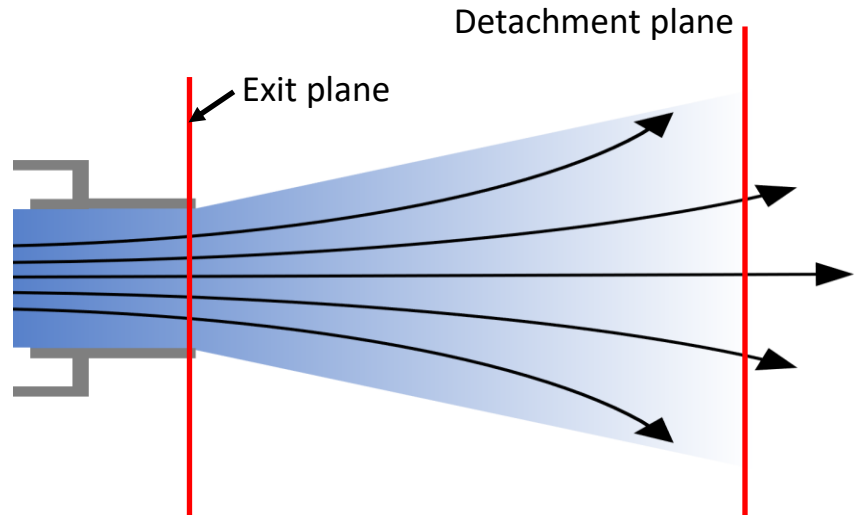
| | |
|-------------------|--------------------------------------|
| Source | ECR (2.4 GHz) based on ONERA design* |
| Gas | Xenon (1 sccm) |
| Power | 20 W (Forward) |
| Peak B | 859 G |
| Source dimensions | 1.25 cm (radius) x 2 cm (length) |

Approach: experimental measurements of spatial distribution of ion velocity (LIF) and background pressure

Major finding: Acceleration of ions depressed with increasing facility pressure



Pressure-related effects in MNs: ion acceleration



| | |
|-------------------|--------------------------------------|
| Source | ECR (2.4 GHz) based on ONERA design* |
| Gas | Xenon (1 sccm) |
| Power | 20 W (Forward) |
| Peak B | 859 G |
| Source dimensions | 1.25 cm (radius) x 2 cm (length) |

Approach: experimental measurements of spatial distribution of ion velocity (LIF) and background pressure

Major finding: Acceleration of ions depressed with increasing facility pressure

Hypothesis: Inelastic collisions of electrons with ambient neutrals absorbs power

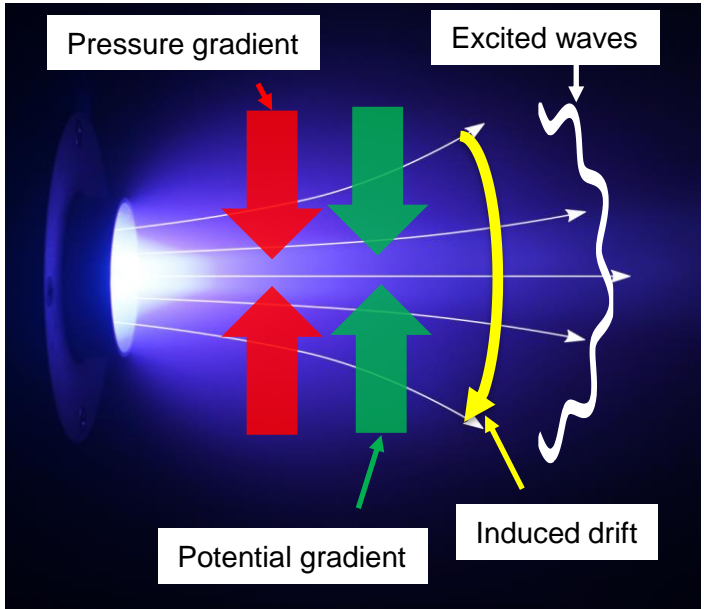
Supporting evidence: 0D scaling law accounting for power absorption matches trends in change in ion velocity

Implications: Facility pressure critical for accurate testing. May be possible to extrapolate, however, from measurements.

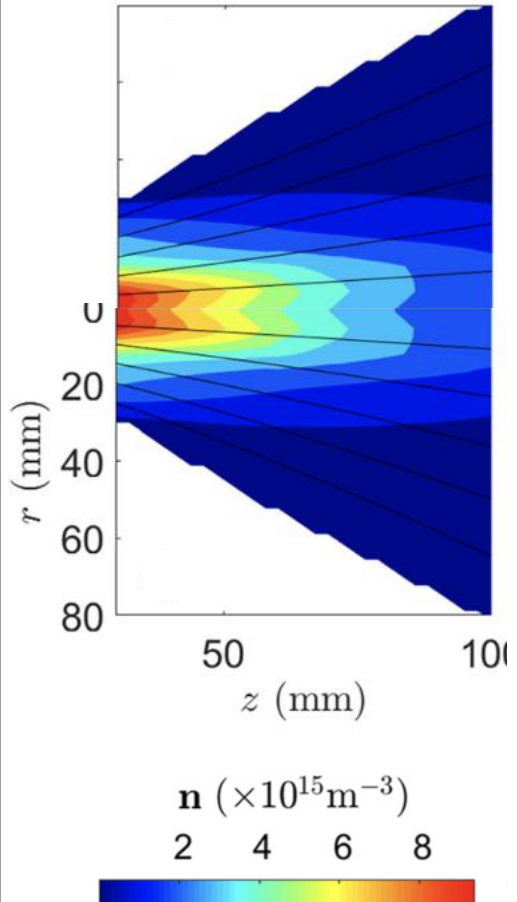


Oscillations and instabilities in MNs

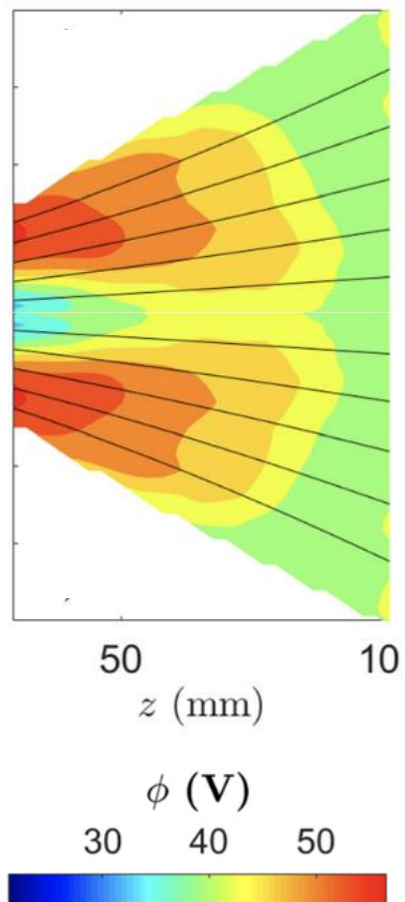
ECR nozzle



Plasma density



Plasma potential

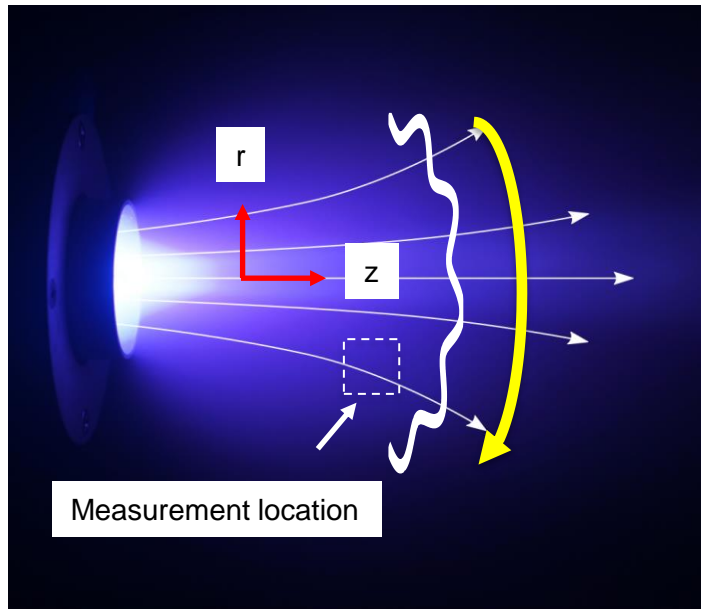


- Gradients in magnetic nozzles can lead to strong azimuthal drifts.
- These can serve as energy source for instabilities



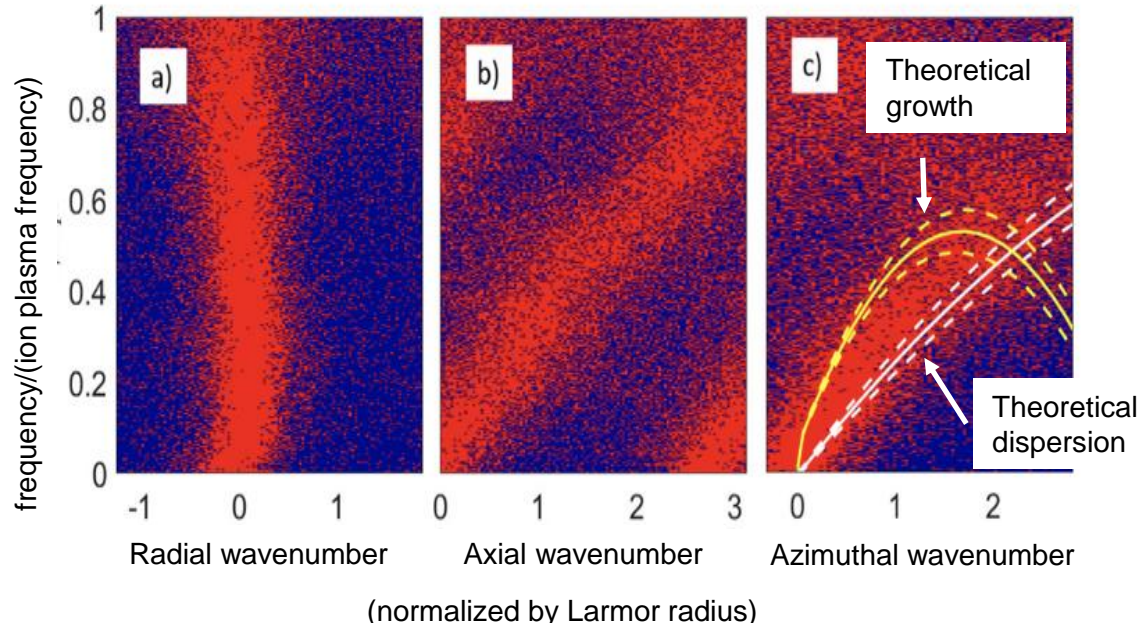
Oscillations and instabilities in MNs

ECR nozzle



| | |
|-------------------|--------------------------------------|
| Source | ECR (2.4 GHz) based on ONERA design* |
| Gas | Xenon (2 sccm) |
| Power | 17 W (Forward) |
| Peak B | 859 G |
| Source dimensions | 1.25 cm (radius) x 2 cm (length) |

Experimental measurements of plasma dispersion

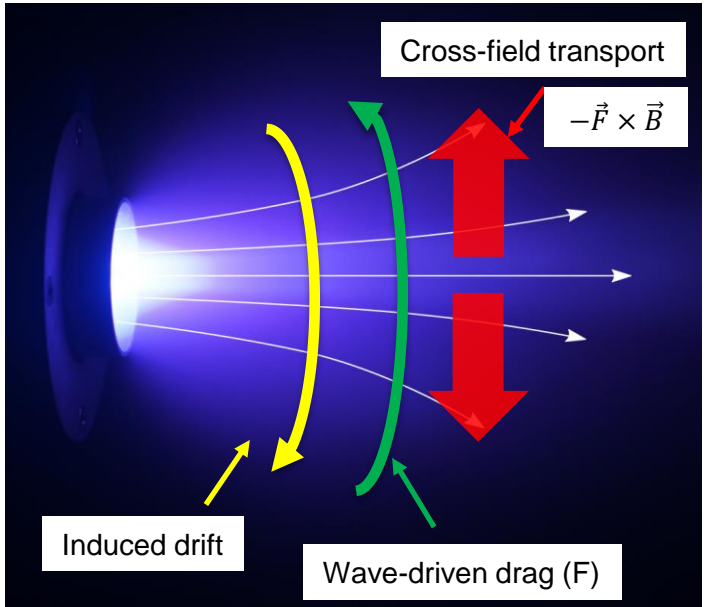


- Experimental measurements show evidence of a **lower hybrid drift instability** induced in plume of magnetic nozzle
- Spectrum observed at nearly all locations



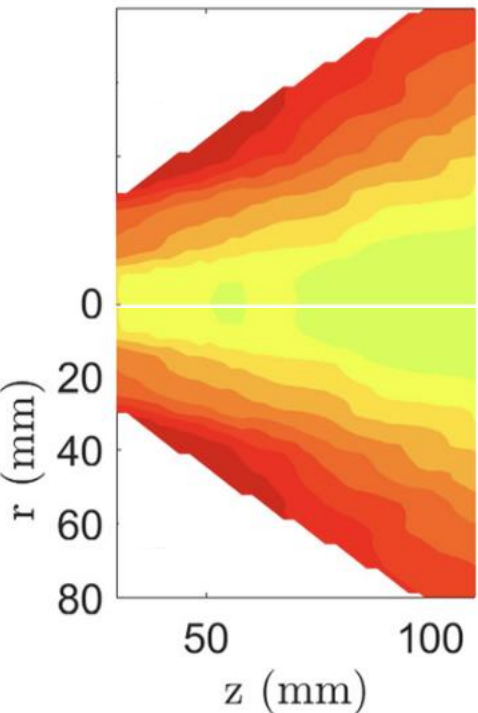
Oscillations and instabilities in MNs

ECR nozzle

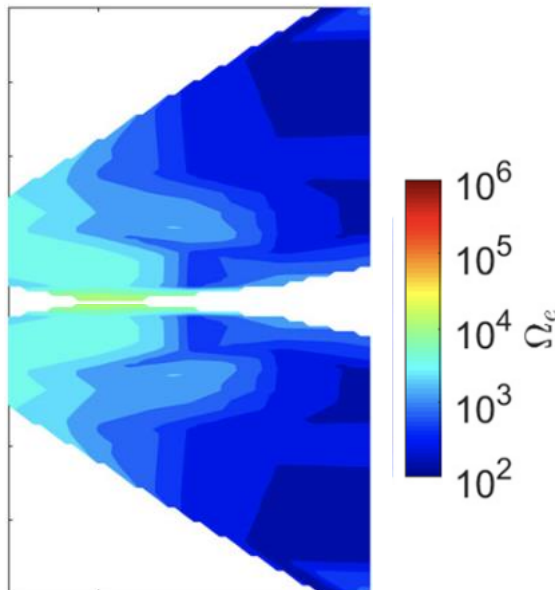


- Cross-field transport is in divergent direction, leading to electrons that flow radially outward
- This mechanism cannot explain convergent detachment that must occur downstream but does show that waves can be major driver of plasma dynamics

Classical Hall parameter



Anomalous Hall parameter

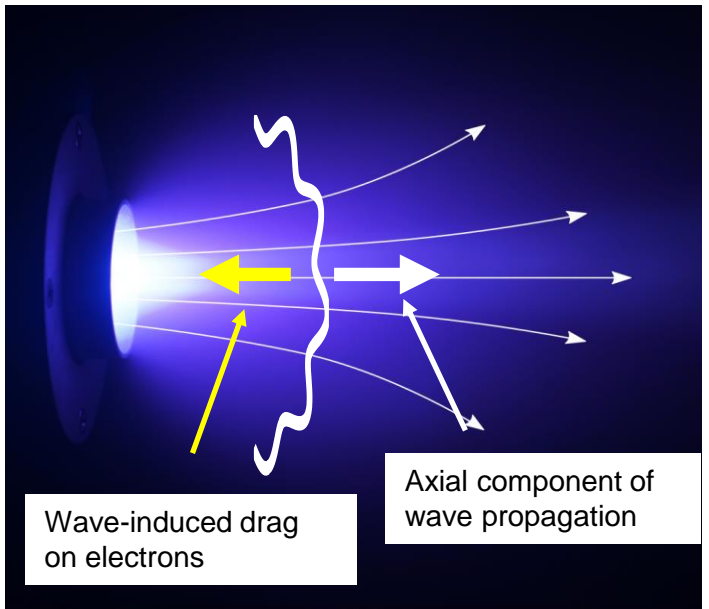


- Growth of waves leads to an effective drag on the electron drift. This can be approximated as an effective collision frequency
- Using quasi-linear, found that presence of LHDI can increase collision frequency in plasma by 1000. This can lead to cross-field transport
- **Major implication: anomalous resistive effects may have an impact on electron detachment**



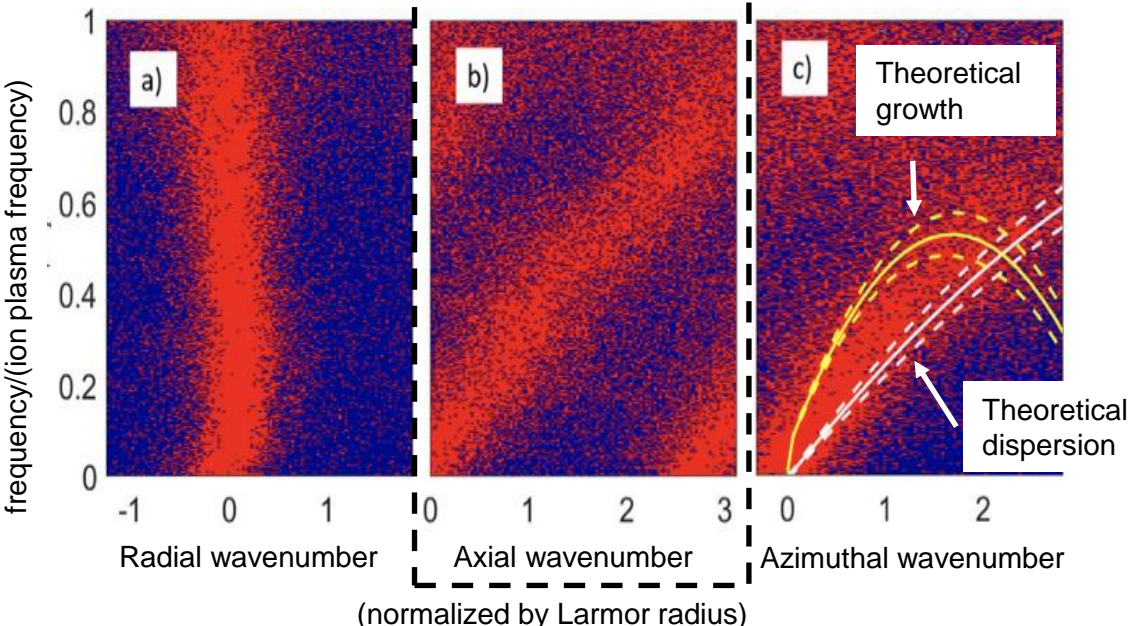
Oscillations and instabilities in MNs

ECR nozzle



- Lower hybrid drift instability also has an axial component along field lines during propagation.
- From QL theory, this also can lead to an anomalous drag on electrons in parallel direction and thus an enhanced effective collision frequency

Experimental measurements of plasma dispersion



QL theory to measure wave-driven collision frequency

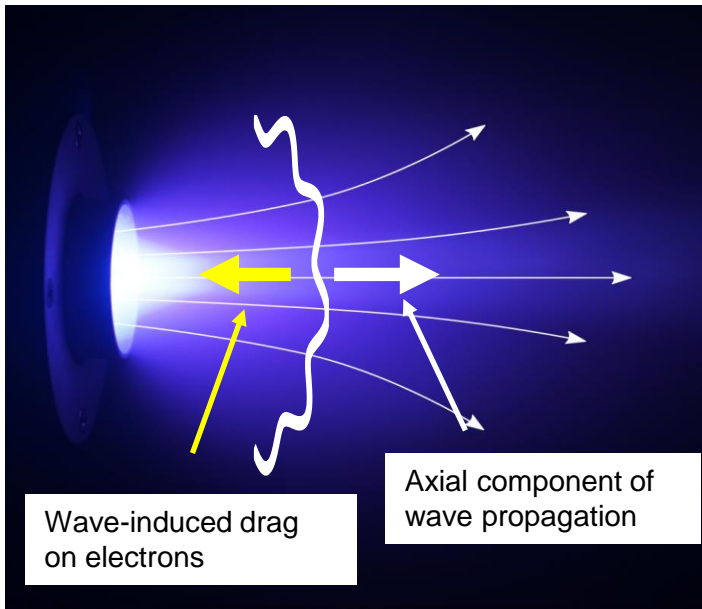
Substitute anom. collision frequency into Fourier law for heat conduction

Estimate heat flux and polytropic index



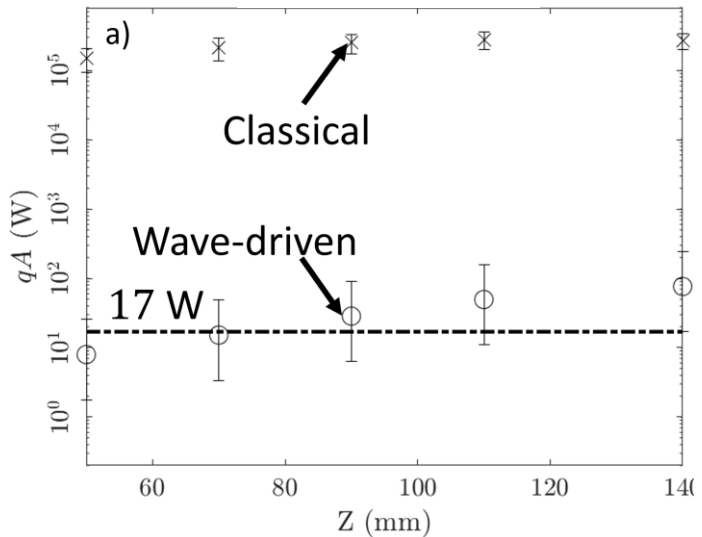
Oscillations and instabilities in MNs

ECR nozzle (17 W)

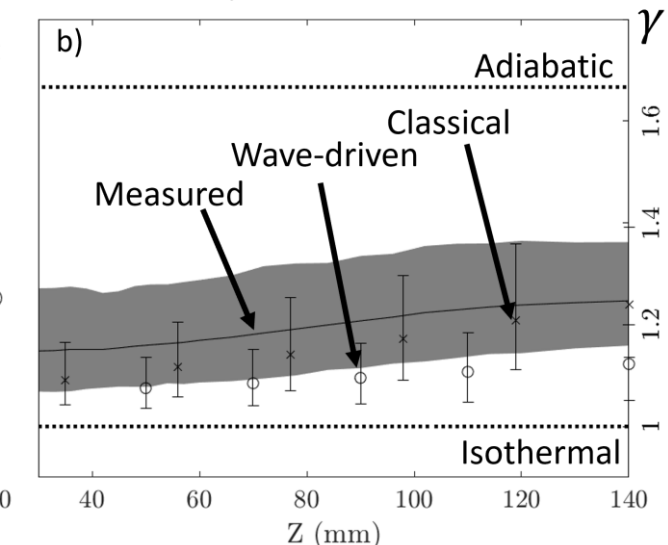


Major implication: including wave-driven heat flux may in part explain the electron cooling in ECR magnetic nozzle

Heat flux (W)



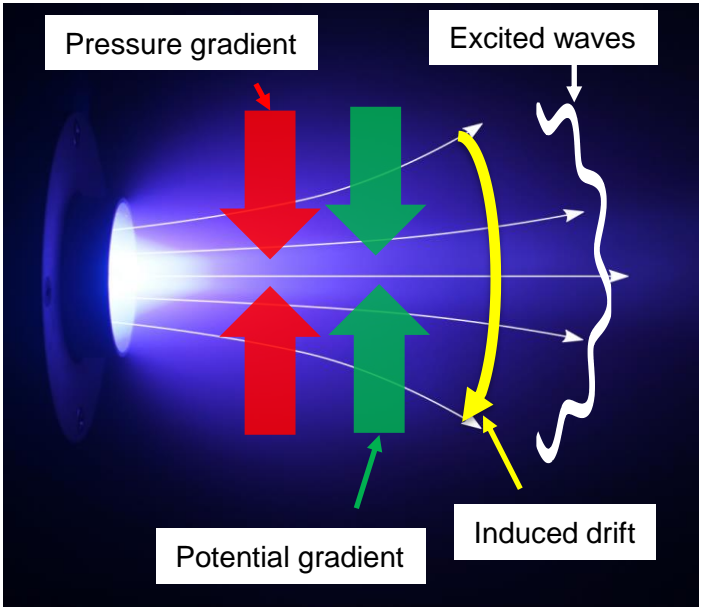
Polytropic index





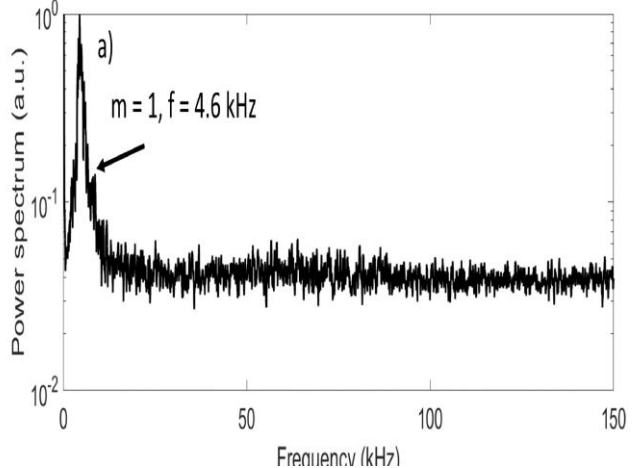
Oscillations and instabilities in MNs

ECR nozzle

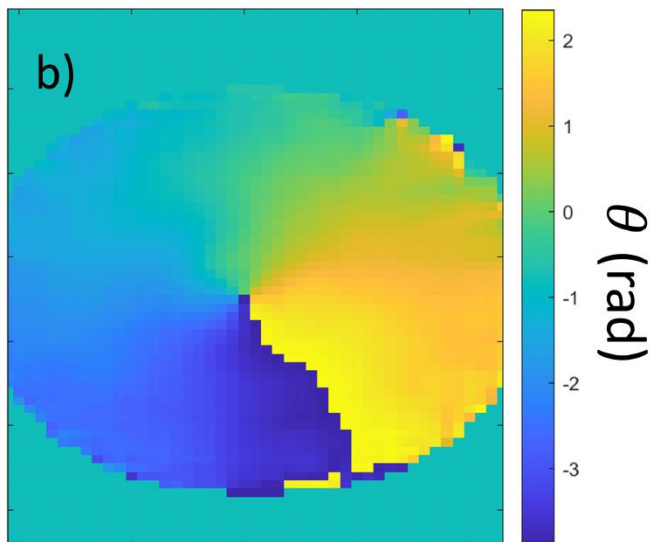


- High speed imaging and probes also show a low frequency rotating wave with large amplitude (~50% background)
- Dispersion is consistent with an anti-drift wave.
- May also be connected to convergent detachment

Power spectrum from high-speed imaging

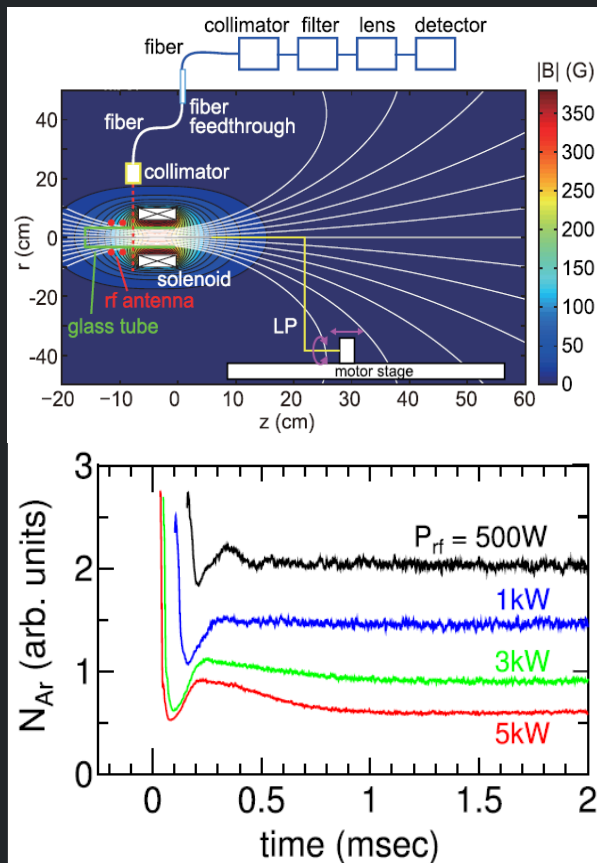


Cross-correlation analysis showing $m = 1$ mode

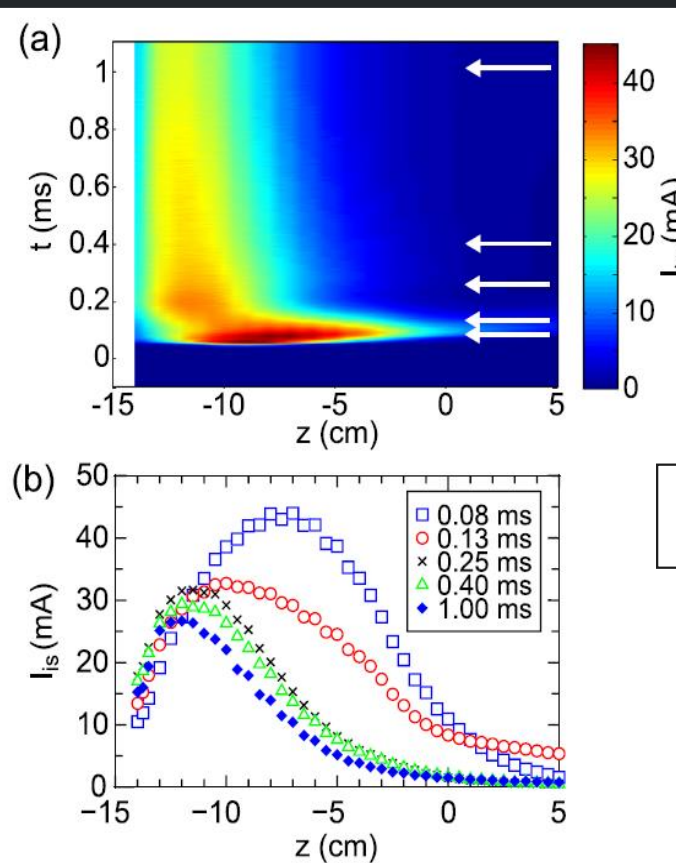


Neutral depletion effect in a high-power helicon thruster

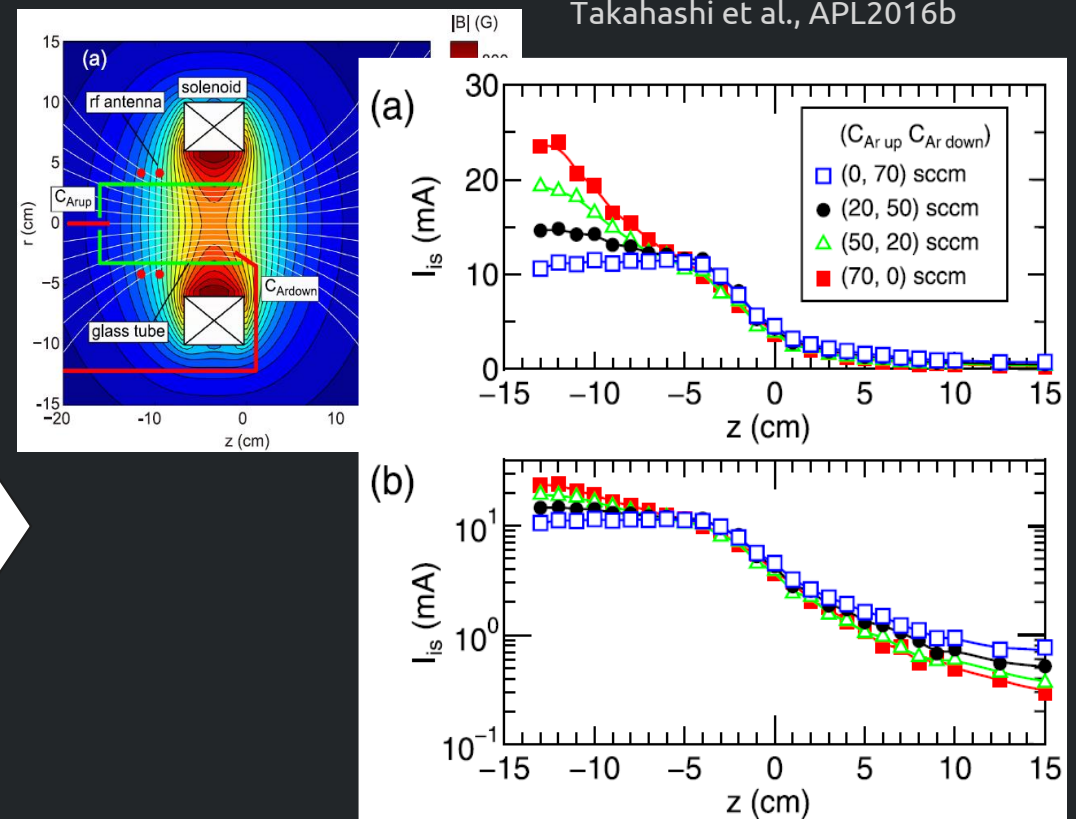
Takahashi et al., APL2016a



Neutrals are depleted in the source, resulting in the density profile near the back wall and the reduction of the density in the MN.



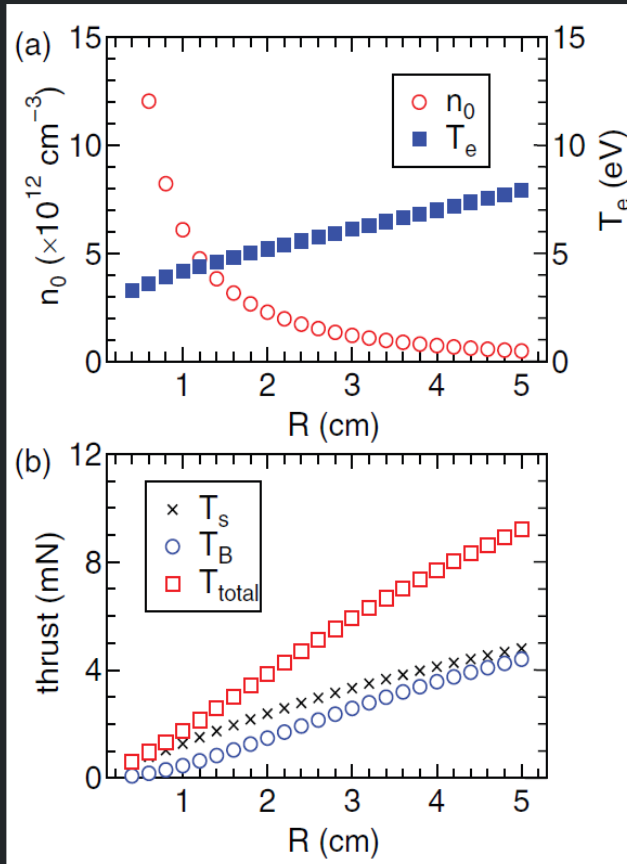
Takahashi et al., APL2016b



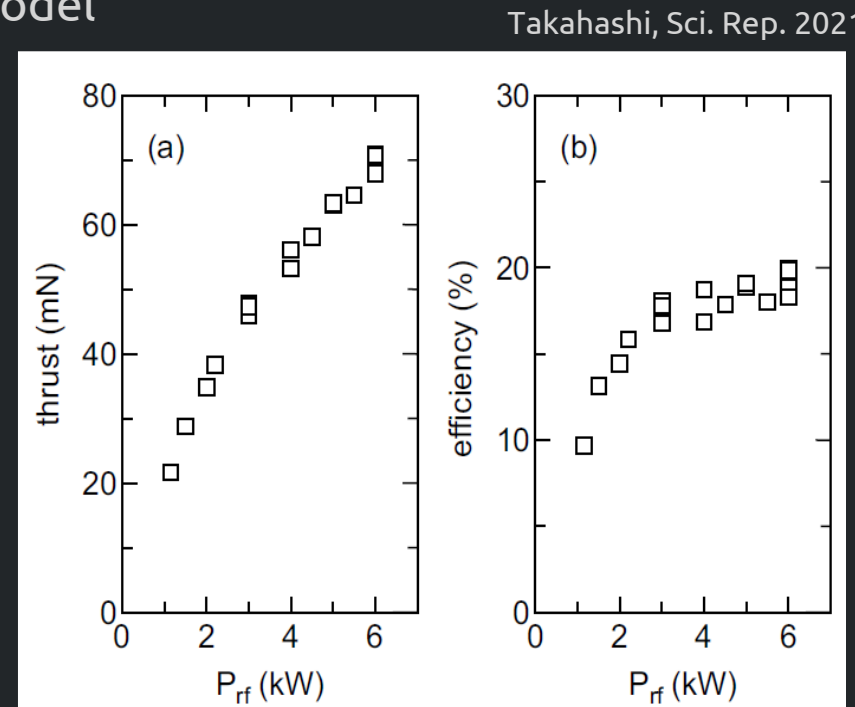
By injecting the propellant near the thruster exit, the upstream density peak (inducing the plasma loss to the wall) can be reduced and then the downstream density increases, providing the larger electron-diamagnetic thrust by the MN.

Advances in the thruster performance (efficiency)

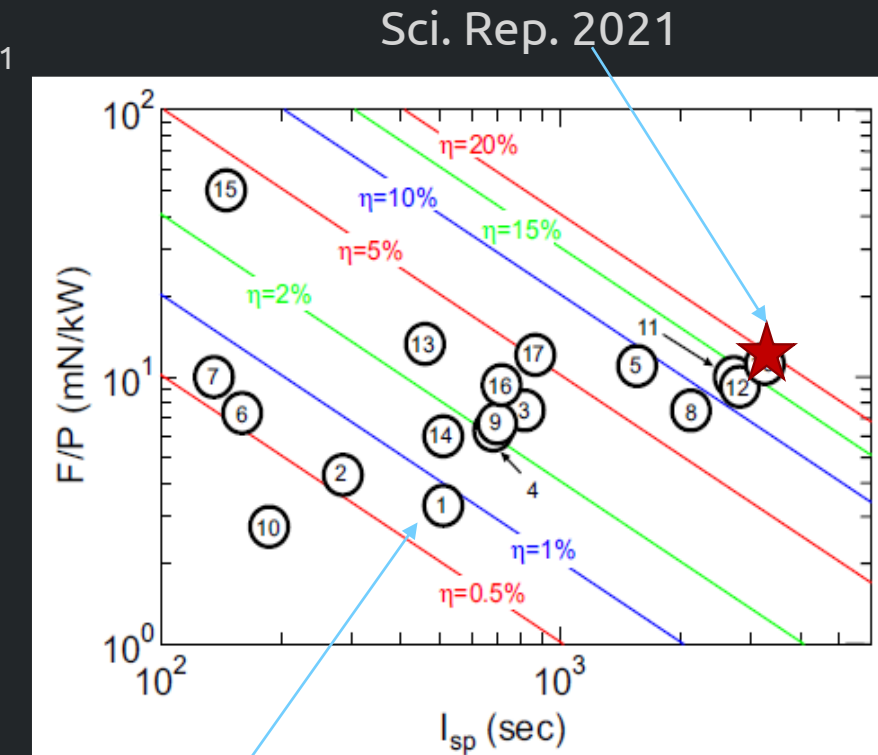
Global source model and 1-D MN model



Large diameter source will give better performance.

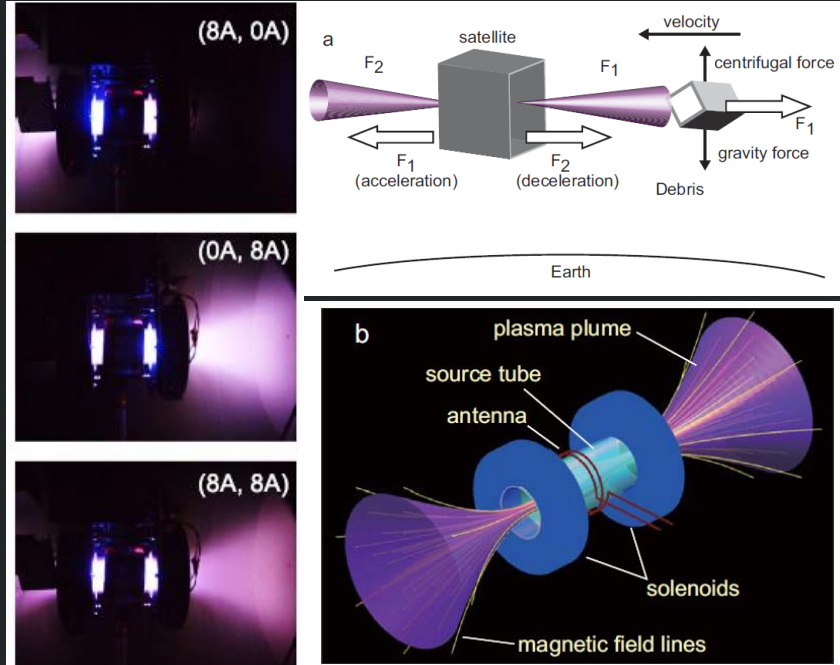


1st thrust measurement (APL2011)

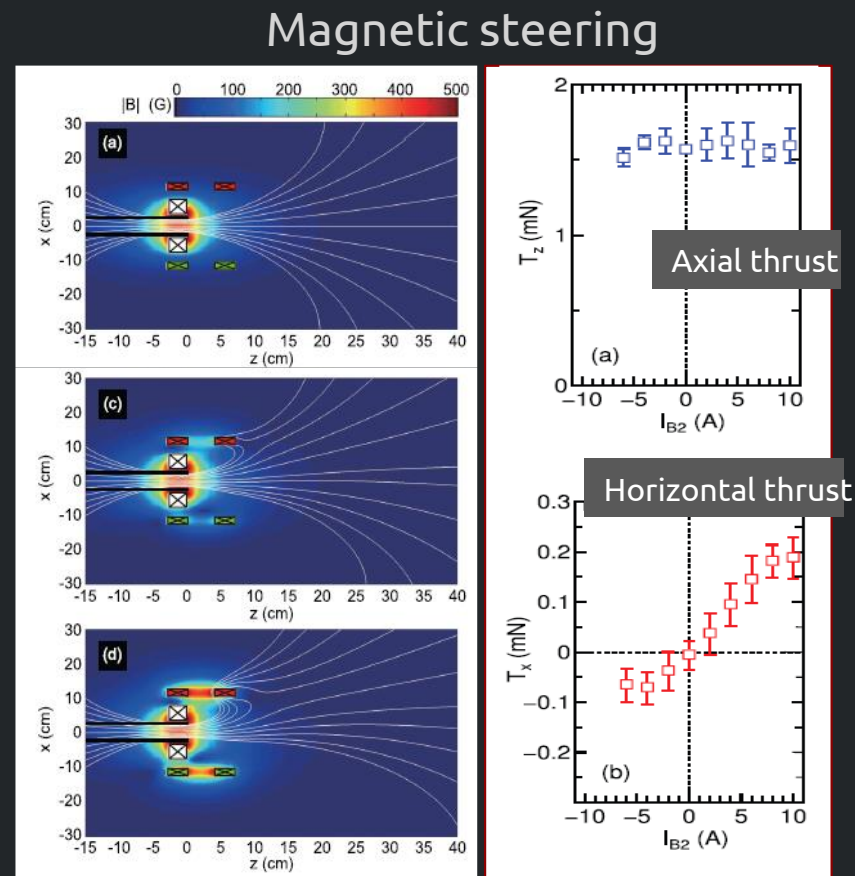


Advances in the thruster performance (controllability)

Active Debris Removal

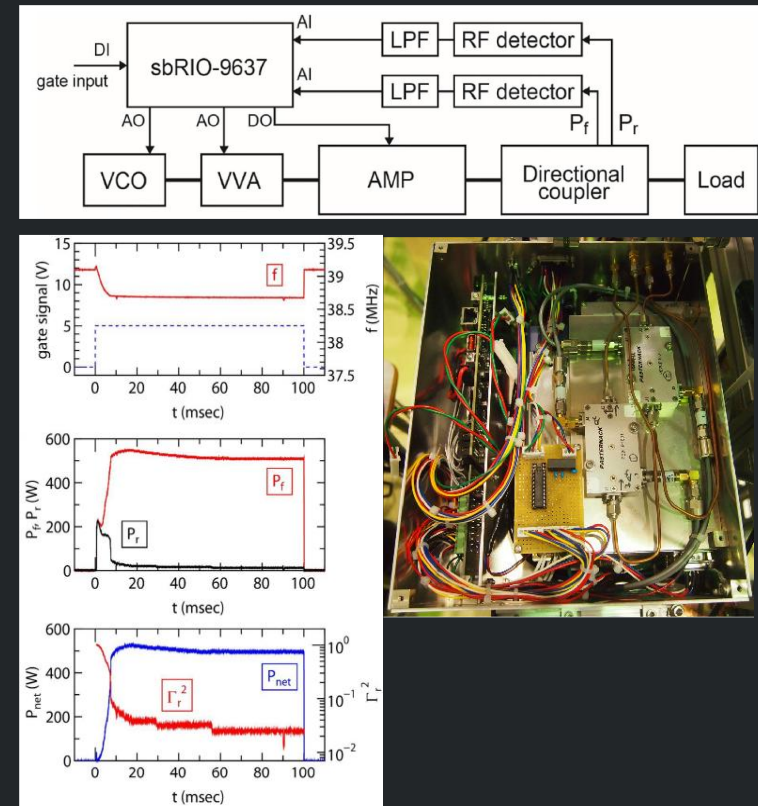


Takahashi, Sci. Rep. 2021



Imai and Takahashi, Appl Phys Lett 2021

Automatic and fast control of frequency-tunable rf matching



Takahashi et al., Front Phys 2020 & 2021

MHD detachment scenario

PHYSICS OF PLASMAS 12, 043504 (2005)

Magnetohydrodynamic scenario of plasma detachment in a magnetic nozzle

Alexey V. Arefiev and Boris N. Breizman

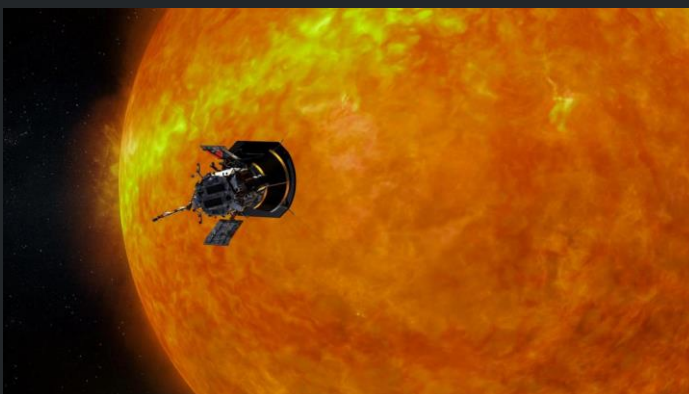
Institute for Fusion Studies, The University of Texas, Austin, Texas 78712

(Received 22 July 2004; accepted 20 January 2005; published online 25 March 2005)

A plasma flow can detach from a spacecraft together with the field lines that become stretched along the flow. This is actually occurring around the Sun.

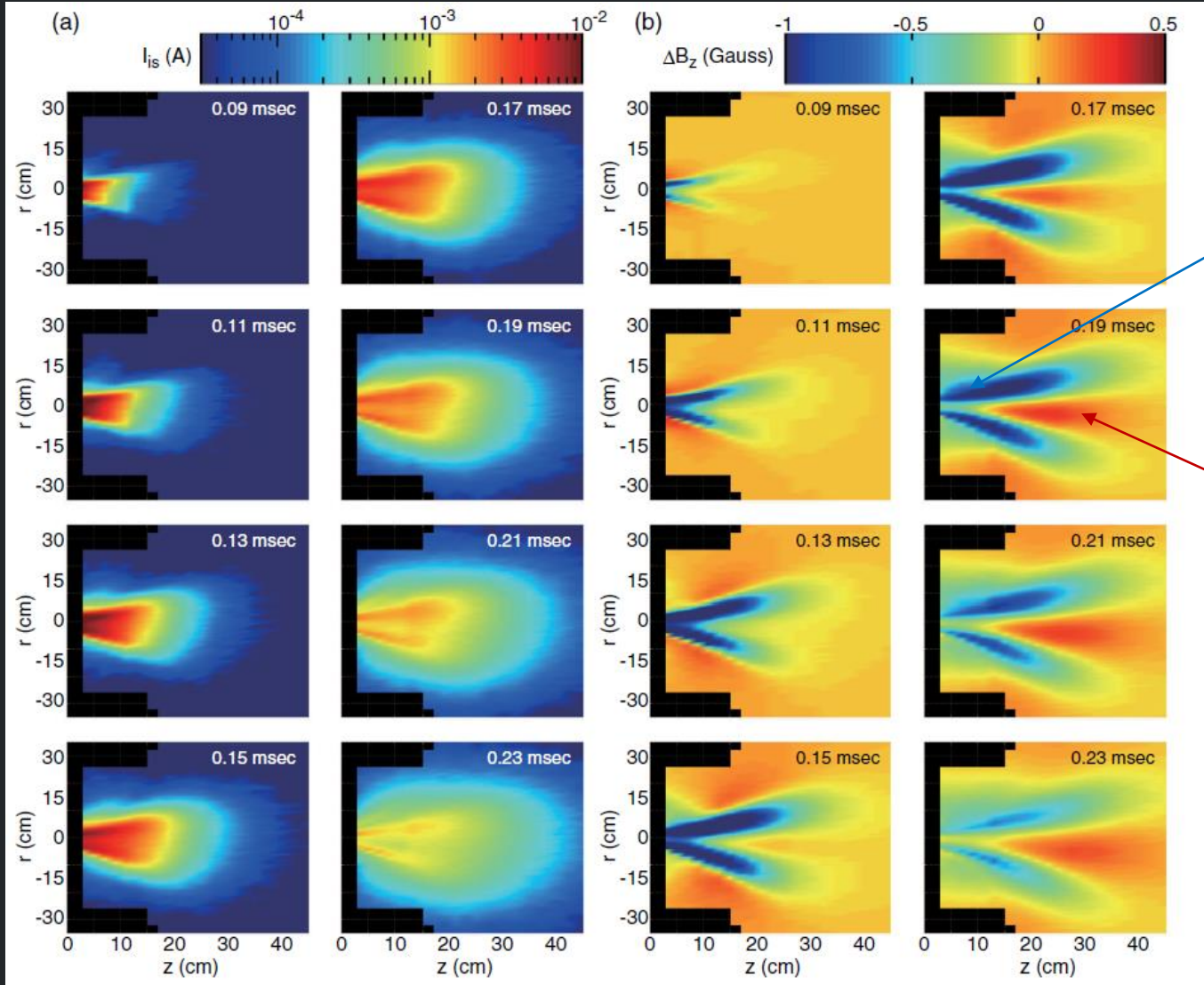
This can occur when the plasma flow energy overcomes the magnetic field energy, corresponding to the case of *super Alfvénic flow* ($M_A = v/v_A > 1$)

$$\frac{1}{2} mn v^2 > \frac{B^2}{2\mu} \rightarrow v > \frac{B}{\sqrt{\mu mn}} = v_A$$



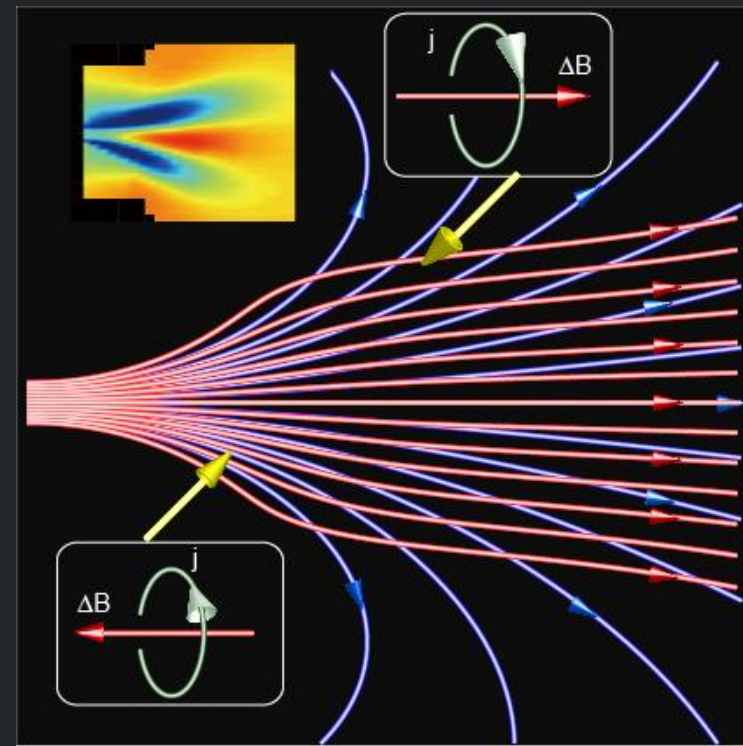
NASA's Parker Solar Probe touch the Alfvén surface ($v=v_A$) recently!
Are there any common physics between the Sun and the MN thruster?
Can the thruster experiment simulate some of Sun's phenomena?

Magnetic field stretch



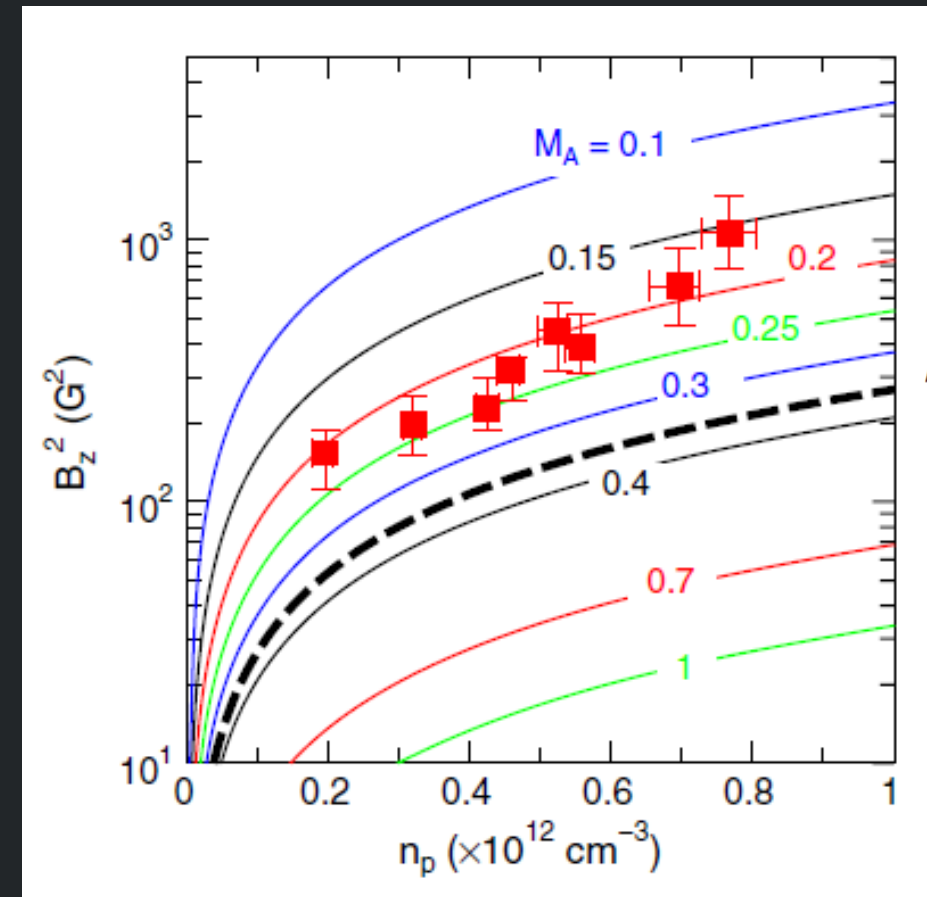
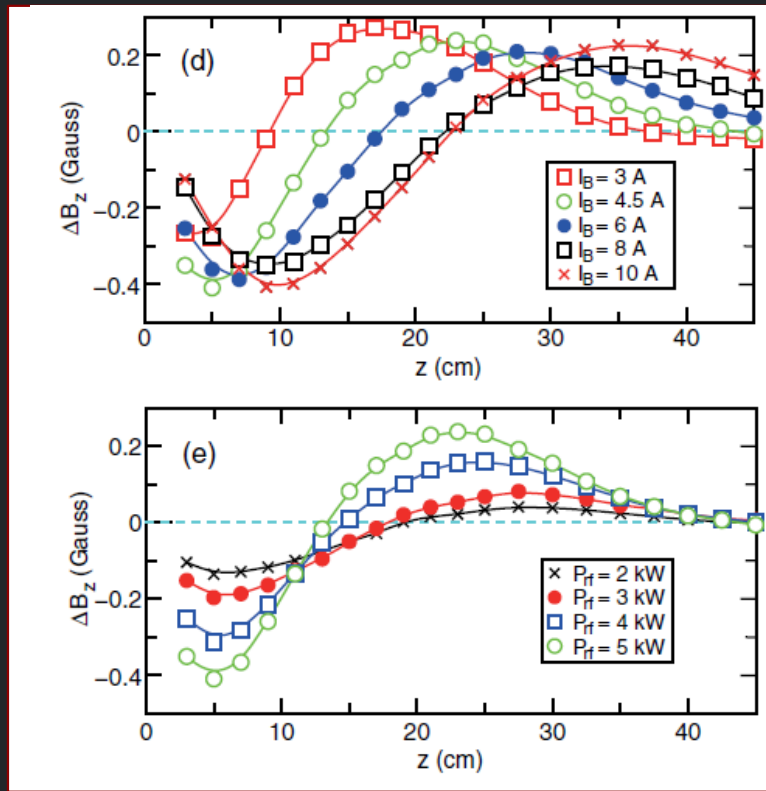
$\Delta B_z < 0$

$\Delta B_z > 0$



The change in the field is only a few percent of the applied field. However, it would be important to understand the flow dynamics in the high-power thruster.

Where does the stretch occur?



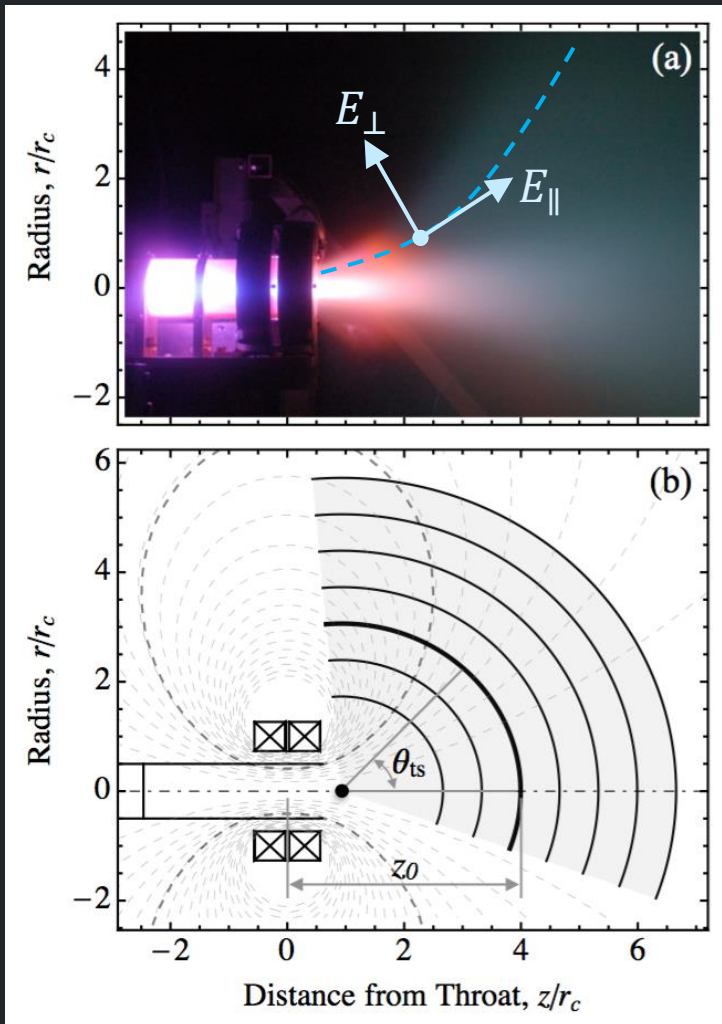
$$\rho(\mathbf{v} \cdot \nabla) \mathbf{v} = -\nabla p - \frac{\nabla B^2}{2\mu} + \frac{(\mathbf{B} \cdot \nabla) \mathbf{B}}{\mu},$$

$$v^2 \sim \frac{1}{2} V_A^2 - C_s^2 = \frac{1}{2} \frac{(B_{vac} + \Delta B)^2}{mn\mu} - C_s^2$$

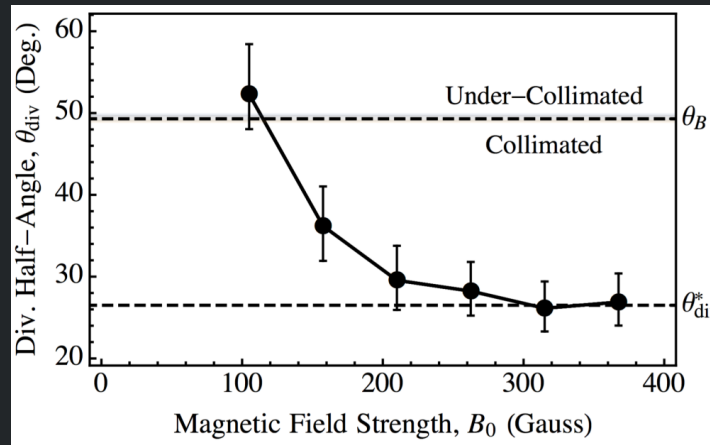
This is the first observation of the stretch of the MN in laboratory plasmas.

The stretch of the magnetic nozzle could occur even if the flow velocity is lower than the Alfvén velocity.

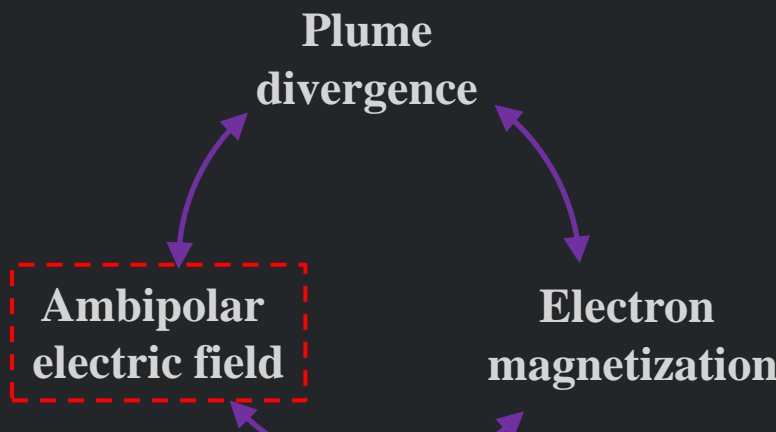
Electron Demagnetization from a Magnetic Nozzle



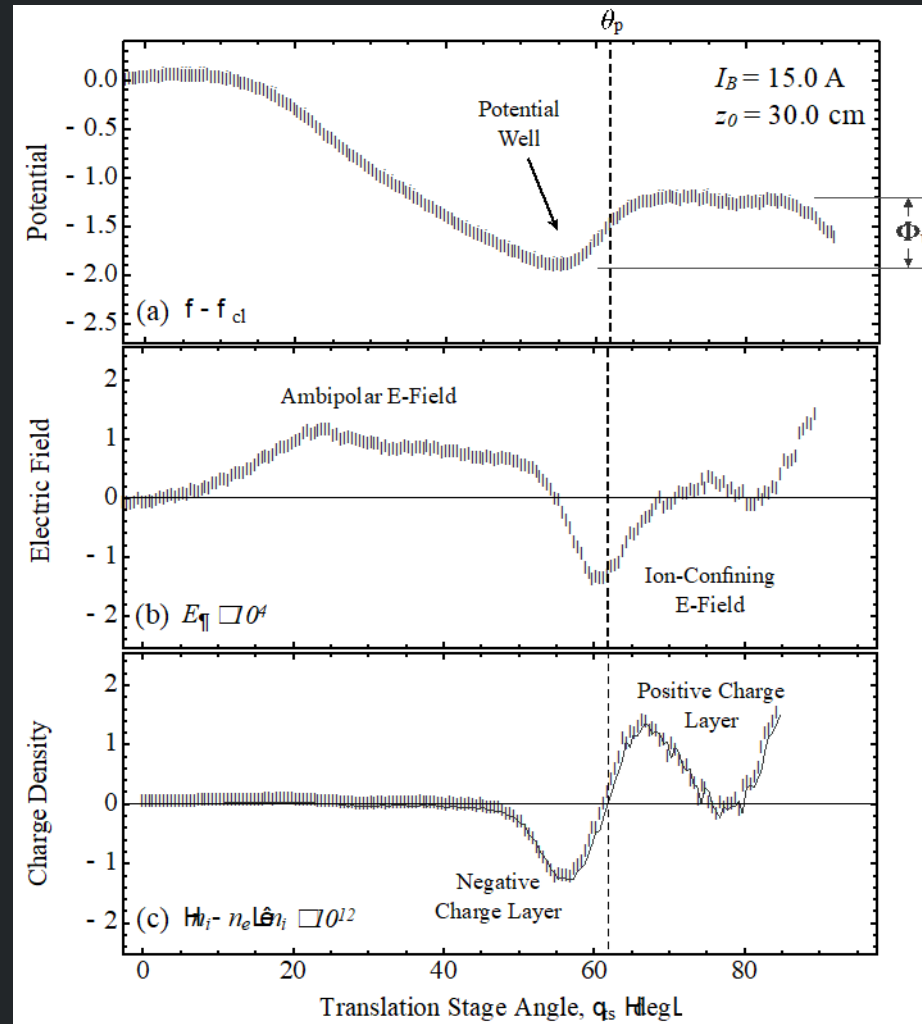
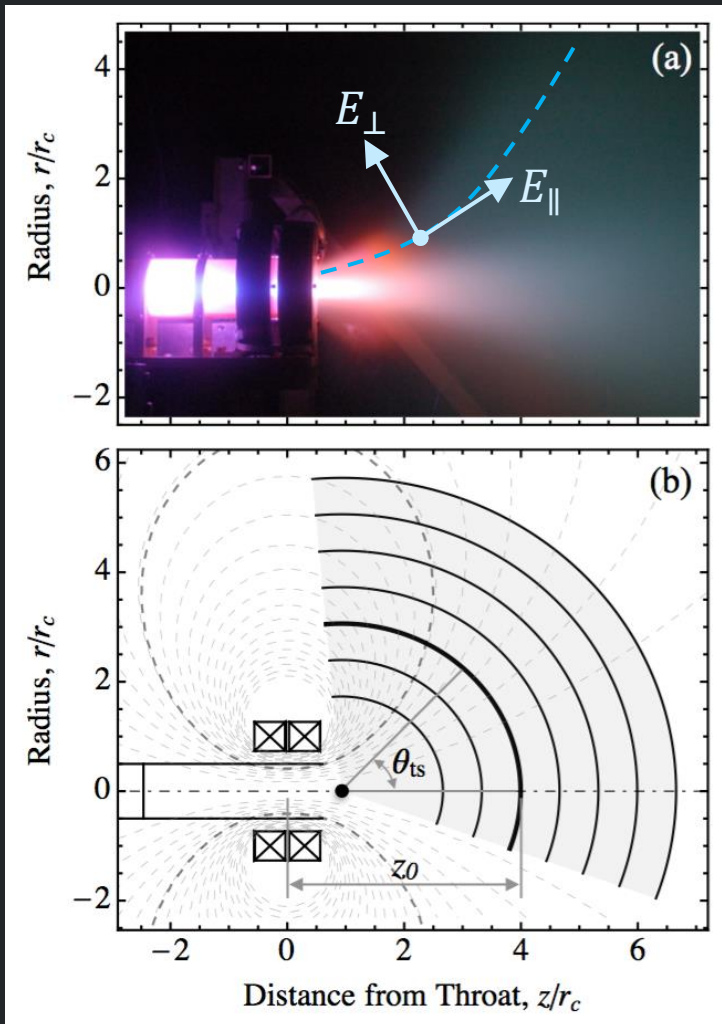
Little and Choueiri, PRL, 2019.



Why does divergence decrease with field strength?

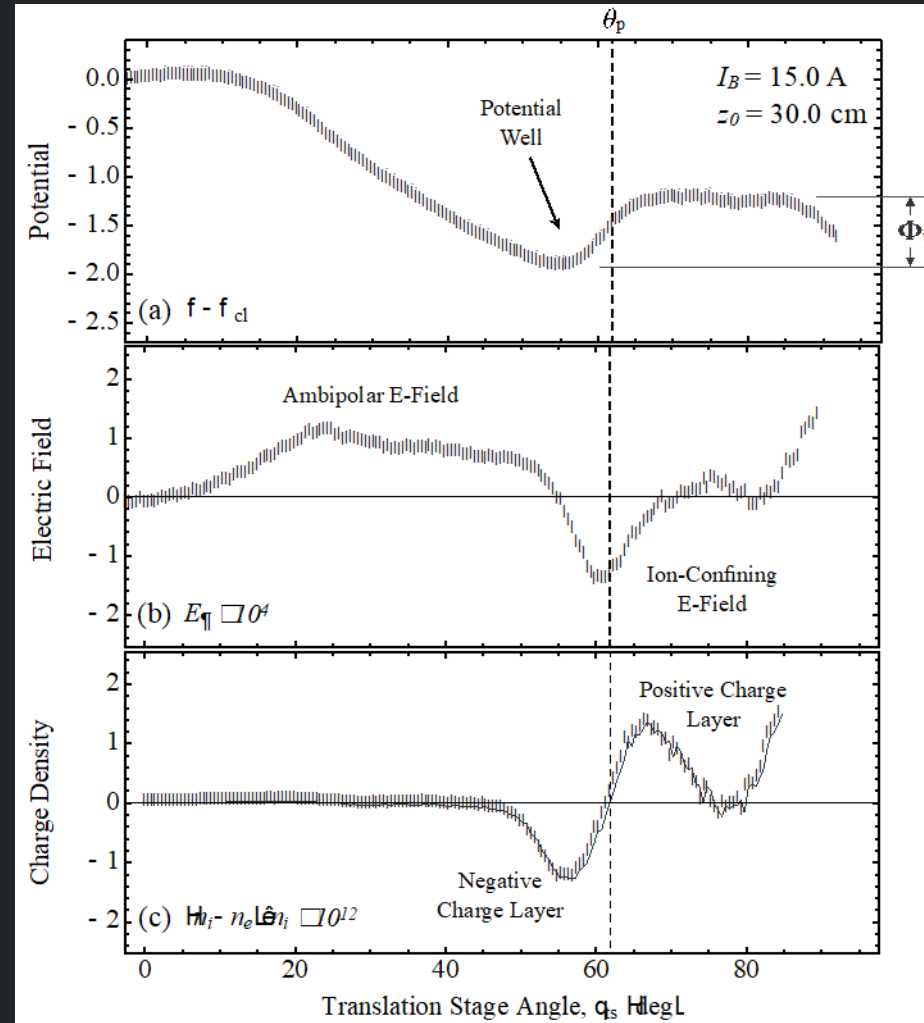
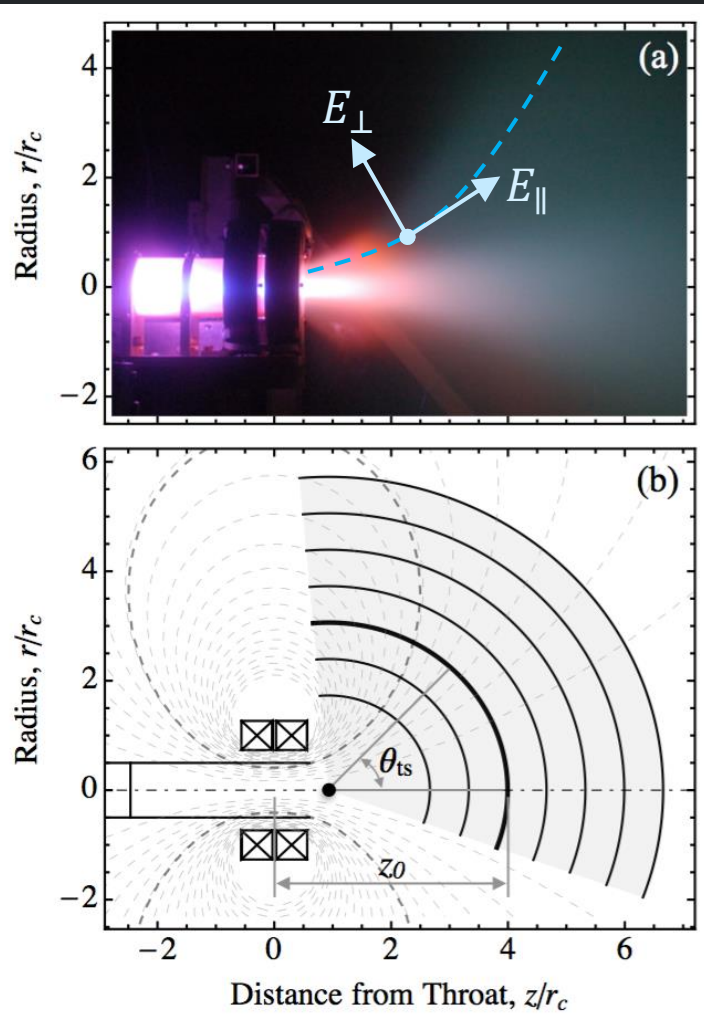


Electron Demagnetization from a Magnetic Nozzle

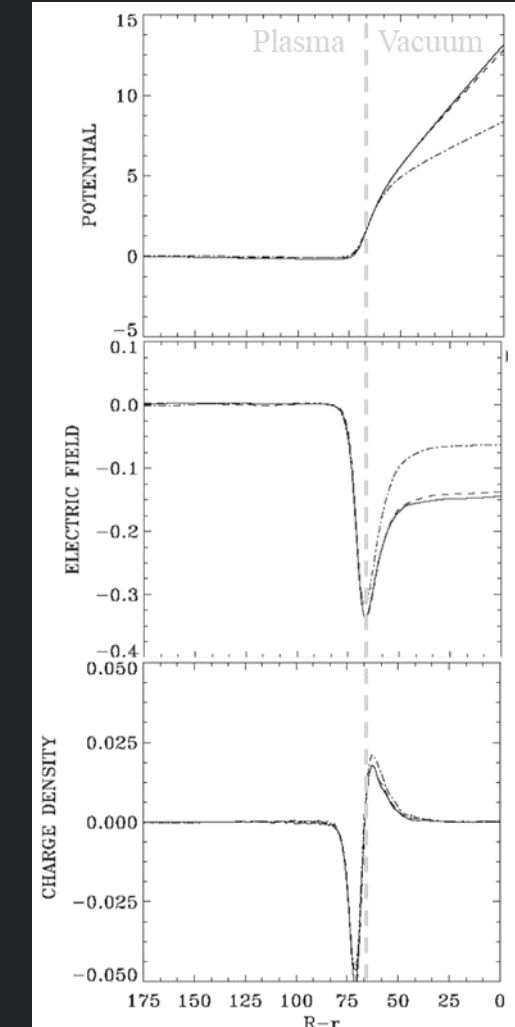


Little and Choueiri, PRL, 2019.

Electron Demagnetization from a Magnetic Nozzle



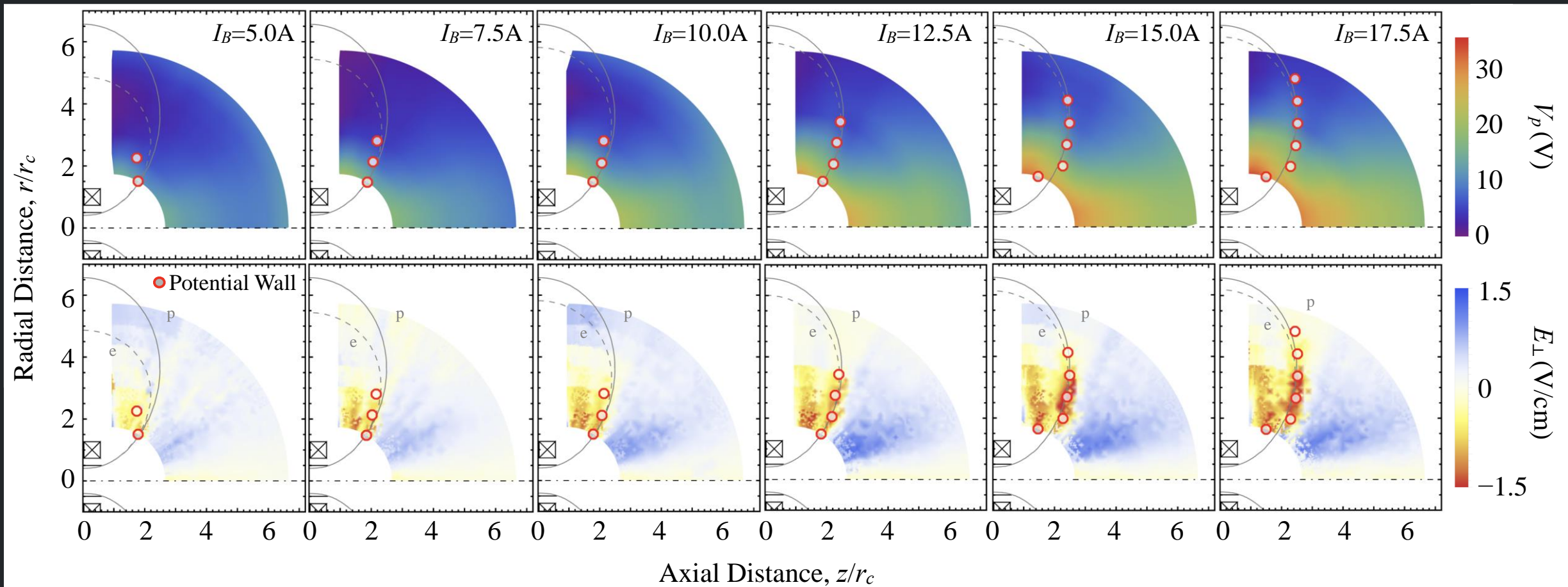
Little and Choueiri, PRL, 2019.



Shoucri, M. Numerical Simulation, 2012.

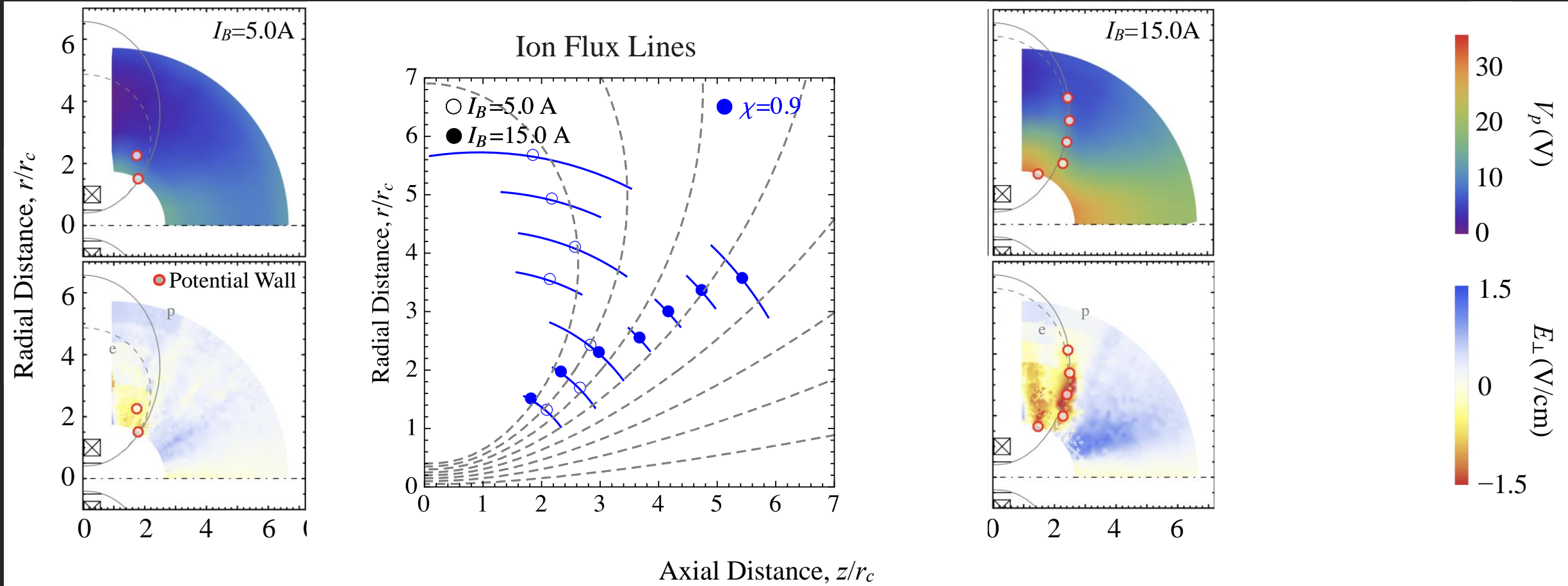
Electron Demagnetization from a Magnetic Nozzle

Little and Choueiri, PRL, 2019.



Electron Demagnetization from a Magnetic Nozzle

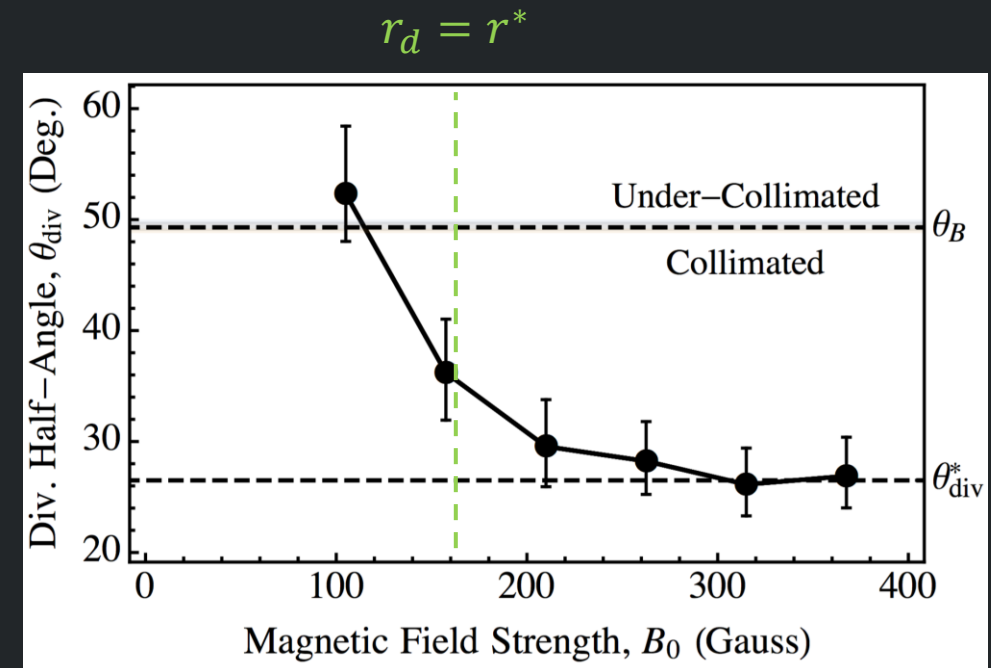
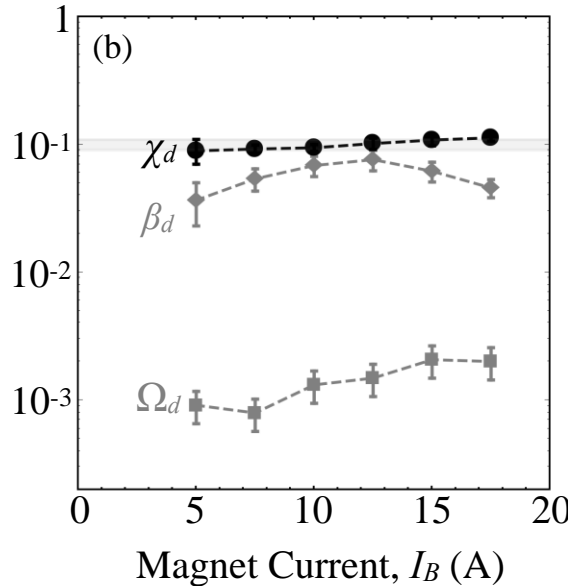
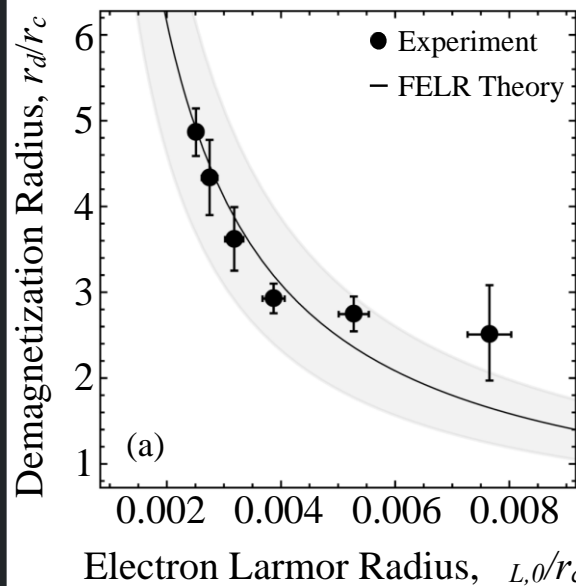
Little and Choueiri, PRL, 2019.



Disappearance of potential wall drives outward expansion of plasma

Electron Demagnetization from a Magnetic Nozzle

Little and Choueiri, PRL, 2019./



$$\chi_d = \rho_{L,e} / l_{\nabla B}$$

Demagnetization when electron Larmor radius
increase to 1/10 x B-gradient length scale

$r_d < r^*$: underexpanded magnetic nozzle

$r_d \gg r^*$: overexpanded magnetic nozzle

r^* = MN turning point

Modeling plasma plume expansions under a geomagnetic field

- Modeling plasma plume expansions in vacuum is essential for:
 - Accurate plasma plume S/C interaction
 - Understanding the physics of **plasma plume current neutralization** in vacuum
 - Correct modeling of plume interaction with downstream objects (e.g. space debris in ion beam shepherd scenarios)
- The problem is generally **three-dimensional**, with **large required simulation domains** (tens of m)
 - Full particle-in-cell or fully kinetic models are generally unaffordable, unless tricks are used (e.g. reduced mass ratios)
 - Hybrid models with PIC ions/ neutrals and fluid electrons are more adequate
 - Very few studies in literature have dealt with this problem [Korsun 2004, Cichocki 2020]

Magnetized electron fluid model

- A simplified model is considered for the electron momentum balance equation [Cichocki 2020]:
 - Polytropic electron closure: $p_e = n_e T_{e0} (n_e/n_{e0})^{\gamma-1}$
 - Quasineutral plasma: $n_e = \sum Z_s n_s$
 - Electric current continuity equation: $\nabla \cdot \mathbf{j}_e = -\nabla \cdot \mathbf{j}_i$
 - Electron momentum balance equation: $\mathbf{j}_e = \bar{\sigma} \cdot \left[-\nabla \phi + \frac{1}{en_e} \nabla p_e \right] + \mathbf{j}'_e$
- with: $\bar{\sigma} = \sigma_e \begin{bmatrix} 1 & \chi b_z & -\chi b_y \\ -\chi b_z & 1 & \chi b_x \\ \chi b_y & -\chi b_x & 1 \end{bmatrix}^{-1}$
- Electron tensor conductivity
- GREEN MAGNITUDES ARE INPUTS FROM THE PIC ION MODULE
- Collisional current density (with heavy species)
- $\chi = \frac{m_e v_e}{eB} = \text{Hall parameter}$
- $(b_x, b_y, b_z) = \vec{B}/B$
- In terms of a thermalized potential with gradient $\nabla \Phi = \nabla \phi - \frac{\nabla p_e}{e n_e}$ $\Rightarrow \mathbf{j}_e = -\bar{\sigma} \cdot \nabla \Phi + \mathbf{j}'_e$
- Resulting system of equations:

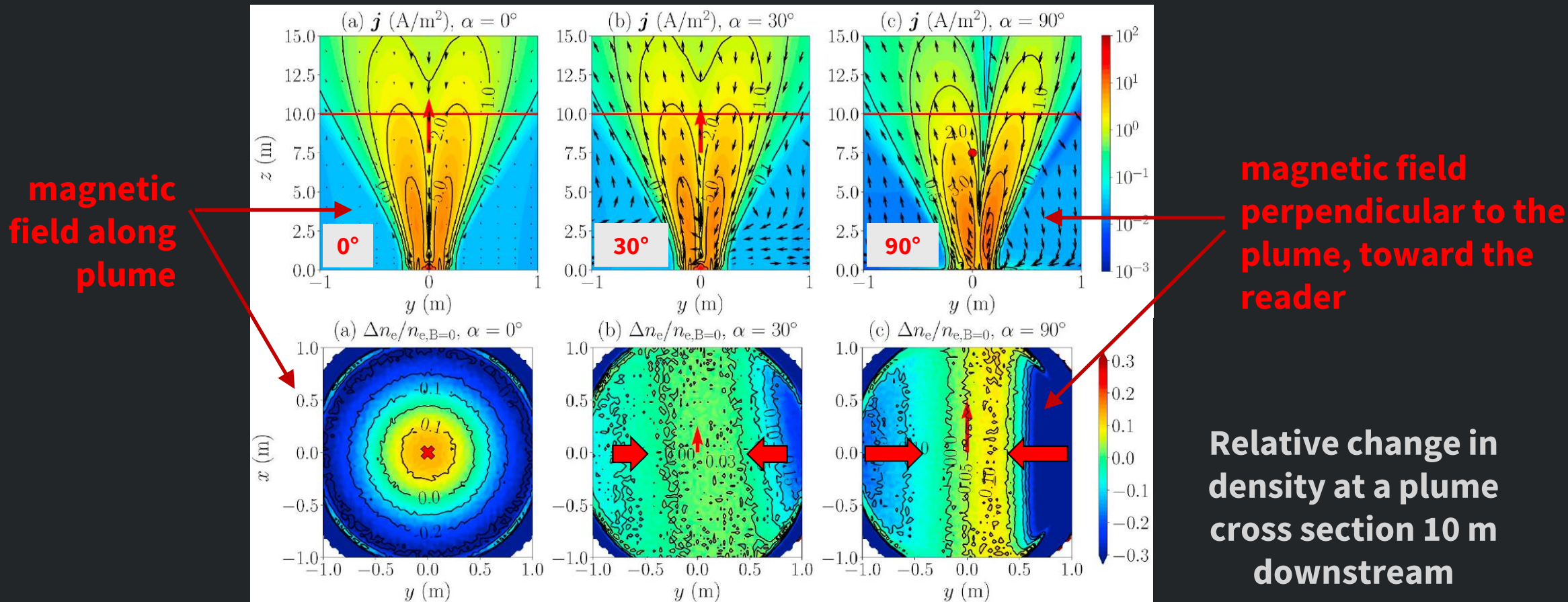
$$\begin{cases} \nabla \cdot \mathbf{j}_e = -\nabla \cdot \mathbf{j}_i \\ \mathbf{j}_e = -\bar{\sigma} \cdot \nabla \Phi + \mathbf{j}'_e \end{cases}$$
- Local boundary conditions imposed on electric current:

$$(\mathbf{j}_e + \mathbf{j}_i) \cdot \mathbf{1}_n = 0$$
- normal unit vector to boundaries

Magnetized electron fluid model results

- The electric field due to the magnetized electron response balances the Lorentz force on ions \rightarrow no net plume deflection
- The geomagnetic field induces **longitudinal current loops** when it is not aligned with the plume centerline \rightarrow the $\mathbf{j} \times \mathbf{B}$ volume force compresses the plume cross section along the direction perpendicular to both the magnetic field and the plume axis

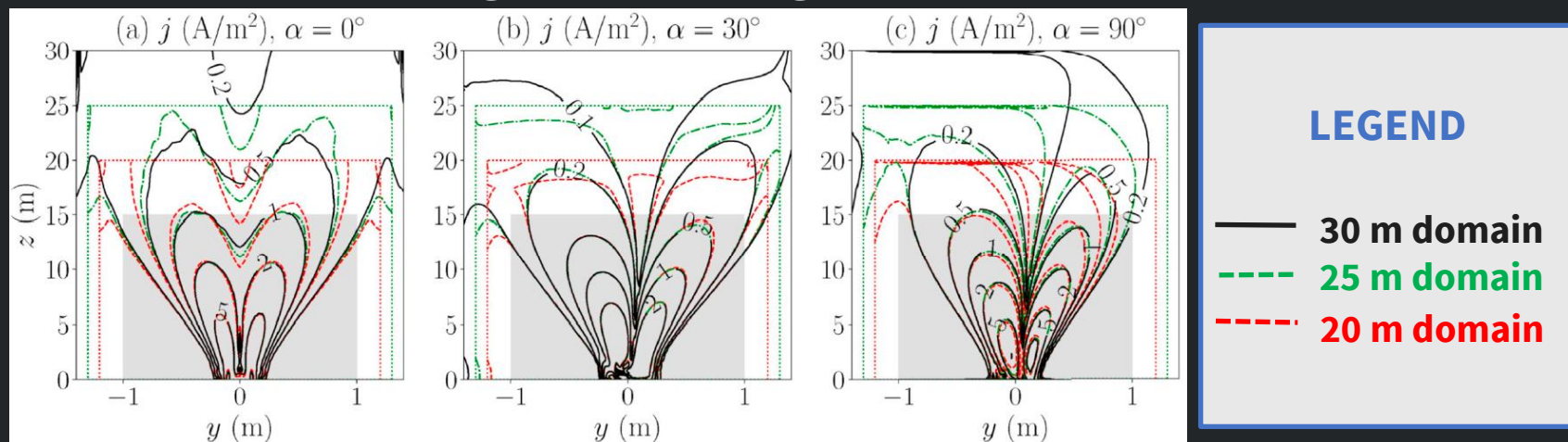
Electric current density in plume for 3 magnetic field angles



Conclusions and open issues/questions

- Geomagnetic field can significantly deform the plasma plume cross section far downstream when it is not aligned with the plume centerline
- The presented 3D magnetized electron fluid model presents some criticalities:
 - Electron polytropic behavior is a strong assumption → challenging implementation of an electron energy equation
 - Any enhanced electron transport must be included through unknown **anomalous transport coefficients**
 - Local boundary conditions introduce **non-local effects** that can travel a certain distance upstream → need for **global boundary conditions**

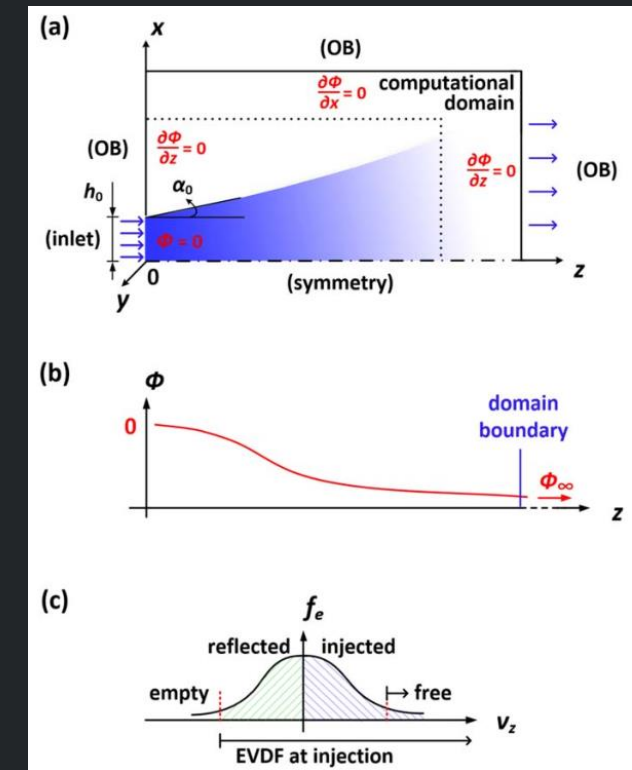
Electric current density for 3 magnetic field angles and 3 different simulation domains



- Electron transport is highly anisotropic → **very high Hall parameters** → **very large condition number** of the resulting linear system → slow convergence of iterative solvers (if convergence at all) → **Hall parameter** typically **limited to approx. 100-200**
- **How and when do electric current loops close downstream?** → Need of larger domains, with electron cooling (to increase Coulomb collisional frequency and lower the Hall parameter) → Self-consistent simulation without forcing strong boundary conditions downstream

Numerical boundary conditions for plumes

- Particle codes boundary conditions:
 - Simply removing the electrons that reach the boundary does not work: leads to ‘numerical pump instability’ [Brieda 2018]
 - Most electrons in the plume EEDF are confined (i.e. reflected) by the downstream potential to infinity, beyond the numerical simulation box
 - Injection BCs also tricky: if near-quasineutral $n_i \simeq n_e$ behavior is desired, amount of injected electrons must “know” the amount of reflected electrons
- Fluid codes boundary conditions:
 - Electron current boundary conditions are tricky:
 - Local current ambipolarity $\mathbf{j}_e = \mathbf{j}_i$? This leads to strong boundary effects into the domain, especially in magnetized plumes where electron motion is essentially along magnetic tubes (2D instead of 3D)
 - Higher-moment codes also need boundary conditions e.g. on the heat fluxes, which need to be modeled.
- Quasi-steady field boundary conditions are also problematic
 - Neumann conditions for ϕ downstream? Assume some slope?
 - Cannot have Neumann ϕ everywhere if there is net charge in the domain

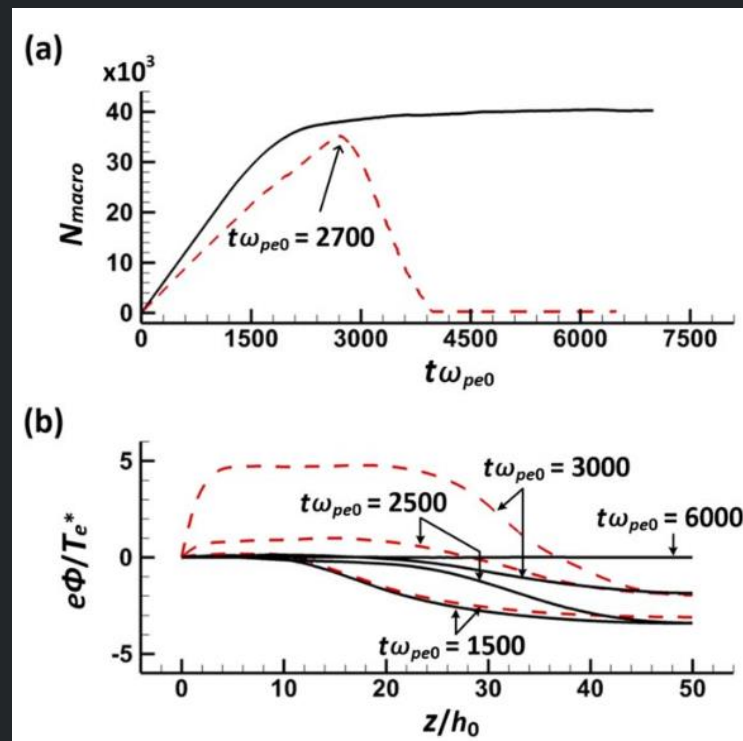


Numerical boundary conditions for plumes: PIC codes

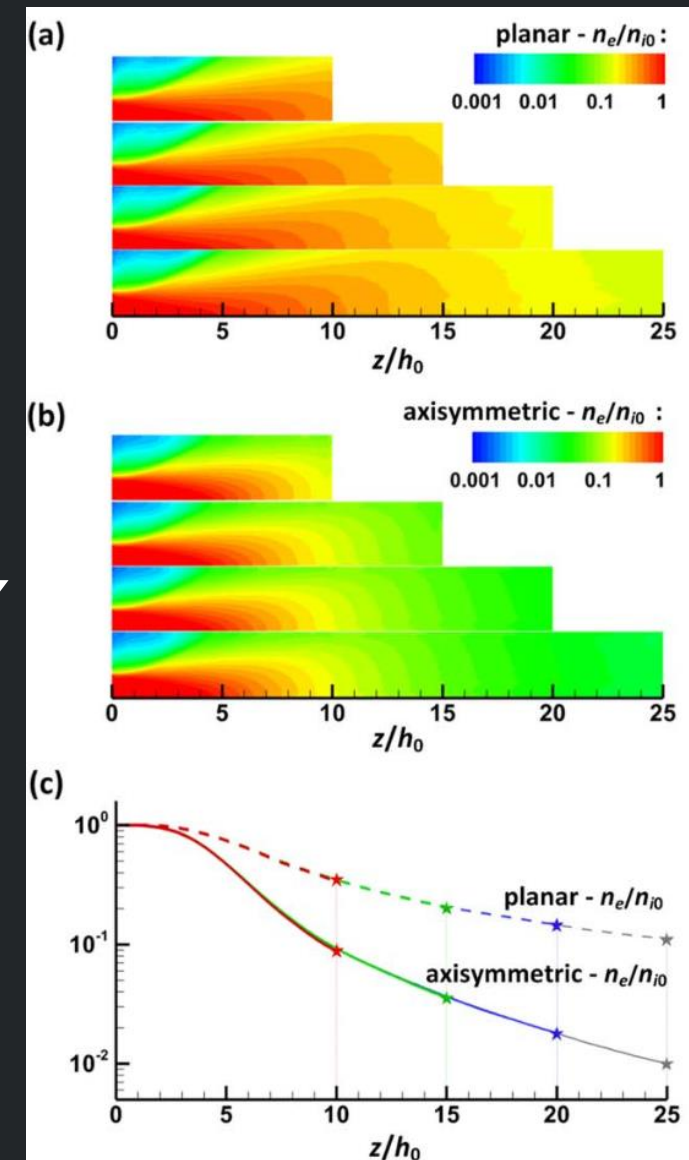
- [Li et al 2019]:

- Electrons reaching the outer boundaries are sorted by mechanical energy
- Lowest energy electrons are specularly reflected to maintain $\int j_i = \int j_e$
 - The critical energy E_{crit} for reflection is computed as a moving time average in practice, to keep PIC noise low
- n_e used for the injection population needs to be changed dynamically, depending on the amount of reflected electrons

Comparison: red is “open boundary” conditions, used in previous works. Black is the new BCs

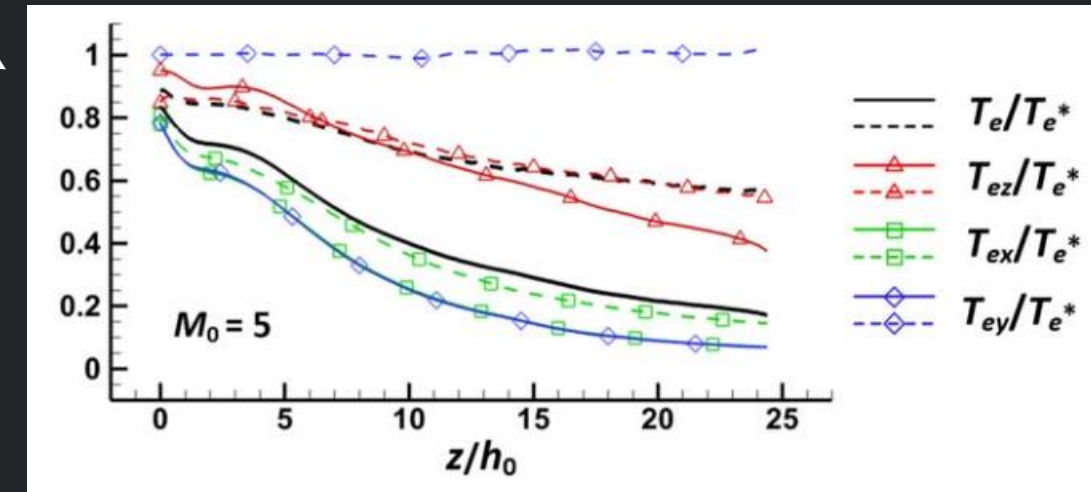
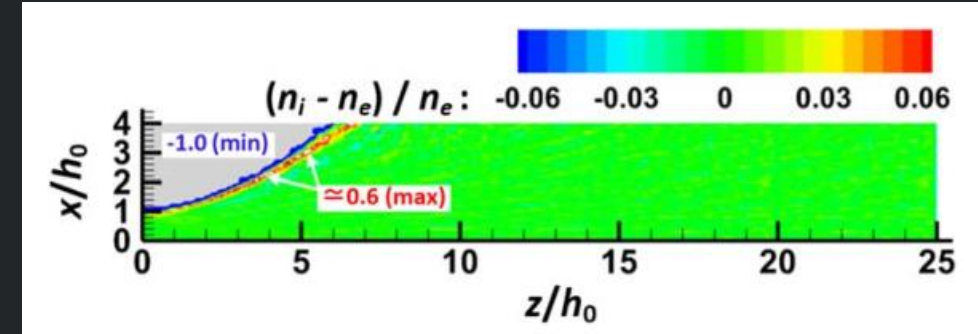
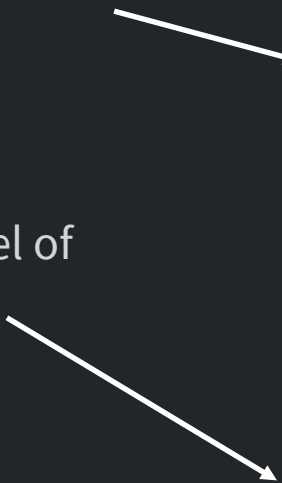


Great domain size convergence



Numerical boundary conditions for plumes: PIC codes

- Domain is essentially quasineutral everywhere, except at plume edge where electrons lead the expansion
- Great agreement with semi-analytic kinetic model of unamgnitized plumes [Merino 2018]

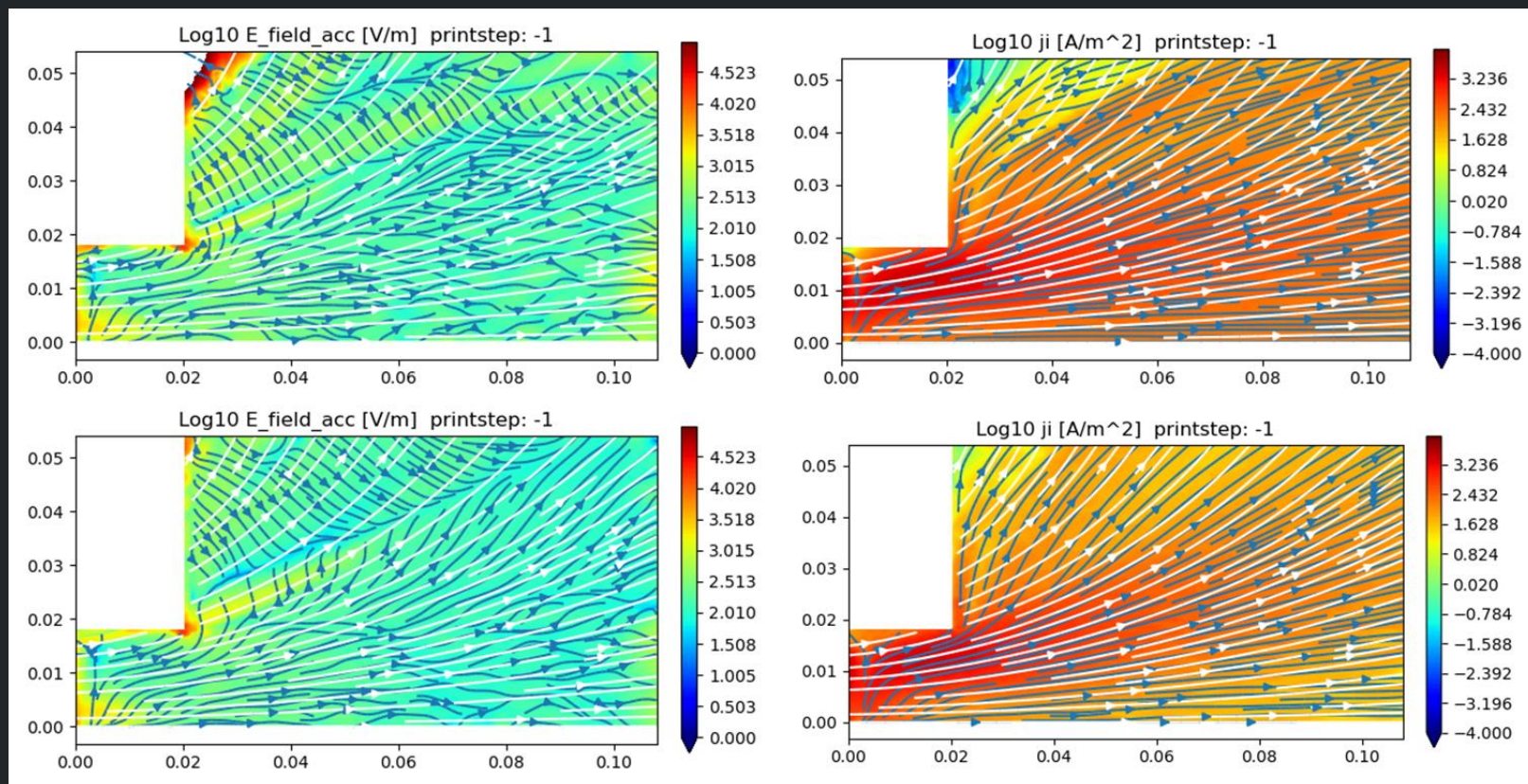


Numerical boundary conditions for plumes: Fluid and Hybrid codes

- Imposing local current ambipolarity $\mathbf{j}_e = \mathbf{j}_i$ leads to artificial boundary effects in the domain
 - Ion trajectories change to accomodate electron transport
 - This is accomplished by a change in the electrostatic potential, to guide the ions
 - These effects are artificial and prevented when a global $\int j_i = \int j_e$ condition is used
- Example: waveguide ECRT simulations (by Marco Inchingolo, unpublished work)

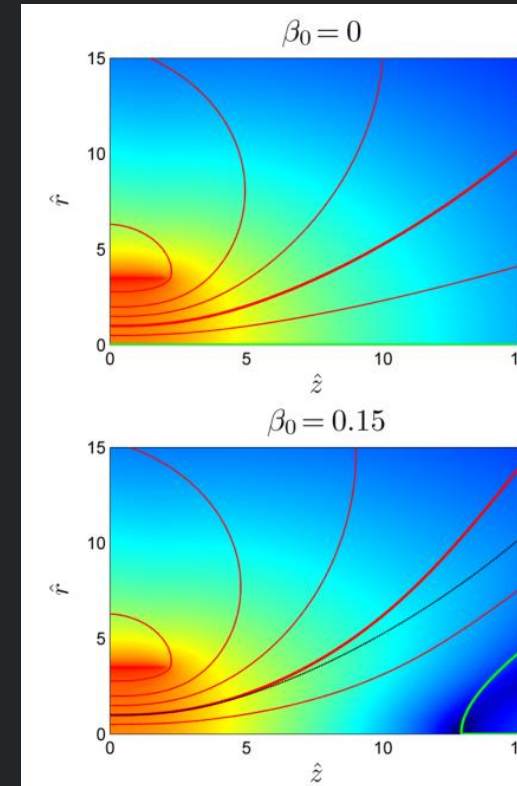
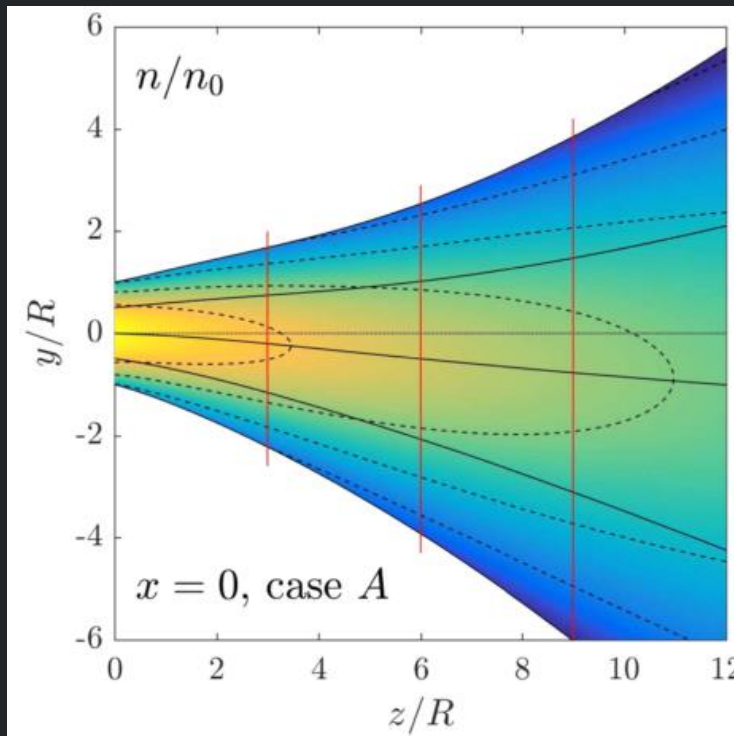
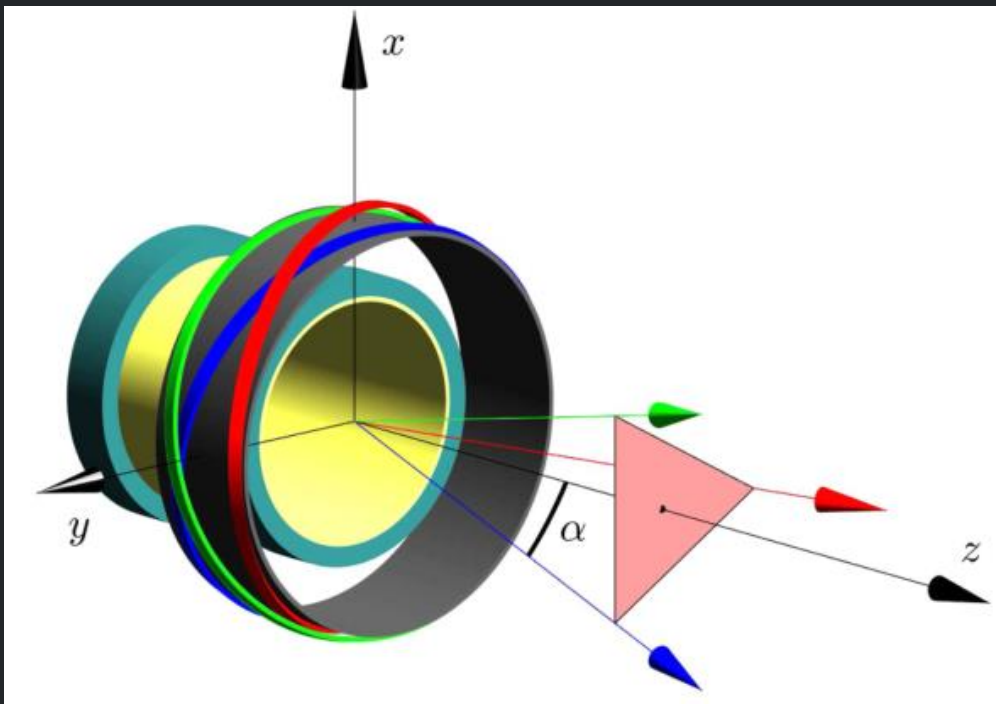
Local 0 Current
(wrong ion stream line curvature, underpredicts plume divergence, wrong radial electric field)

Global 0 Current



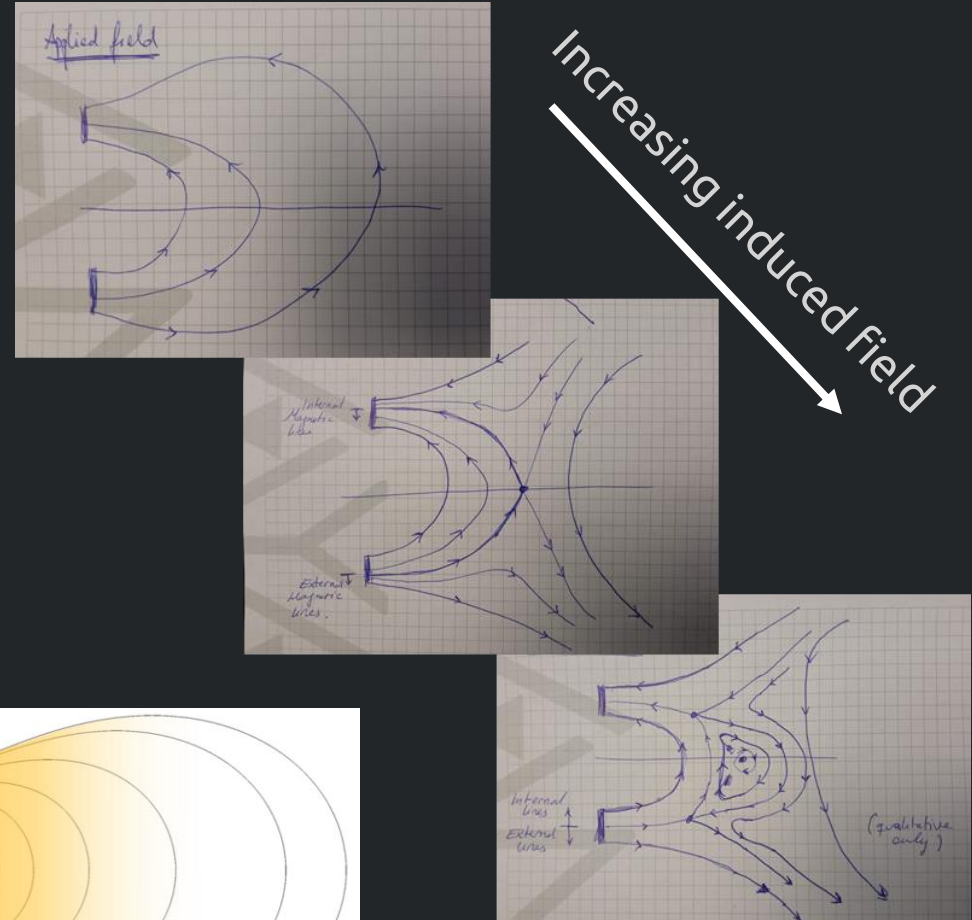
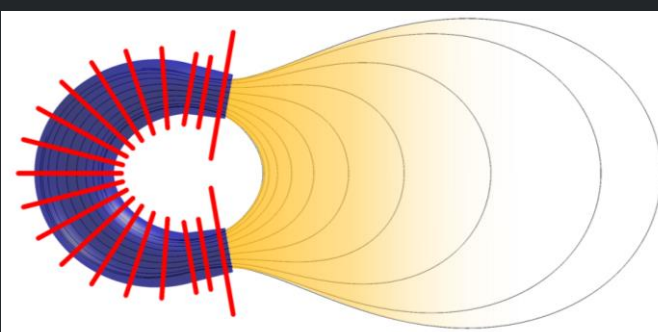
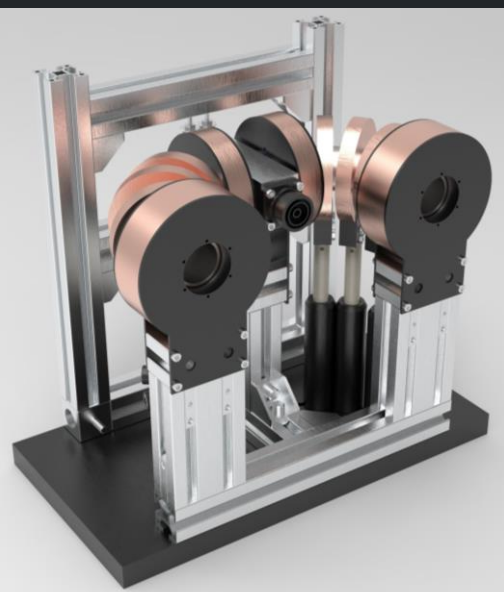
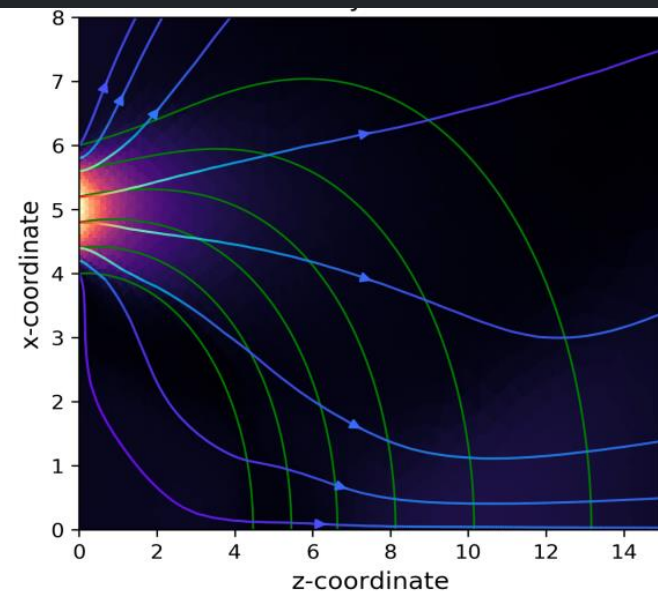
Advanced MN magnetic configurations

- Traditional MN consists of converging-diverging \mathbf{B} field.
Plasma is diamagnetic, pushing back against field [Merino 2016]
 - Generates magnetic thrust
 - Increases MN divergence
- 3D MN** based on 3 (or more) intertwined, tilted coils
proposed for contactless thrust vector control without moving parts [Merino 2017]



New configurations?

- A “Magnetic arch” forms combining two MNs with opposite polarities
- New, interesting physics occur:
 - Diamagnetic plasma will now stretch and open the magnetic lines, changing the topology completely
 - New family of trapped electrons connecting the two sources
 - Lower divergence plasma jet?
- Planar, two-fluid simulations of traditional MN and magnetic arch (by Diego García-Lahuerta, preliminary unpublished work):



Discussion

- What is the trapped electrons population in a magnetized/unmagnetized plume?
 - How sensitive this population is to collisionality, initial transient, etc?
 - What experiments can be designed to study electrons kinetically, in particular the trapped population?
- What is the degree of freedom of electrons and ions in magnetic nozzle device
- Proper closures at pressure level and heat flux level: simplified electron cooling models
 - How can kinetic studies help obtain proper closures?
 - How can experiments be designed for obtaining proper closures?
- Oscillations in the magnetic nozzle and their relation to perpendicular transport?
 - Ranges of frequencies, mechanisms involved.
 - What models/simulations to carry out?
 - What experiments to design?
- Electron detachment. What mechanisms are at play? How to characterize it numerically and experimentally?
- What is the effect of charged obstacles on the performance of magnetic nozzles?
- What boundary conditions for the electron fluid downstream? Local vs global conditions, which ones enable the smallest simulation domain?